UNIVERSITY OF OKLAHOMA
GRADUATE COLLEGE

APPLICATION OF BASALT FIBER REINFORCED POLYMER REBAR FOR PRESTRESSED CONCRETE BEAMS

A THESIS

SUBMITTED TO THE GRADUATE FACULTY

in partial fulfillment of the requirements for the
Degree of

MASTER OF SCIENCE

By

WASSIME SOMATRI
Norman, Oklahoma
2022

APPLICATION OF BASALT FIBER REINFORCED
POLYMER REBAR FOR PRESTRESSED
CONCRETE BEAMS

A THESIS APPROVED FOR THE SCHOOL OF CIVIL
ENGINEERING AND ENVIRONMENTAL SCIENCE

BY THE COMMITTEE CONSISTING OF

Dr. Jeffery S. Volz, Advisor

Dr. Royce W. Floyd

Dr. Shreya Vemuganti

ABSTRACT

All steel reinforced concrete infrastructure that is facing a chemical environment and corrosion will have their service life greatly reduced. With time it will lead to a premature and an inevitable failure of the steel reinforced members. After the World War II in the 1940s, the development of fiber reinforced polymer (FRP) composites has found extensive applications in different fields such as aerospace and the defense industry thanks to the expanded use of composites and recently it has found applications in the construction industry. FRP composites are characterized by various beneficial features such as high strength-to-weight ratios and excellent corrosion resistance and can be used as a substitute for steel.

This research focused on investigating the implementation of a new materiel, basalt fiber reinforced polymer (BFRP) for prestressed concrete members. Using BFRP rods instead of traditional prestressing steel tendons could increase the durability of reinforced concrete structures. To assess the behavior of prestressed members made with tensioned BFRP rods, and determine if it would be suitable for prestressing applications, three prestressed BFRP concrete beams were fabricated. For each one, a companion nonprestressed BFRP concrete beam was fabricated at the same time. The nonprestressed BFRP concrete beams had the same characteristics as the prestressed BFRP concrete beams. This would enable an assessment of the effectiveness of BFRP for prestressing.

After developing an anchoring system using a steel sleeve that will confine the BFRP rod from slipping through an expansive mortar, the prestressed BFRP beams could be fabricated. The transfer length as well as the prestress losses were measured through the use of DEMEC points. The transfer length results were dispersed depending on the method used to calculate them.

Prestress losses were also evaluated, and a prestress loss of approximately 10% was observed after 28 days. The results of the flexural testing of the beams lead to a conclusion that prestressed BFRP concrete beams are 20% stronger than nonprestressed ones, and they could sustain a load five times greater before the appearance of cracks in the prestressed BFRP concrete beams. As a result, BFRP prestressed concrete beams will have a greater service life expectancy than regular reinforced BFRP members.

ACKNOWLEDGMENTS

First, I would like to thank my advisor, Dr. Jeffery Volz for the help and support throughout this research journey. I would also like to thanks my committee members, Dr. Royce W. Floyd and Dr. Shreya Vemuganti, for their time and advice. Additionally, I would like to give a special thanks to the lab manager John Bullock, for his help and recommendations to fabricate all the BFRP concrete beams. I would like also to extend my thanks to V-ROD company who provide us BFRP rods for this research. Additionally, I owe a lot to the member of the research team composed of Choate Jacob, Milner Jackson C., Martin Johnathan D, Stephen Roswurm, Vargas Jorge E., Reed, Clay M., and Haibe Abdirahman A, for donating their time and effort to help me with my research. Working with everyone was always a pleasure, and I could never have completed my work without the help of the lab technician and my colleagues. Finally, I would like to thank my parents, my sisters, and my friend Hodzic Uzeir for their consistent support.

TABLE OF CONTENTS

LIST OF ILLUSTRATIONS

LIST OF TABLES

1. INTRODUCTION

1.1 Background

In civil engineering, stresses and loads become more important in construction such that civil engineers have to design structural elements to be able to sustain loads during the service life of the structure. New methods and technologies are constantly developed to face these challenges. In particular, for long span bridges, prestressed beams were developed to improve long term performance as the prestressing reduces or eliminates the potential for cracking of the concrete, significantly improving its capacity and durability. Normally, steel is used to counter the tensile stress in the beam, but a new material called basalt fiber reinforced polymer (BFRP) has come into the market, which plays the same role as steel to support the tensile stress in the beam. The important benefit of BFRP is that unlike steel, it is not susceptible to corrosion. Fiber reinforced polymers (FRP) also have high strength to weight ratios, as well as the inherent resistance to corrosion. These characteristics are particularly beneficial when building structures exposed to water and aggressive agents such as salts. However, FRP also has some disadvantages, particularly due to its elastic properties (low modulus), which can be a problem for the dynamic behavior of structures constructed using BFRP. For prestressed beams, the failures of strands directly lead to the failure of the beam and all the structures that it supports. As a consequence, BFRP must be an efficient and reliable alternative to steel.

1.2 Objective

In order to investigate the general behavior of prestressed BFRP concrete beams, and determine if BFRP can serve as prestressing for concrete, this research was conducted. The first main objective was to develop a viable anchor in order to tension the BFRP rod. In order to apply a prestressing force to the beam, the BFRP rod must be tensioned enough to create a compressive force to counter the tensile stresses due to the loads on the beam. Thus, to tension the rod, a method is needed to anchor the bars to transfer the jacking stress without slipping along the BFRP rod nor crushing the bar during the operation.

The second main objective was to test prestressed and nonprestressed BFRP concrete beams and compare their strength and ductility. Indeed, BFRP rods are very resistant to corrosion and chemicals attacks whereas typical strand or steel rebar are not. As a consequence, introducing BFRP rods for prestressing applications will solve a number of problems for the sustainability and the durability of infrastructure facing corrosion attacks and harsh environments. Furthermore, evaluating the transfer length and prestress losses of BFRP prestressed concrete beams will enable the evaluation of this alternative to steel.

1.3 Scope

In order to evaluate potential anchoring systems first, a literature review was conducted. Based on the literature review, a research plan was developed to find a suitable anchoring system to tension the BFRP rod safely. The mechanical properties of the BFRP rod from the literature review enabled an understanding of how BFRP materials behave in general, and how they could be prestressed safely. To prestress a series of three concrete beams using BFRP rod, the concrete was designed to have enough compressive strength to resist the prestressing force after one to two days, so the prestress release would be effectuated sooner. For each prestressed BFRP concrete beam, one nonprestressed concrete beams was fabricated as a control in order to have an accurate comparison with the effect of prestressing. Demountable mechanical strain gage were implemented for the prestressed BFRP concrete beams to evaluate the transfer length as well as the prestress losses at prestress release and over time.

1.4 Outline

This thesis is composed of six chapters and 10 appendices numbered from A to J. Chapter 1 gives a brief introduction to the subject area and explains why this research was pursued. Chapter 2 presents the literature review made in order to gather information about BFRP materials and prestressing. Chapter 3 examines potential anchoring systems developed to tension BFRP rods. Chapter 4 outlines all the steps necessary to design and fabricate the prestressed and nonprestressed BFRP concrete beams as well as how the prestressing procedure was effectuated. Chapter 5 provides the results obtained from measurements and the testing of all the beam specimens, as well as analyzing those results. Finally, Chapter 6 summarizes the findings and provides a final set of conclusions for this research, as well as some recommendation for further research applications. The appendices provide details of calculations and results from measurements.

2. LITERATURE REVIEW

2.1 History of BFRP

Basalt fiber reinforced polymer (BFRP) is fabricated from basalt, which is a natural stone that comes from the frozen lava that volcanoes produce when they are active. Basalt is composed from two essential minerals, pyroxene and plagiocene which is around 80% of its composition (JiriiMilitky et al., 2002). The fibers are extruded through small nozzles to produce continuous filaments of basalt fiber from the molten rocks heated to between 1500-1700°C (Fareed Elgabbas et al., 2016). Then there is a resin applied to bond together all the basalt fibers, and the fabrication process of bonding together the fibers is termed pultrusion (A. M. Fairuz et al., 2016). Pultrusion is a composite fabrication technique where continuous fibers are impregnated with the thermoset polymer matrix through a heated die to form the composite (A. M. Fairuz et al., 2016). Originally, this new material was derived from a material named Bekelite, which is the first plastic made from synthetic components recognized by the American Chemical Society and formed from the condensation reaction of phenol and formaldehyde (David Trejo, 2018). It was developed by a chemist named Leo Baekeland in New York in 1907.

After this discovery, the development of fiber-reinforced plastics for commercial use was being extensively researched in the 1930s. Then, in 1981, the American Concrete Institute (ACI) published an article on fiber reinforced polymer (FRP) for the first time by Fardis et al. (1982). The article focused on using FRP for cast-in-place concrete. Then, in 1991, S. Paul Bunea proposed using glass fiber reinforced polymer (GFRP) instead of steel for lunar exploration and settlement. Since 1991, more than 200 research articles have been published in the ACI’s journal because companies, including construction, aeronautics, and automotive, were interested in studying this material's behavior.

Nowadays, application of FRP in different fields has grown considerably, and in the 2000s China became the largest user of FRP in new construction, especially used from underground work to bridge design (ACI Committee 440, 2015). Basalt fibers found their application for the production of chemically inactive products, molded products such as pipes, flag stones, or for insulation using basalt wool (Fareed Elgabbas et al., 2016). The largest demand for electrically nonconductive reinforcement, like FRP, was in facilities for medical equipment. However, it was not only in this domain of construction that FRP was demanded, it was especially for all constructions related to a water environment, because FRP is free from corrosion, thus FRP reinforcement became better known and desired, specifically in seawall construction design (ACI Committee 440, 2015). An image of BFRP rod is presented in Figure 2-1.

Figure 2-1: Image of a BFRP rebar (Raghavendra Vasudeva Upadhyaya, 2018)

2.2 Mechanical properties of BFRP rod

2.2.1 BFRP composite material

BFRP composites and bars are obtained by embedding continuous fibers of basalt in a resin mix made of polymers which bind together the fibers and keep them straight, which facilitates the distribution of stresses between each fiber. These fibers determine the various control characteristics of composites and bars (David Trejo, 2018). The end products and polymers manufactured form these fibers are termed BFRP. The letter “P” which stands for polymer is added at the end of BFRP, because we use a resin matrix (e.g., vinylester, epoxy) to embed the fibers together. Resins also play the role of a layer protecting fibers from external environmental stresses (Mohammed A. J. Alsalihi, 2014). Figure 2-2 is an image captured from a microscope of the BFRP rebar where fibers and resin can be observed.

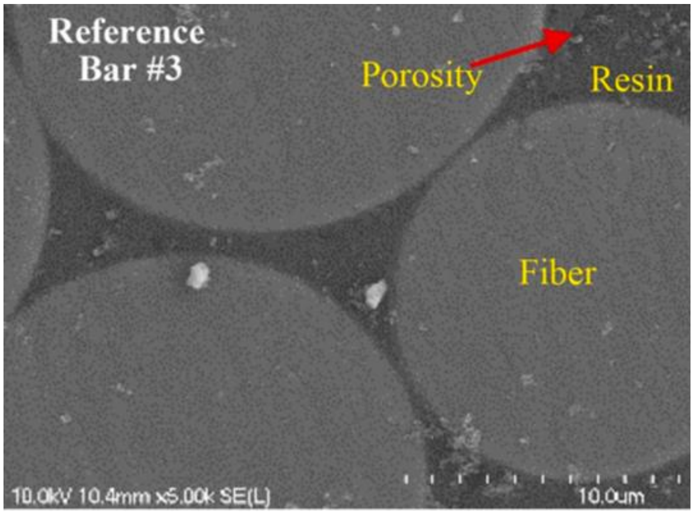

Figure 2-2: Cross section of #3 BFRP rebar, image cropped from figure 10 (Ahmed H. Ali et al., 2021)

The Rule of Mixtures describes the mechanical properties of BFRP, which has an anisotropic behavior, with the high tensile strength associated with the direction of the fibers when used as a reinforcement for concrete. The effect of the relative properties of the fibers and the resin is usually described through the "rule of mixtures" (David Trejo, 2018). In equation 2-1, P_{FRP} represents the mechanical property of the FRP, P_f is the mechanical property of the fibers, P_m is the mechanical property of the matrix, υ_f is the volume fraction of fibers, and υ_m represents the volume fraction of the matrix.

$$\boldsymbol{P_{FRP}} = \boldsymbol{P_f}\upsilon_{\boldsymbol{f}} + \boldsymbol{P_m}\upsilon_{\boldsymbol{m}} \quad (\mathbf{2}\text{-}1)$$

Through this expression, the relative properties of the BFRP material can be determined. For instance, Bakis et al. determined a very close prediction of the modulus of elasticity of BFRP rods using the rule of mixture (David Trejo, 2018).

2.2.2 Mechanical characteristics of BFRP

The company V-ROD based in Canada provided the BFRP reinforcing bars for this research. Table 2-1 contains the BFRP properties based on quality control testing by the manufacturer.

Table 2-1: Mechanical properties of #4 BFRP rod grade III provided by V-ROD company (V-ROD, 2021)

Tensile strength	195.8	ksi
	1350	MPa
Minimum tensile modulus	8702	ksi
	60	GPa
Transverse shear capacity	31.9	ksi
	220	MPa
Type of Resin	Vinylester	
Type of fibers	Basalt	

Table 2-1: (continued)

Effective cross-sectional area (ASTM D7205 including sand coating)	0.223 1.44	in^2 cm^2
Nominal cross-sectional area (ASTM D7957 table 3)	0.2 1.29	in^2 cm^2
Effective diameter	0.56 1.43	in. cm
Linear weight	0.21 0.32	lb/ft kg/m

The BFRP rods have a high tensile strength of nearly 200 ksi, which is greater than regular steel rebar currently in the market, with the additional benefit that it is very light compared to steel, so it is very easy to handle on the construction site, and it has a excellent corrosion resistance.

2.2.3 Advantages and disadvantages of BFRP

According to ACI committee 440, advantages and disadvantages of BFRP compared to steel include the following (ACI committee 440, 2015):

→Disadvantages

- BFRP has a linear elastic behavior until failure whereas steel yields.
- BFRP is anisotropic whereas steel is considered isotropic.
- BFRP has a lower modulus than steel.

- BFRP has a lower creep-rupture threshold than steel.
- Coefficient of thermal expansion is different in longitudinal and radial directions.
- Endurance time in fire and elevated temperature is less than steel.

→Advantages

- Tensile strength is greater than steel.
- Lightweight at 1/4 to 1/6 the weight of steel, with the reduced weight lowering transportation costs and more easily handled on the project site.
- Transparent to magnetic field and radio frequencies.
- Thermally and electrically nonconductive.
- High fatigue endurance.
- Less concrete cover is required.
- Cost effective alternative to epoxy coated and galvanized steel bar and stainless steel bar.
- Degradation mechanism benign to the surrounding concrete unlike steel that expands and causes failures of the member.
- Non-corrosive so it is impervious to chloride ion and chemical attack.

With those advantages that BFRP provides, there is significant potential as a replacement of steel in prestressed concrete beams. BFRP is lightweight, high strength, and non-corrosive. It is also a competitive replacement for conventional steel reinforcement, suggesting high durability and low impact construction projects. For example, corroded steels are responsible for approximately $276 billion in annual loss, or more specifically around $8.3 billion spent on repairing corroded bridges in the United States (Koch et al., 2002). Therefore, BFRP has the potential to save a significant amount of money if it can be used to replace steel reinforcement in concrete beams.

2.2.4 Stress-strain diagram

The stress-strain response of BFRP is shown in Figure 2-3 compared to other FRP bars, prestressing steel, and mild steel. In examining Figure 2-3, it is apparent that BFRP has a slope less than steel, and thus a modulus of elasticity significantly lower than that of steel reinforcement or prestressing steel tendons. This means that BFRP is less stiff than steel reinforcement. Furthermore, with no plateau in the stress-strain response, it is also less ductile than steel and can fail at any moment without warning when it reached its ultimate strength.

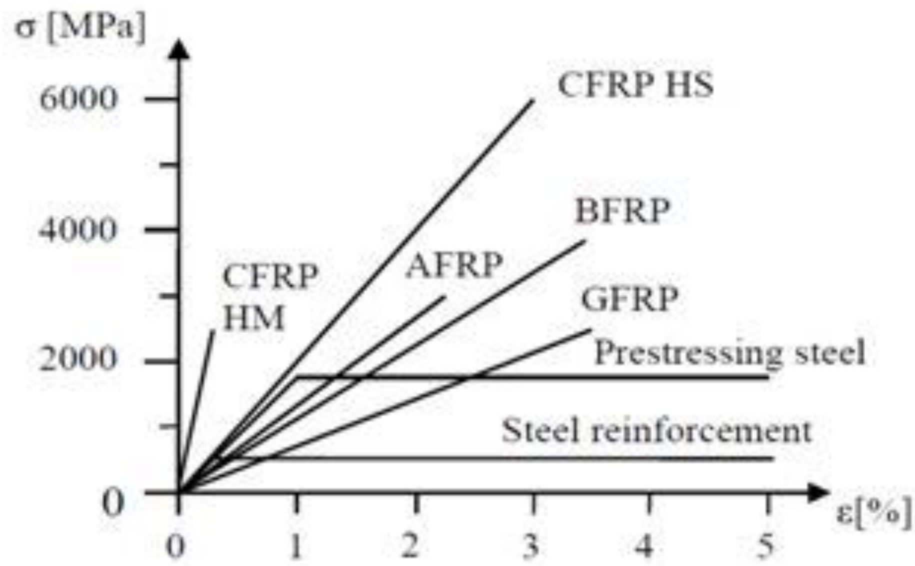

Figure 2-3: Stress-strain diagram for different type of FRP and steel rebar or tendons (Raghavendra Vasudeva Upadhyaya, 2018)

2.3 BFRP Prestressing application

2.3.1 Prestressed concrete

Concrete is strong in compression, but weak in tension, with a tensile strength that varies from 8 to 14 percent of its compressive strength. In order to counter the low tensile strength of concrete, steel prestressing tendons or strands are used to impose stresses in the beams that will counter the stresses due to load. The imposed longitudinal force is called a prestressing force, it is a compressive force that prestresses the sections along the span of the structural element prior to the application of the transverse gravity dead and live loads. Contrary to a simple reinforced concrete beam, the prestressed beam will have a camber, which will minimize the deflection when loaded, as illustrated in Figure 2-4.

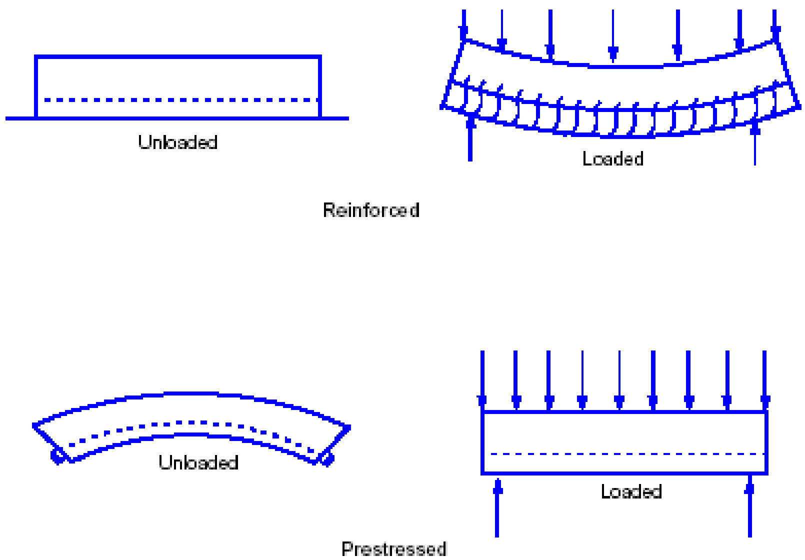

Figure 2-4: Difference between reinforced and prestressed concrete beam (Ash, 2022)

2.3.2 BFRP rebar

The compressive force used to prestress the beam is usually applied to the beam through a tensioned steel tendon, but BFRP tendons could also be used. Unfortunately, BFRP tendons are currently unavailable in the marketplace, and only prototypes have been developed at this point in time. BFRP solid rebar, which is typically not well suited for prestressing due to their difficulty to be coiled, are usually used for reinforced concrete. However, due to its very high tensile strength, it may be possible to use BFRP solid rebar as prestressing bars similar to steel prestressing bars without the corrosion concerns. The No.4 BFRP rod could provide around 72% the tensile capacity of a Grade 270 steel tendons. Furthermore, few research related to BFRP prestressed beams have been conducted, and no standard or guidelines cover this subject yet (Eythor et al., 2012).

2.3.3 Anchorage characterization

The various types of anchorages used with FRP tendons can be classified as clamp, plug and cone, resin sleeve, resin potted, metal overlay, and split wedge anchorages, and are shown in Figure 2-5 (ACI Committee 440, 2015).

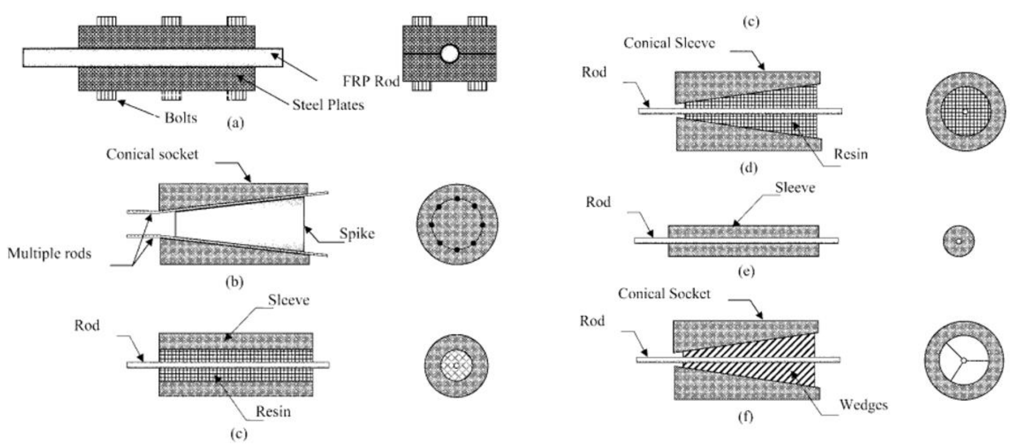

Figure 2-5: (a) clamp (b) plug and cone (c)straight sleeve (d) contoured sleeve (e) metal overlay (f) split wedge anchorage

These methods will need to be adapted to find a viable solution for the anchorage and stressing of BFRP solid bars. In the article published by Alraie et al. (2021) about the "Development of Optimal Anchor for Basalt Fiber–Reinforced Polymer Rods", the authors insert the rebar inside a steel sleeve and use expansive grout cement to bond together the rod and the anchor. This technique avoids crushing the bar when placed under tension and is shown in Figure 2-6, to illustrate the shape of this anchor:

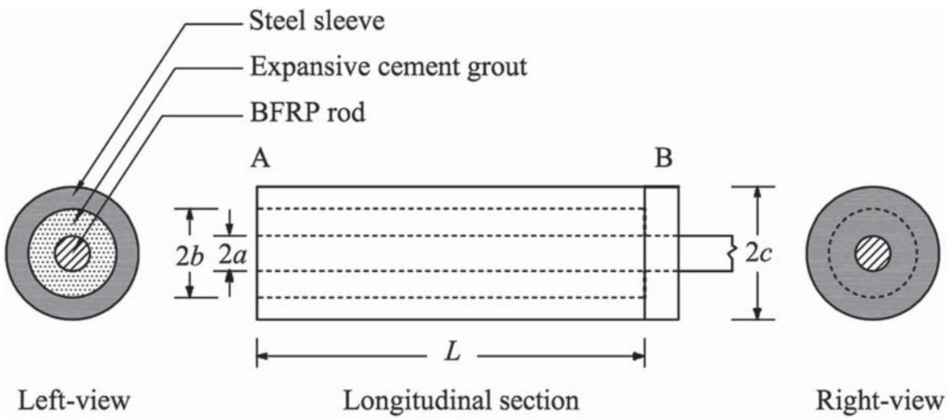

Figure 2-6: Schematic drawing of the anchor used by Ali et al. (2021) where they inserted their BFRP rod inside a steel sleeve and used an expansive cement grout to bond them

Eythor et al. from the University of Reykjavik (Eythor et al., 2012) used a steel pipe for the anchor for their BFRP tendons and glued to that pipe using HIT-RE-500, an epoxy from the manufacturer Hilti. Similarly, the company V-ROD for their tensile test used the same procedure but instead of using the epoxy to glue the rebar with the steel pipe, they used an expansive mortar in order to achieve a better bond.

2.3.4 Conclusion

As a conclusion, by investigating the evaluation of prestressed BFRP beams, this research will adds to the literature by providing more data about the behavior of prestressed BFRP concrete beams. After testing the flexural strength of prestressed BFRP concrete beams and nonprestressed BFRP concrete beam, the comparison of strength enabled to determine if prestressing was worth it and suitable. The anchoring system suggested in this literature review was tested in order to find if the anchoring system was suitable, in order to tension the BFRP rod.

3. DEVELOPMENT OF AN ANCHOR FOR PRESTRESSING BFRP RODS

3.1 Introduction

To assess the properties of the basalt fiber reinforced polymer (BFRP) and its general behaviors when pretensioned for prestressed concrete beam applications, a series of beams that can be tested in the laboratory were constructed. In order to fabricate those prestressed BFRP concrete beams, the BFRP rod had to be tensioned safely. To make that possible, an anchor to transfer the tension stress to the BFRP rod without damaging it needed to be designed. For this research, one of the main tasks consisted of developing a suitable anchor in order to tension the BFRP rebar. The BFRP rods for this research, donated by the V-ROD company, are sand-coated to increase bonding with the concrete. These rods are not as flexible or ductile as a traditional prestressing tendon. This difference will also have an impact on the general behavior of the beam. In the ACI 440.4R-04 guide (ACI Committee 440, 2004) it is recommended for FRP tendons an allowable jacking stresses between $0.40f_{pu}$-$0.65f_{pu}$ depending of the type of FRP tendons. Thus, the objective was to tension this BFRP rebar to at least 50% of its ultimate tensile capacity, which is reasonable in terms of safety regarding this type of brittle material. According to the V-ROD specification sheet for the #4 BFRP rod provided, the ultimate tensile capacity is 195.8 ksi.

As a consequence, it was decided to set the objective to tension the rod to 20 kips, which corresponds to a tensile stress of approximately $0.46f_{pu}$, close to the goal of 50% of its ultimate tensile capacity.

3.2 Test Setup for BFRP Anchoring System

In order to test the proposed anchoring systems for the BFRP rod, a test setup was fabricated for the Baldwin Universal Testing Machine (Baldwin) located at the Donald G. Fears Structural Engineering Laboratory. This test setup provided a transition from the Baldwin grips to the BFRP rod anchoring system that was used for prestressing purposes. The first anchoring system that was explored was a traditional steel strand chuck, the next one was a steel pipe filled with HILTI epoxy, and finally the last one tested was a steel pipe filled with expansive mortar. To test the efficacy of those different anchoring systems, a tensile test was conducted using the Baldwin. The test setup required a slot to allow installation of the BFRP rods and proposed anchoring systems. Unfortunately, during initial testing, the top and bottom flanges of the test setup were overstressed prior to reaching the required load of 20 kips, as shown in Figure 3-1.

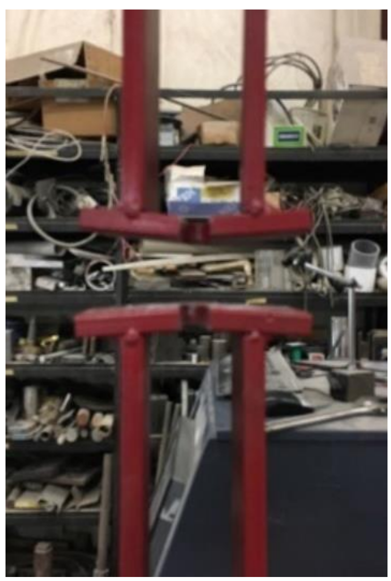

Figure 3-1: Damaged BFRP anchoring system test setup

The test setup was revised with a thicker top and bottom flange. Details of the revised design and the fabricated test setup are shown in Figure 3-2.

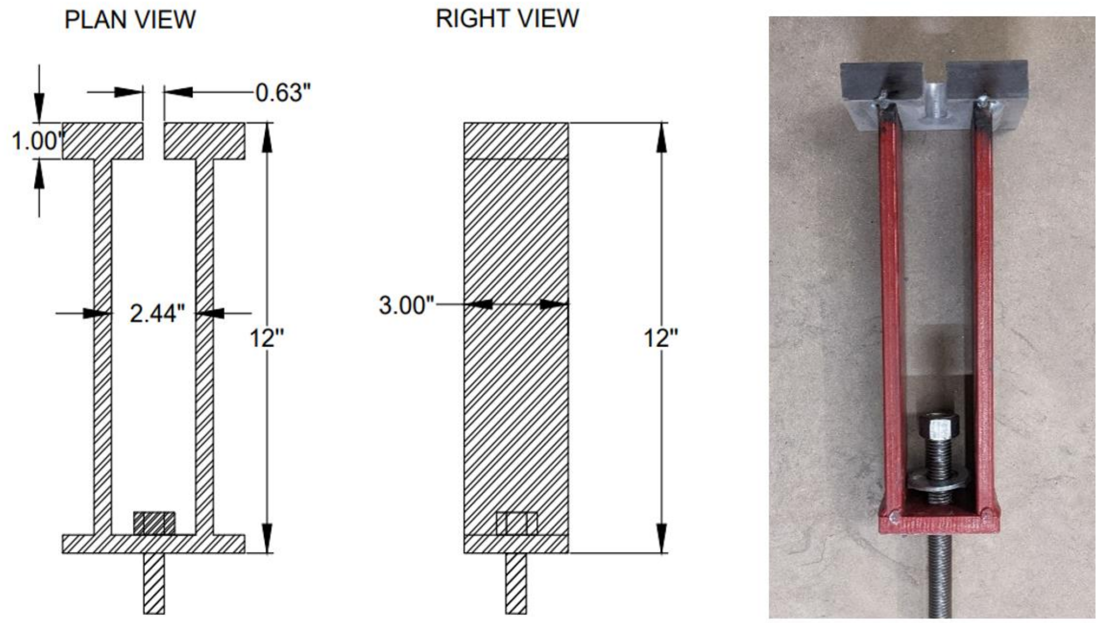

Figure 3-2: Revised design of the BFRP anchoring system test setup

3.3 Traditional steel strand chuck

In the prestressed concrete industry, steel chucks are used to anchor traditional steel tendons, which play the role of securing the tendons during the prestressing process. This anchor is suitable for steel tendons, but it is not recommended for FRP bars in general. In the process of finding an anchor which would enable the goal of achieving a tension force of 20 kips, it was decided to investigate whether a standard steel chuck would be able to successfully anchor the BFRP rods. Figure 3-3 shows one regular set of prestressing chucks that was tested.

Figure 3-3: Photograph of one set of prestressing chucks used for testing

After sectioning a 13 in. long BFRP rod specimen, a steel chuck was installed at each end. It is also worth noting that because the chuck is designed for 0.5 in. diameter steel strand and because the BFRP rod has a diameter of 0.56 in., the insertion of the BFRP rod had to be forced a little bit. Once all those steps were realized, the tension test was conducted using the Baldwin. The BFRP rod was tensioned to 15 kips, which corresponds to a tensile stress of approximately 67 ksi. At this load, slippage of the BFRP rod inside the chuck was observed, which decreased the load. Subsequently, the load was applied again, until it reached 15 kips where the slippage occurred once again. Thus, it was decided to stop the test since the load could not be maintained without slipping.

The BFRP specimen is shown in Figure 3-4a with the steel chucks installed at both ends. Figure 3-4b shows the specimen within the test setup fabricated for the Baldwin. After removing the specimen from the test setup, it was observed that the BFRP rod slipped within the wedges causing grooves in the specimen, as shown in Figure 3-5.

(a) (b)

Figure 3-4: Picture of the BFRP rod used with two chucks (a) inserted in the test set up (b)

Figure 3-5: BFRP rod after removing the chucks that slipped during testing

3.4 Steel pipe with HILTI epoxy

At the University of Reykjavik (Thorhallsson et al. 2012) researchers used a steel pipe for the anchoring system and a high strength epoxy for their prestressed BFRP tendons. The product they selected was HIT-RE-500 manufactured by HILTI, which they poured between the steel sleeve and the BFRP rebar. The curing of the epoxy usually required 24 hours, although it depends on the temperature and the specific type of the epoxy. When cured, the tendon is fixed within the steel pipe, restrained from any movements, due to the adhesion between their BFRP tendon and the steel sleeve.

For the case considered in this research, it was decided to test the HILTI product HIT-RE-200 that was already available in the laboratory. It was expected that the HIT-RE-200 would develop less bond strength compared to the HIT-RE-500 based on the product literature provided by the manufacturer. To begin, the steel sleeve needed to be chosen. It was decided to try a wall thickness of 1/8 in., and for its length, the pipe needed to be as long as possible to develop sufficient bonding between each component, forming the anchor. The maximum length available depended on the steel test frame length, which was fabricated to allow a maximum length of 11.5 in.

Finally, two 10 in. long steel pipes were cut to make one anchor specimen for the pull-out test. The pipes were cleaned with water, then paper towels soaked in acetone were used to clean the inside so that the epoxy would bond well to the inside wall of the steel pipe. Once this was done, the BFRP rod was inserted inside the pipe, and four 5/8-in.-diameter washers were welded on the end of the anchor to maintain the correct position of the BFRP rod inside the steel pipe. Then, the HILTI epoxy gun was used to inject the HIT-RE-200 from one edge of the anchor. Afterward, the epoxy could cure during the 24 hours period prior to testing. Figure 3-6a is a photograph of the BFRP rod, steel sleeve, and HILTI epoxy installation tool. Figure 3-6b is a photograph of the completed anchorage system.

(a) (b)

Figure 3-6: Epoxy anchoring components (a) and completed anchorage system (b)

Once all the required steps were completed, the tension test was conducted using the Baldwin. The result of that experiment was that the BFRP rod could not achieve a tension force above 3 kips without exhibiting slippage. Therefore, this anchor was deemed unacceptable. I think that this early failure could be attributed to the epoxy that was not strong enough as mentioned previously, and another factor could be that the epoxy was not distributed uniformly around the BFRP rod during its injection within the anchor.

3.5 Steel pipe with expansive mortar

The other anchoring system proposed consisted of a steel pipe and expansive mortar. It was inspired by the BFRP manufacturer, V-ROD, as this was the method they followed for tensile testing of their BFRP rods, as described in the CSA S806 Annex C and Annex B of the Canadian Standards Association (CSA, 2002). In these types of anchors, they use a steel pipe where they bond the FRP bar with a resin and sand mixture filling. However, the V-ROD company instead used an expansive mortar that when it expanded and due to the confined space between the BFRP rod and the steel sleeve, creates an internal pressure inside the steel sleeve. This pressure provides significant friction between the BFRP, the mortar, and the sleeve, preventing the bar from slipping (Alraie et al., 2021). V-ROD recommended a different expansive mortar brand for their tensile test.

It was decided to choose the brand DEXPAN, as it was readily available in Oklahoma.

The same procedure described in Section 3.3 was followed. However, instead of using the HILTI epoxy, the expansive mortar was used. The expansive mortar also needed at least 24 hours to cure. Because the expansive mortar is more flowable than the epoxy, the edge of the steel sleeve was taped to prevent leakage during the pouring. The anchor was fabricated by inserting the BFRP rod inside the 1/8-in. wall thickness and 10-in.-long steel pipe. It was centered using 5/8-in.-diameter washers placed inside the steel pipe. The first anchor was placed vertically and fixed at the bottom with two pieces of plywood held by two steel clamps, as shown in Figure 3-7a.

The expansive mortar was poured vertically from the top through the space between the BFRP rod and the steel pipe. Once the expansive mortar cured for 24 hours, the set up was turned upside down and the next anchor could be installed by following the same procedure.

After curing of the expansive mortar, washers were welded to the steel pipe where the specimen would bear on the top and bottom flanges of the test setup. Two completed specimens are shown in Figure 3-7b.

(a) **(b)**

Figure 3-7: Specimens after pouring 2 anchors (a) and after pouring second set (b)

To make the expansive mortar, the DEXPAN cement had to be mixed with cold water. This type of expansive mortar is used in the industry for concrete demolition and rock breaking. The mix design ratio recommended in the company literature is 11 lb of DEXPAN powder for 0.4 gallons of water. For the pouring of one anchor, it was mixed at a ratio 0.44 lb of DEXPAN powder to 60 ml of cold water using a plastic container.

After all those steps were realized, the tension test was conducted using the Baldwin. The two BFRP rods were tested to a maximum load of 23 kips. The rate of the testing was controlled manually, and the load was increased slowly. They could have been tensioned to more than 23 kips, but because the steel test frame started to experience noticeable bending, the testing was stopped. The result of that experience was satisfying, because this anchor is suitable for the research, since 23 kips is larger than the objective of 20 kips.

3.6 Steel pipe with expansive mortar for prestressing application

Although the anchoring system using the expansive mortar was found suitable, for the beam prestressing application, an issue considering the casting of those anchors was raised. Indeed, pouring the expansive mortar vertically when the BFRP rebar was inserted in the prestressing frame is problematic. By pouring the expansive mortar vertically, it requires that all the prestressing setup will need to be in a vertical position, enabling the mortar to flow inside the anchor.

Thus, a solution was developed to remedy this problem. It consisted of drilling a 3/8-in.-diameter hole in the middle top of the steel pipe. Hence, the expansive mortar would flow uniformly by gravity from the top of the anchor down to all the spaces remaining inside. By this manner, the beam prestressing setup can remain horizontal. To verify the homogeneity of the mortar inside of the steel sleeve, an anchor was fabricated in this manner and then sectioned to expose the inside.

A photograph of the anchor when it was poured, Figure 3-8a, and after sectioning, Figure 3-8b, reveals complete filling of the annular space within the tube with expansive mortar.

As a consequence, pouring from the top through the drilled hole would not affect the homogeneity of the mortar around the rebar, and this method was used to cast the anchors in the prestressing setup.

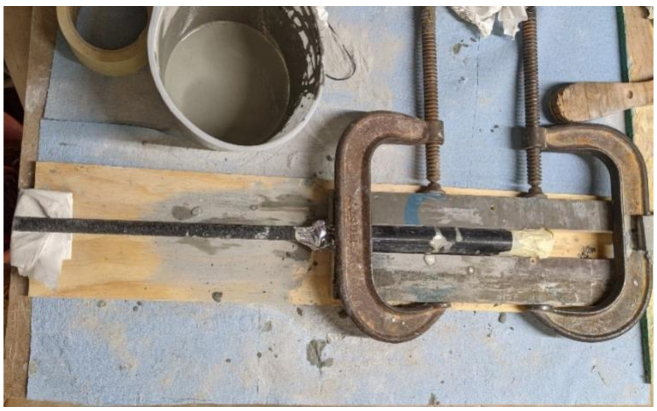

(a) **(b)**

Figure 3-8: Anchoring pouring setup (a) and sectioned anchor (b)

3.7 Conclusion

To conclude, the first experiment using the steel chuck gave a reasonably high- tension force of 15 kips before slipping. However, this anchoring system could not reach 20 kips for the application of this research. The next type of anchor tested using a steel tube and the HILTI epoxy was also unsuccessful because it reached a tension load of only 3 kips, which is very low compared to the required 20 kips. As a result, this anchor was not suitable. A stronger epoxy might have been successful but was not pursued.

Finally, the steel tube anchor using the expansive mortar was successful, since the goal of 20 kips was reached and surpassed by reaching a tension force of 23 kips. A modified procedure was also developed so than the anchors could be installed in a horizontal position, which was necessary for the beam prestressing application. As a consequence, the last anchor with the expansive mortar was used to prestress the BFRP concrete beams. Table 3-1 gather all the results from the tensile test of each anchor specimen. All the results were read from the manual gauge of the Baldwin.

Table 3-1: Results of the tensile test of all anchors tested

Anchoring System	Load before slippage
Traditional steel strand chuck	15 kips
Steel pipe with HILTI epoxy	3 kips
Steel pipe with expansive mortar number 1	> 23 kips
Steel pipe with expansive mortar number 2	> 23 kips

4. DESIGN AND FABRICATION OF THE PRESTRESSED AND NONPRESTRESSED BFRP CONCRETE BEAMS

4.1 Introduction and objectives

The development of a suitable anchoring system was accomplished, as discussed in Chapter 3, enabling the tensioning of the BFRP rod to the required load without damaging it. The next step of this research consisted of fabricating prestressed and nonprestressed BFRP concrete beams. In order to compare the efficacy of prestressing BFRP concrete beams, a nonprestressed BFRP concrete beam had to be fabricated. In this process, the design of a suitable cross section, as well as the method to fabricate and prestress the BFRP concrete beam was developed and discussed in this chapter. For this research, the main objectives consisted of building three similar prestressed and nonprestressed BFRP concrete beams. Building those two types of beams will provide information enabling the comparison of prestressed and nonprestressed BFRP members. A total of six beams, with three prestressed BFRP concrete and three nonprestressed BFRP concrete beams were fabricated. Measurements of the strain at the level of the BFRP rod with the demountable mechanical strain gage enabled to determine prestress losses occurring over time, as well as the transfer length. Prestress losses and transfer length were taken to assess the properties of the prestressed BFRP concrete beams.

4.2 Design of the cross section

4.2.1 Introduction

The design of the cross section was based on the ACI 318-19 code (ACI Committee 318, 2019) for the concrete reinforcement design, and the ACI 440-1R (ACI committee 440, 2015) and

ACI 440-4R-04 (ACI Committee 440, 2004) guides, which provide guidance for the design of FRP material in general. All calculations for the design of the different types of beams are provided in Appendices A, B, C and D. Since the beam length was restricted to a maximum length of 5 ft. due to the existing prestressing frame, the cross section needed to be smaller in comparison. Furthermore, the prestressing frame can accommodate a section with a width no larger than 8 in. The prestressing frame also has only one hole, so only one BFRP rod could be tensioned. Those constraints guided the design toward a beam cross section of 4 in. wide by 6 in. deep. These beams had shear reinforcement, consisting of No.3 steel rebar with a yield strength of 60 ksi. A No.4 steel rebar was used at the top of the section to hold those stirrups as well as providing tensile strength for the concrete in tension during prestressing release. Finally, a No.4 BFRP rod was used in the bottom of the beam in the tension zone, and depending of the type of beam, was pretensioned or not.

4.2.2 The BFRP nonprestressed beam

The nonprestressed beam had the same cross section as the prestressed beam. The calculation of the flexural strength of this beam is presented in Appendix A. The result of the calculation using the strain compatibility method gave a nominal moment capacity of 111.8 kip-in. The BFRP rod and the No.4 steel rebar used at the compression zone are located at 1.41 in. from the bottom and top fiber, respectively, of the concrete cross section. This distance was selected to take into account the No. 3 stirrup, as well as the concrete cover taken as ¾ in., which is the minimum recommended by the ACI 318-19 code (ACI Committee 318, 2019).

The goal was to bring the beam to a flexural failure. In order to attain this objective, the beam had to be over reinforced for shear to avoid shear failure. Concerning the shear design, calculations are presented in Appendix C. The beam was to be subjected to three point loading arrangement, with one point load situated at the midspan and the other two, representing the reactions, situated at the supports. As a consequence, the shear reinforcement was designed to resist the shear force from the ultimate moment that would bring the beam to fail in flexure. The point load calculated was 7.4 kips, and the result of the shear reinforcement calculations for one No. 3 single leg stirrup, gave a required spacing of 8.11 in. However, for the design to meet the ACI 318-19 specification, as presented in table 9.7.6.2.1 (ACI Committee 318, 2019), the minimum required spacing had to be 2.29 in. To make the construction process easier, a spacing of 2.25 in. was chosen. Choosing a smaller spacing also helped to over reinforce the beam against shear failure. Another important result that helped over reinforce the shear capacity of the beam is the fact that during the fabrication of the stirrup, it was impossible to fabricate a single leg stirrup. Particularly because of the small space within the beam cross section. Indeed, to follow the stirrup reinforcement details in the ACI 318-19 Table 25.3.1 (ACI Committee 318, 2019), the embedment length for a 180° hook would be 2.5 in, thus, the two ends of the stirrup had to overlap, otherwise they will not fit inside the 6 in. deep cross section.

As a result, the shear reinforcement was fabricated as a No. 3 double leg stirrup. By choosing that, it is obvious that the beam has far greater strength in shear than in flexure, insuring the desired flexural failure. Two No. 3 lifting hooks were also added to attach to the overhead crane for transport. The final steel reinforcement design details are show in Figure 4-1.

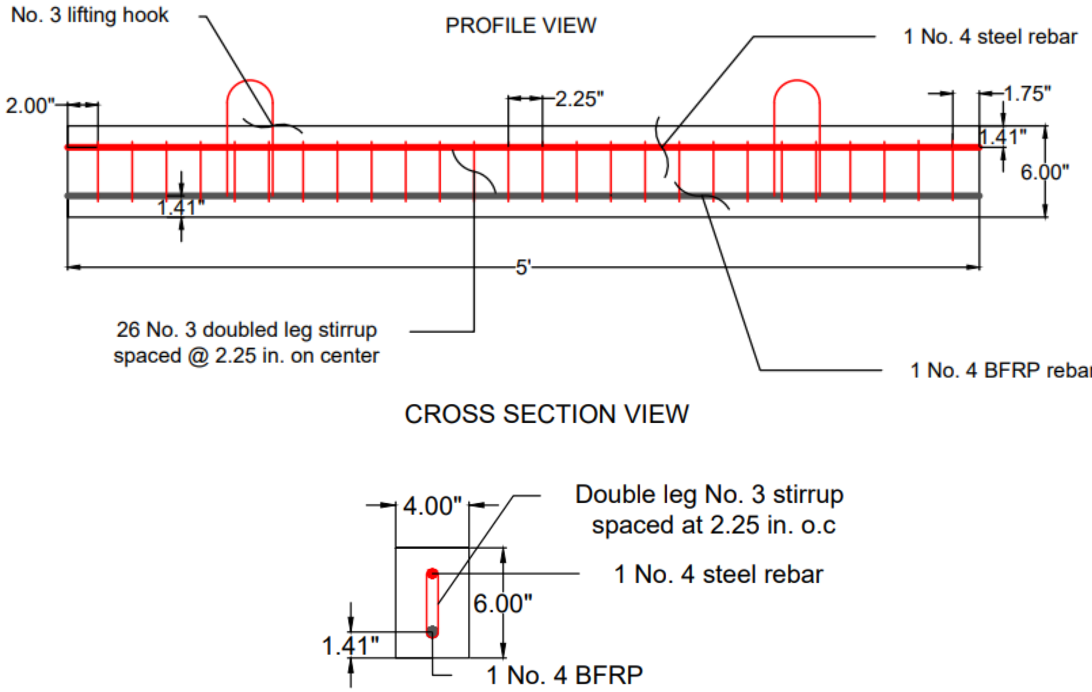

Figure 4-1: Reinforcement details for the nonprestressed BFRP concrete beam

4.2.3 The BFRP Prestressed beam

The prestressed beam had the same cross section as the nonprestressed beam. The calculation of the flexural strength of this beam is presented in Appendix B. The result of the calculation using the strain compatibility method gave a nominal moment capacity of 141.24 kip-in., which is greater than the nominal moment capacity calculated for the nonprestressed beam. Using the Zia et al., (1979) method, an estimation of the total prestress losses was calculated. The details can be found in Appendix B. By prestressing the BFRP rod to 20 kips, and after taking into account all the losses due to elastic shortening of the concrete, creep, shrinkage of the concrete and finally the relaxation of the BFRP rod, it was estimated that the effective prestressing force would be 17.37 kips, which is an approximate prestress loss of 13.15%. One of the main hypotheses is that the nominal moment capacity calculated is based on the effective prestress stress f_{se}. The effective stress is calculated by subtracting the prestress losses from the jacking stress f_j. Because those prestresses losses calculated are an approximation, the calculated nominal moment capacity is also an approximation but it could have been calculated using the measured prestress losses. Ideally, the prestressed losses should have been measured during testing day and the prestress losses could have been used to refine the estimated nominal moment of the prestressed BFRP concrete beams.

Regarding the shear strength, the same procedure was used as the nonprestressed beam, and all the details can be found in Appendix D. The point load calculated was 9.35 kips, and the result of the shear reinforcement for one No. 3 single leg stirrup gave a required spacing of 6 in. However, for the design to conform to the ACI 318-19 specification presented in Table 9.7.6.2.1, (ACI Committee, 2019), the minimum required spacing would have been 4.5 in. Indeed, for prestressed concrete, the shear reinforcement can be spaced farther apart than for nonprestressed concrete since the angle of the critical shear crack is less than 45°. A spacing of 4.5 in. was finally chosen, and because of the limited space within the cross section, a No. 3 double leg stirrup was used as was done for the nonprestressed beam. The final steel reinforcement design details are shown in Figure 4-2.

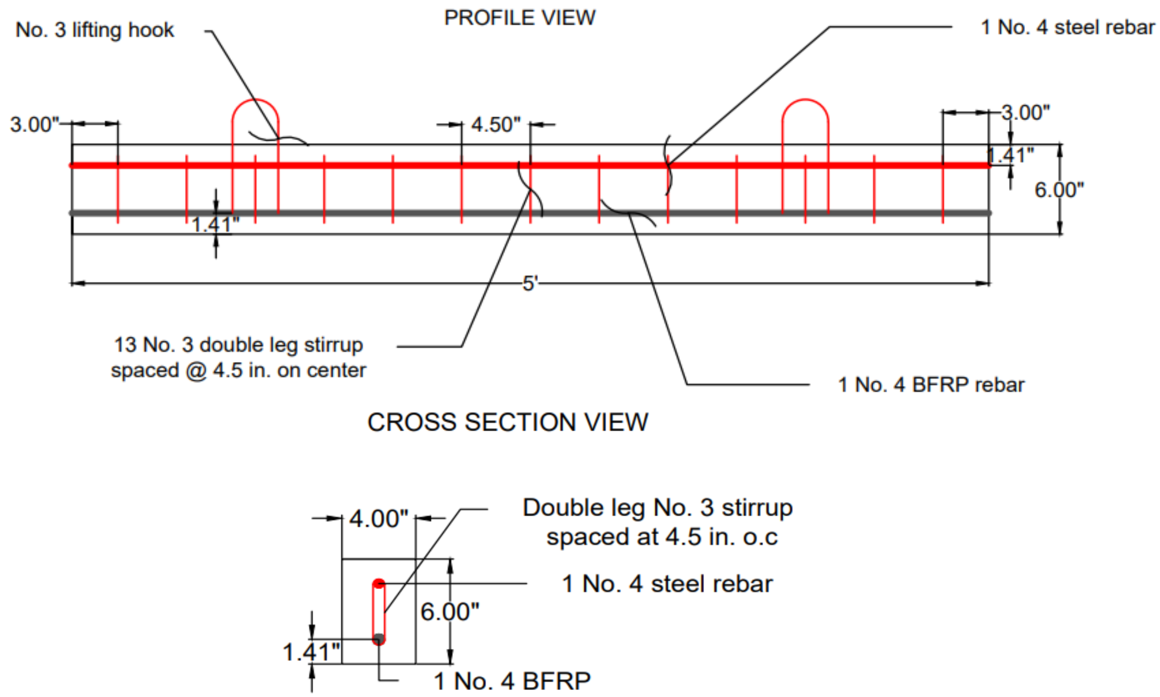

Figure 4-2: Reinforcement details for the prestressed BFRP concrete beam

4.3 Construction of the specimen formwork

4.3.1 Formwork for the nonprestressed beams

The formwork was designed to hold the fresh concrete of the beam to cure during the casting. Three 5-ft-long, ¾-in.-thick plywood were used to fabricate the formwork, as well as screws to hold the different parts of the formwork together. All elements constituting the formwork were predrilled to avoid splitting of the wood. The screws were drilled from the bottom of the wood planks, going through them as well as the two lateral wood planks. The completed form is in the shape of a "U" ready to welcome the concrete inside of it. To maintain a distance of 1.41 in. from the bottom for the BFRP rebar, a hole was drilled at both ends of the formwork located at 1.41 in. on center from the bottom. Thus, the BFRP rebar could be slid through it, keeping the eccentricity chosen and preventing any movement. The distance between the steel reinforcement from the top was maintained by tying it to the stirrups, so once the steel rebar was placed within the stirrup, it was positioned approximately at 1.41 in. from the top concrete fiber. A 6-ft-long BFRP rod was used as it didn't need to be longer since no anchors was used to tension it. After the pouring of the concrete, the extra 1 ft each bar was cut. Figure 4-3a shows the details of the formwork for the nonprestressed beam, as well as a photograph of the pieces prior to assembly (Figure 4-3b).

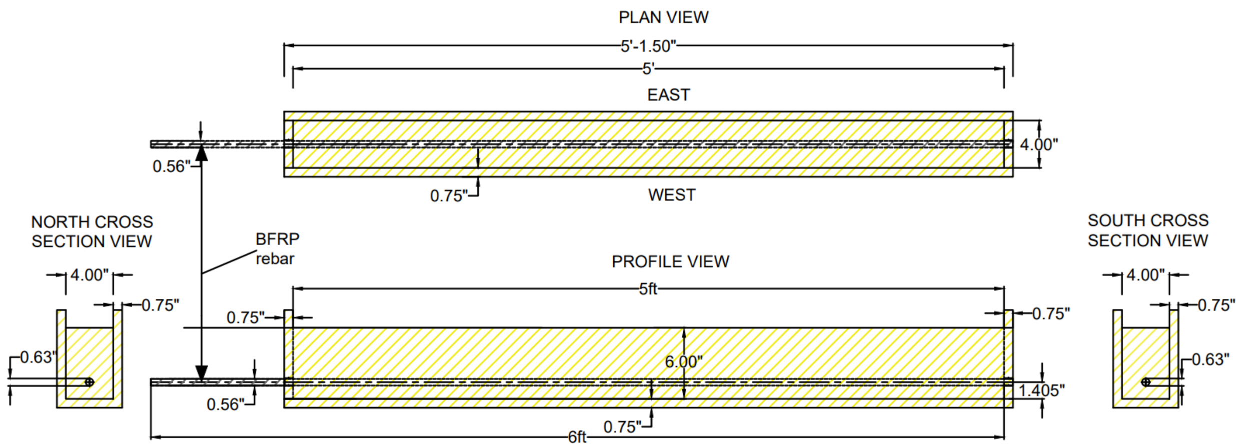

(a)

(b)

Figure 4-3: Blueprint of the Formwork for the nonprestressed BFRP concrete beam (a) and a photograph of the segments ready to be assembled (b)

4.3.2 Formwork for the prestressed beams

The formwork was designed to hold the beam to cure concrete during the casting. Three 5-ft-long, ¾-in.-thick plywood were used to make the formwork, as well as screws to hold the different parts of the formwork together. The wood planks were predrilled to avoid splitting of the wood. The difference in the formwork compared to the nonprestressed beam formwork is that four pieces of OSB were added to brace the formwork, with two along each edge. This was done mainly because the screws were drilled from the side of the two lateral wood planks forming the "U" and not from the bottom. The reason is because there was no room to remove the screws from the bottom as it was not possible to move the formwork while it was inside the prestressing steel frame. The other reason is because DEMEC points were used, and it was required to take measurements before the release of the prestress force, and to do that, the formwork containing the beam needed to be removed while the prestress force was yet to be released. The fabrication of the setup for the DEMEC points inside the formwork is discussed in Section 4.3.3. To maintain a distance of 1.41 in. from the bottom for the BFRP rebar, both ends of the formwork received one hole drilled at 1.41 in. on center from the bottom, similar to the formwork for the nonprestressed beam. Figure 4-4a shows the details of the formwork for the prestressed beam, as well as a photograph of the pieces prior to assembly (Figure 4-4b).

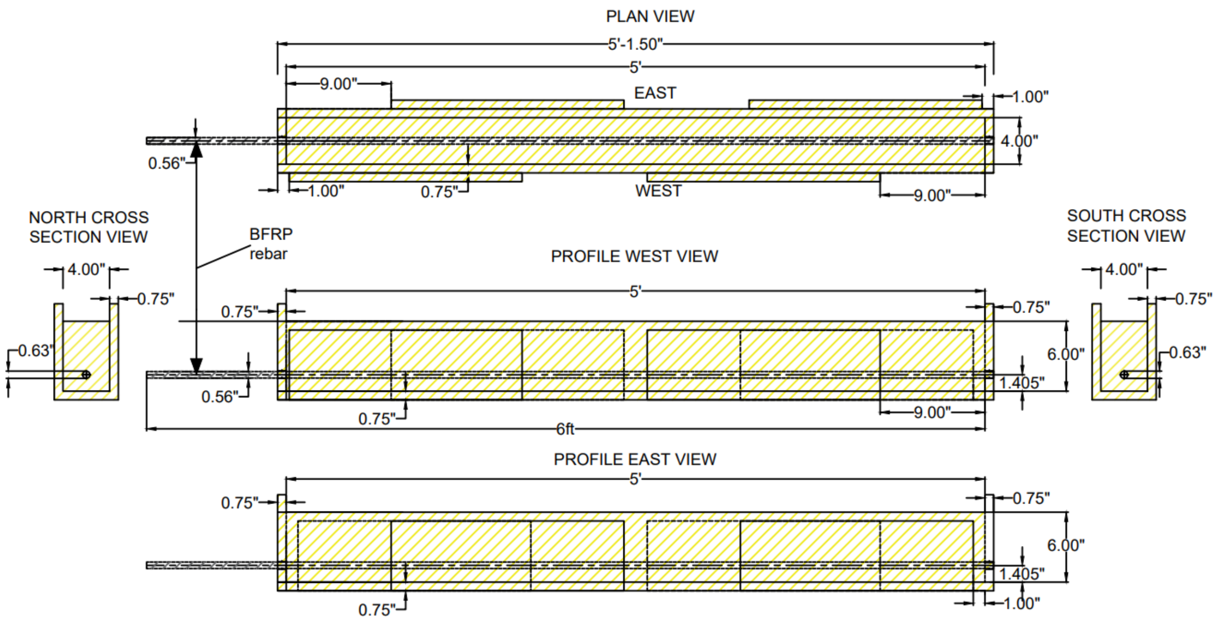

(a)

(b)

Figure 4-4: Formwork of the prestressed BFRP concrete beam (a) and a photograph of the segments ready to be assembled (b)

4.3.3 DEMEC points

In order to measure the prestress losses as well as the transfer length of the prestressed BFRP concrete beam, the distribution of the strain over time of the beam needed to be recorded. Thus, demountable mechanical strain gauge (DEMEC) points were used. Those points are assumed to be fixed in the beam, so when the beam shrinks or creeps, for example, the DEMEC points are also deforming following the deformation of the concrete. These DEMEC points were situated at the same level as the BFRP rod, so they can give information about the strain at the level of the tensioned BFRP rod. The DEMEC gauge consists of a standard dial gauge which is attached to an invar bar composed of two conical points mounted at each edge of the instrument. One of those conical points can move whereas the other one is fixed, and this pivoting movement is measured by the dial gauge. In Figure 4-5a a photograph of the box containing the standard dial gauge is shown, and the profile view of the dial gage is shown in Figure 4-5b.

(a) **(b)**

Figure 4-5: Box containing DEMEC dial gauge (a) and profile view of the dial gauge (b)

Each division of the dial gauge corresponds to 0.0784 microstrain according to the manufacturer's product literature. Two steel strips of ¼ in. thickness were predrilled to position nine 8-32 internal stainless-steel threads along the beam. They were staggered in the formwork on each side of the beam. With a length of 35.5 in each, they covered the full span of the beam. The two sides of the formwork were drilled from the inside so the steel strips would fit inside. Glue was used to make sure that the steel strips remain inside the carved wooden strip. The holes drilled in the steel strip were space at 100 mm from each other, which corresponds to 3.937 in. on center. The first hole was situated at 1.5 in. from the edge of the beam. Figure 4-6 is a photograph of the steel strip inserted inside the formwork as well as the DEMEC points inserted after predrilling the formwork from the outside.

Figure 4-6: Photograph of the steel strip mounted inside one side of the formwork pieces with the internal stainless-steel threads shown

When the formwork was assembled, the 8-32 internal stainless steel threads were fixed using a temporary hexagonal cap screw, and after the concrete was placed and cured, this temporary screw was removed so the formwork could be removed. Then a similar shorter screw having a small hole in the middle of the cap was inserted inside the stainless steel threads. With that screw, it was possible to use the invar bar composed of those two conical points. Figure 4-7 is a photograph of the stainless steel threads, the screw to read strain from the invar bar, and the temporary screw to fix the threads.

Figure 4-7: From the left to the right: stainless-steel threads, final screw used to read strain from gage, temporary screw

4.4 Fabrication of the reinforcing steel cage

4.4.1 Vertical reinforcement

The vertical reinforcement is composed of No. 3 double leg stirrups. For the 6 beams, a total of 117 stirrups needed to be fabricated. The stirrups were fabricated manually. At the beginning, it was complicated to get a consistent double leg stirrup of 4.5 in. deep from edge to edge because the bar had a tendency to slip in the bender when trying to get a 180° angle hook. The final solution was to use a pipe and a steel clamp to prevent the bar from moving, then insert the pipe along the bar, and rotate the pipe to bend the bar. These stirrups are not conventional since the inside bend diameter of the stirrup is less than the minimum of 6 times the bar diameter for a 180° hook, according to Table 25.3.1 in the ACI 318-19 code (ACI Committee, 2019). Also, the straight extensions were bent not in the same plane so they had to overlap in order to achieve the minimum straight extension length required by the code. Figure 4-8a is a photograph of the No. 3 rebar ready to be sectioned using the circle disc cutter. A photograph of the rebar being bent using a steel pipe is shown in Figure 4-8b, and a fabricated No. 3 double leg stirrup is shown in Figure 4-8c.

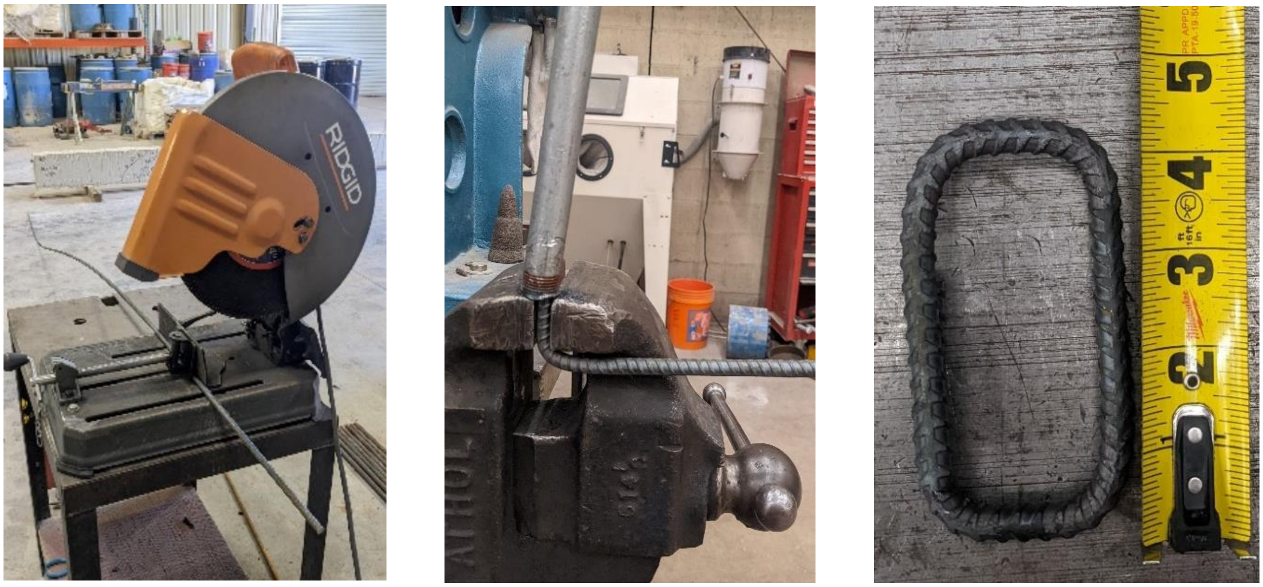

(a) **(b)** **(c)**

Figure 4-8: No. 3 rebar cut (a) then bent using a steel clamp and a pipe (b) and a completed No. 3 double-leg stirrup (c)

4.4.2 Longitudinal reinforcement

The longitudinal reinforcement consisted of two 5 ft lengths of rebar. The rebar located at the bottom was the No. 4 BFRP rod whereas the second rebar located at the top of the beam was a No. 4 steel rebar. For the prestressed beam, a 9 ft long BFRP rod was used to take into account the anchors, as well as the extra length required to fit inside the prestressing frame. For the nonprestressed beam, the BFRP rod used was 6 ft long. The reason is that the rod needed to be longer than the formwork in order to be properly positioned and secured at both ends.

4.4.3 Assembling the cage

To fabricate the six cages, longitudinal and vertical reinforcement needed to be assembled.

Two steel sawhorses were used, and the No. 4 longitudinal steel reinforcement was placed first. Then the No. 3 double leg stirrups were slid along the steel rebar and positioned according to the required spacing. Two ties were used to fix each stirrup to the No. 4 steel longitudinal rebar.

Once all the steel rebar ties were made, the cage was set inside the frame and the BFRP rod was slid through the two holes of the formwork. In order to have the set composed of the stirrups and the No. 4 steel rebar leveled, as well as enabling the bottom stirrup to be positioned around the BFRP rod, the cage was suspended in the form. Three plastic zip ties were attached to extra pieces of rebar supported by the top of the formwork. Afterward, two lifting hooks were fabricated and tied to the steel cage for each beam in order to facilitate movement of the specimens. Figure 4-9a is a photograph of the process of tying of the No. 3 double leg stirrups to the No. 4 longitudinal steel rebar. The set composed of the stirrups and the No. 4 steel rebar suspended in the form is shown in Figure 4-9b, and the fabricated cage inserted inside of the formwork is shown in Figure 4-9c.

(a)

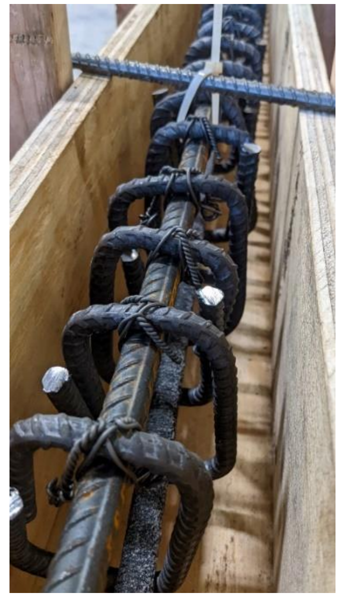

(b)

(c)

Figure 4-9: Tying of the cage (a), cage suspended on top of the formwork (b) as well as the fabricated cages inside their formwork (c)

4.5 Procedure for prestressing

For the prestressed BFRP beam, once the formwork and rebar cage were ready, they were inserted inside the steel prestressing frame. The steel frames are composed of two 2 in. thick plates and 4-HSS (2 x 1/4) sections welded together. Inside those two steels plate located at both ends, there are five holes. One is located in the middle with a diameter of 0.6 in., giving enough space for the BFRP rod to pass through. The other four holes were made to insert 8 threaded rods, four in both sides, to connect the steel frame to two other similar steel plates for anchoring and stressing the BFRP rod. Plate B is connected to the frame with four threaded bars going through Plate A. Twelve nuts completed the assembly. The first four nuts on the right of Plate A prevented the four threaded rods from moving during the prestressing procedure because the anchor was pushed against Plate B. As a result, four other nuts were inserted between Plates A and B preventing Plate B from moving. The last four nuts located behind Plate B are used just for safety in case it goes in the other direction. Figure 4-10 is a photograph of the dead end of the prestressing frame. The dead end is the end of the BFRP rod which is anchored in the prestressing frame whilst stressing takes place from the opposite (live) end.

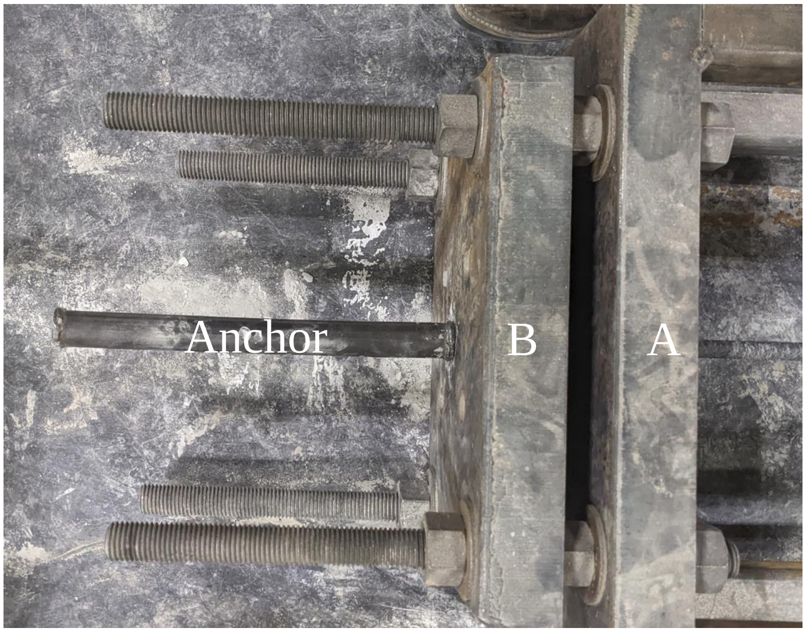

Figure 4-10: Dead end anchor in contact with the prestressing frame

On the other side, the part to tension the BFRP rod is more complex since mores plates are used in order to apply the prestressing force. The same setup for the dead end can be seen with

Plates A and B, but the only difference is that the last four nuts situated behind Plate B in the dead end set up were placed between Plates A and B. The reason is that during the prestressing process, Plate B will be able to slide along the 4 threaded rods running along Plates A and B. By sliding to the right in Figure 4-11, the anchor will be pushed to the right, creating a tension force along the BFRP rod which is fixed on the other side. To slide Plate B to the right, four threaded rods run through 4 inner holes of Plates B, C, and D. At plate C, two 200 kips hydraulic jacks were placed and supported on a rolling cart. Plate C has two side plates welded to it forming a "U" that will be in contact with Plate A during the prestressing process. The two hydraulic rams will push Plate D, applying tension to the four threaded rods secured behind Plate D with four nuts. A load cell was placed next to one of the hydraulic rams to measure the prestress force applied. To push evenly, a steel cylinder was added next to the other hydraulic ram, and two large washers were used to distribute the load to Plate D. A photograph of the free end with the hydraulic ram assembly is shown in Figure 4-11.

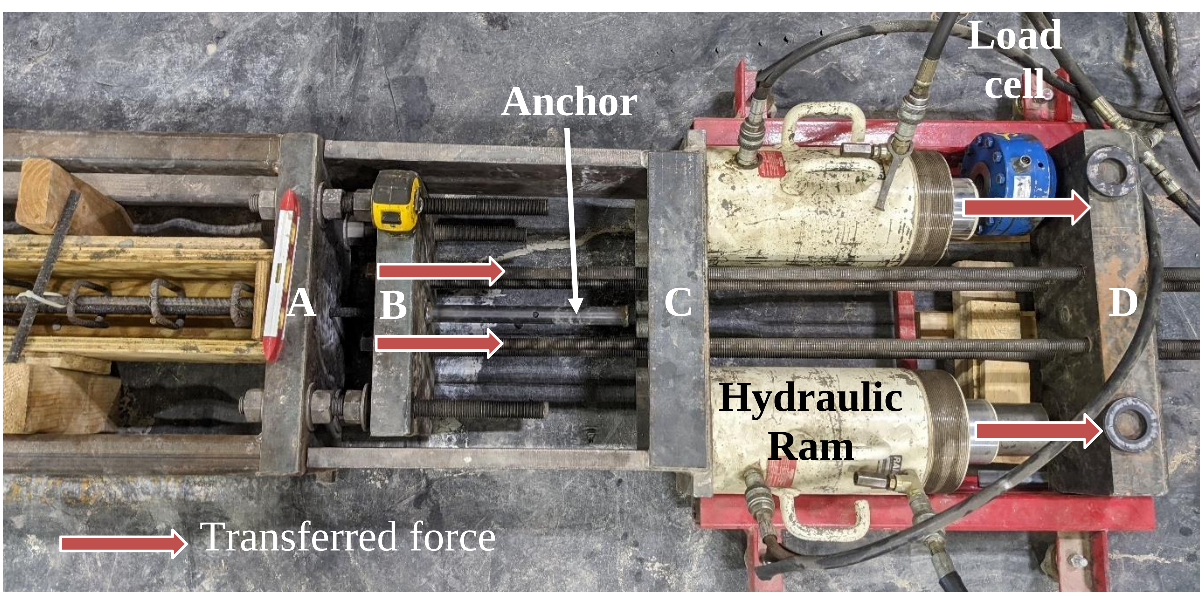

Figure 4-11: Ram assembly attachment

The red rolling cart will enable Plates C and D and the hydraulic rams to slide smoothly during the prestressing procedure. To sum up, the hydraulic rams will extend Plate D, pulling the long, inner threaded rods that are attached to Plate B. As Plate B extends outward, the anchor situated to the right of Plate B will be pulled, tensioning the BFRP rod. All the pieces were leveled to avoid bending the anchor.

The steel cage shown in Figure 4-12a was positioned to protect personnel as well as the computer connected to the load cell. Furthermore, two massive concrete blocks shown in Figure 4-12b were positioned behind the beam in case the BFRP rod failed during tensioning, which can be very dangerous due to the large amount of energy stored inside the rod that can be released suddenly. A red steel cage was also placed on top in case the BFRP rod fractured during tensioning and projected into the air, as shown in Figure 4-12b.

(a) **(b)**

Figure 4-12: Protections during prestressing

Before and after applying the prestress force, the distance between Plate A and Plate B was measured in order to evaluate the elongation of the BFRP rod. This was done as a secondary measure to confirm that the correct prestressing force was applied. Also, because two hydraulic rams were used, they needed to provide a force of compression of around 10 kips each one individually, so a sum of 20 kips will be transferred to the BFRP rod.

4.6 Concrete mix design

The concrete mix design is shown in Table 3-1. This mix design was developed to achieve a 28-day compressive strength of 10,000 psi and a one to two days compressive strength of 6,000 psi to facilitate release of the prestressing force. Several trial mixes were performed to arrive at the final mix design shown in Table 3-1. The strength gain versus time is shown in Figure 4-13.

Table 4-1: Concrete mix design

Material	**Amount**
Aggregate 5/8’’	1554 lb/yd^3
Sand	1554 lb/yd^3
Cement Type I-2	893 lb/yd^3
Water	268 lb/yd^3
High-Range-Water-Reducer	207 ml/ (100 lb/yd^3) cement
Water/Cement ratio	0.30
Fresh Concrete Properties	
Ambient Temperature	65 °F
Mix Temperature	72 °F
Unit Weight	150.74 lb/ft^3

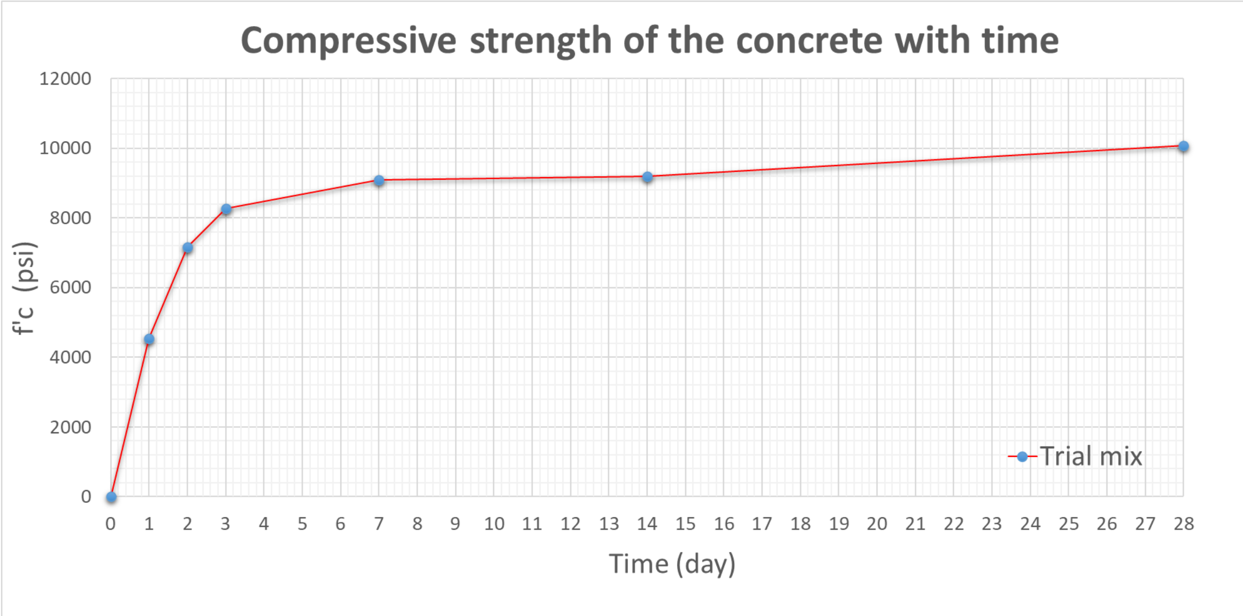

Figure 4-13: Plot of compressive strength versus time for the trial mix

4.7 Anchor correction

During the tensioning of the first prestressed BFRP concrete beam, the anchor resisted the required stress. However, it was noticed that the anchor bent slightly when the prestressing force reached 20 kips. At this stage of the process, everything worked well. However, during the tensioning of the second prestressed BFRP concrete beam, when the prestress force reached 15 kips, the anchor started bending, and at around 17 kips, the anchor failed and it was impossible to tension the BFRP rod. The anchor bent, and one of the hypotheses attributed to that failure was that the set up was not well leveled as well as the hole drilled to pour the expansive concrete was bigger the second time (0.75 in. diameter instead of 0.375 in.). As a result, during the tensioning, the anchor was not pulled straight and because of the reduction of the circular section with a bigger hole, the anchor failed by flexure. On the other hand, the anchor could possibly have buckled. It was chosen to investigate the first option, hence all the set up was disassembled and assembled again to make sure that everything was leveled, even the plywood supporting the framework. Afterward, another attempt was made with the same anchor used for the first prestressed beam with a hole diameter of 0.375 in. During the tensioning, the anchor was bending slowly as the load increased, and failed again around 19 kips. At this point, it was decided to investigate the second option.

The anchor was considered first as a hollow steel column, and as shown in Appendix E, the calculation of the buckling load was determined. The column was considered free at one end and fixed at the other end, where the anchor was in contact with Plate B. The steel yield strength was assumed to be 35 ksi, which is the minimum for steel pipes in general. The result of the calculation gave a buckling load of 4.4 kips using the ASD and 6.57 kips using LRFD including the safety factors, which is considerably less than 20 kips. However, the resistance of the grout was not considered in the calculation. If it was, it will add a significant compression resistance to the anchor. Nevertheless, compared with a steel pipe having a wall thickness two times larger results in an available critical buckling load of 20.34 kips for ASD design and 31.27 kips for LRFD design, which is larger than the required 20 kips.

As a result, switching to an anchor having a wall thickness two times larger was conservative since in those calculations it can be expected for the anchor in general to have more resistance because the resistance of the expansive cement. At the end, it was decided to try a ¼ in. wall thickness pipe. After pouring those anchors, which were heavier, support at their edge was added to avoid bending the BFRP rod when casting the anchor. During the tensioning, those anchors performed well, with no sign of buckling at 20 kips, and fabrication of the second and third BFRP prestressed concrete beams could proceed.

As a conclusion, the reason for the failure of the anchor was buckling, and the first anchor was fortunate to have resisted 20 kips. Figure 4-14a is a photograph of the two anchors that failed, and next to it in Figure 4-14b is the new successful anchor used for the last two prestressed BFRP concrete beams.

(a)

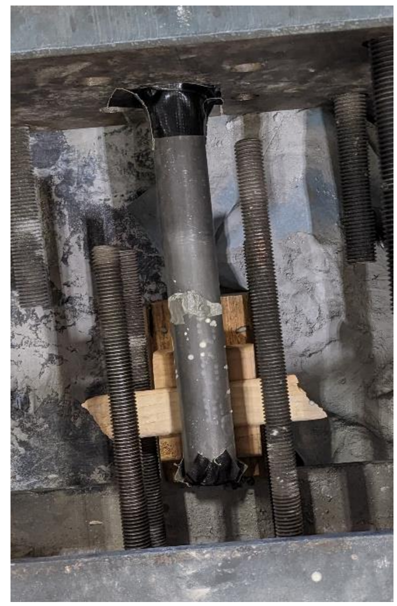

(b)

Figure 4-14: The two anchors with 1/8 in. wall thickness which failed (a) and the successful 1/4 in. wall thickness anchor (b)

5. ANALYSIS OF TEST RESULTS

5.1 Introduction

In this chapter, the results of the measurements and the testing of the BFRP prestressed and nonprestressed beams are presented. An analysis of all those results will enable the understanding of the behavior of the prestressed concrete beams reinforced with the BFRP rods. The first section presents and discusses the results of the concrete strength for each mix. Afterward, the results of the DEMEC point readings as well as the strand end slip are presented and discussed to evaluate the transfer length of the prestressed BFRP rods. The following section presents the prestress losses over time and compares them to the anticipated prestress losses. Finally, the last section presents how the testing of the BFRP beams was conducted, then the results were analyzed and compared to the calculations made which predicted the strength of the sections.

5.2 Concrete mix design results

Three sets of beams were fabricated, and in each set of beams, they included one prestressed and one nonprestressed BFRP beam. For each set of beams, the concrete was mixed according to the testing mix design presented in Chapter 4. Each mix volume was set to be 3.5 ft^3 so there was enough concrete for the two beams as well as a number of concrete compressive strength specimens. Thus, the compressive strength of the concrete could be tested at different times so the release of the prestress force could be closer to the interval set of $0.6f'_c$-$0.7f'_c$. A total of twenty-four cylindrical specimens were made for each mix to determine the compressive strength of the concrete at 1 day, before prestress release, at prestress release, and at 3 days, 7 days, 14 days, 28 days, and beam specimen test day. All of the compressive strength data is plotted in Figure 5-1.

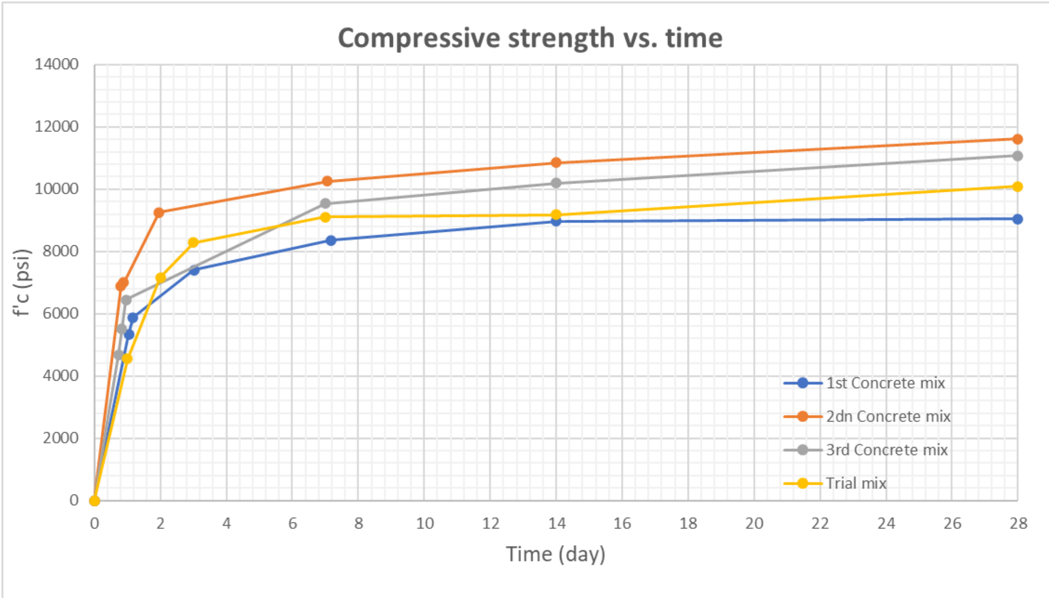

Figure 5-1: Plot of compressive strength versus time for all concrete mix

All the data related to the compressive strength of the concrete for each mix can be found in Appendix G. In Figure 5-1, it can be noticed that the target compressive strength of the concrete was close to the 10,000 psi target strength, varying from 9,039 psi for Mix 1 to a maximum of 11,605 psi for Mix 2, which were close to the trial mix, which provided a result at 28 days of 10,085 psi, closer to the target compressive strength. The results are well within normal variations between concrete mix designs. The actual compressive strength test results were used to revise the section capacity calculations of the beams afterward.

A concrete slump flow test was also conducted to check the workability of the concrete mix by following ASTM C 1611/1611M-14 (2014). The results of the concrete slump flow are shown in the Table 5-1, and a photograph of the slump test for the 3rd concrete mix is shown in Figure 5-2.

Table 5-1: Slump flow results

Concrete mix	Concrete Slump flow
Testing mix	25 in
1st concrete mix	26 in
2nd concrete mix	18 in
3rd concrete mix	27 in

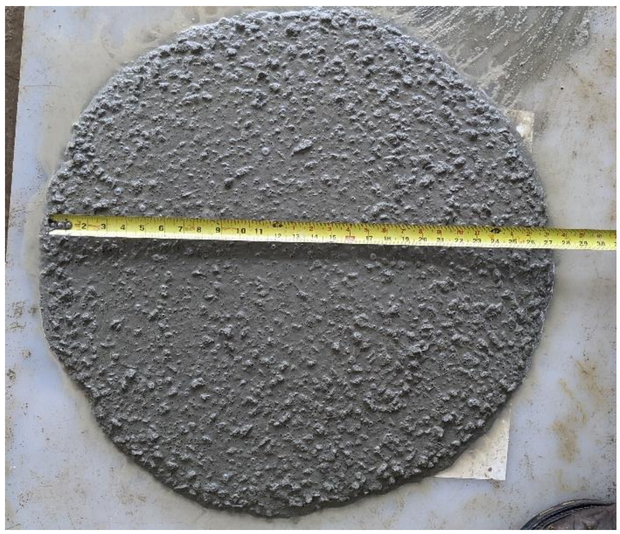

Figure 5-2: Slump flow test for 3rd concrete mix (slump flow =27 in)

The concrete slump flow was more than 18 in., which indicates that the concrete was flowable and self-consolidating, thus it did not need to be mechanically vibrated. According to table X1.1 in ASTM C 1611/1611 M-14 (2014), the Visual Stability Index Value (VSI) was equal to 0 for each of the mixes, which means that they was no evidence of segregation or bleeding of the concrete.

5.3 Prestress release results

During the tensioning of the BFRP rods, the prestress force of 20 kips was the objective, but in practice it is not easy to aim precisely for the prestress force target. The instantaneous prestress losses due to the prestress steel frame elastic shortening and due to the slippage of the BFRP rod occurs. To reach 20 kips prestress force, it is necessary to prestress the BFRP rod to more than 20 kips so the prestress losses can be accounted for and the final tension force will be as close as possible to 20 kips. However, during the tensioning of the BFRP rods, for safety purposes, it was decided to tolerate a prestress force within the interval of 19 to 21 kips, which is within 5% of the desired prestress force. Something important to note is that because they were two hydraulic rams, the tension force imposed on the BFRP rod was two times the jacking force measured. As a consequence, the ideal jacking force needed to be 10 kips. Figure 5-3 is a plot of the load on the instrumented ram vs. time during tensioning of the 1st prestressed beam (PB1).

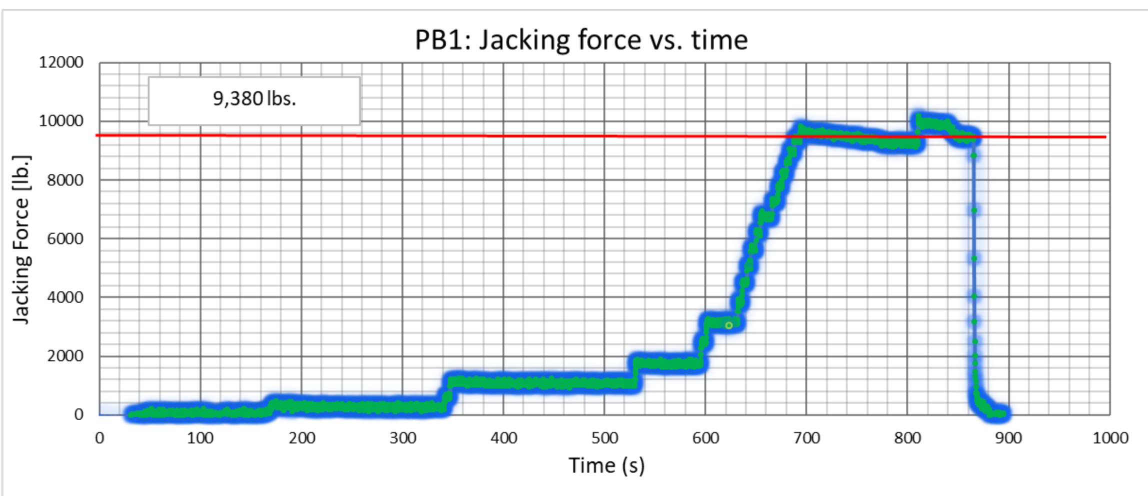

Figure 5-3: Jacking force vs. time for the 1st prestressed BFRP concrete beam (PB1)

When the BFRP rod was tensioned to 20 kips, the bolts were tightened to prevent the anchors of the BFRP rod from slipping. Once the BFRP rod was tensioned and secured, the forces from the hydraulic rams were backed off. In Figure 5-3, it can be observed that after reaching a plateau around 10 kips, the jacking force dropped to 0 kips, which corresponded to the backing off of the hydraulic rams. The last point in this plateau before the sudden decrease of the jacking force was the last tension force number corresponding to one half of the final prestress force. A red line shows the finale tension force of 9,380 lb, which corresponds to 18,760 lb for the prestress force. This jacking force was used to revise the prestress losses as well as the section strength of the prestressed beam. All the jacking force vs. time plots are provided in Appendix F. Table 5-2 summarizes the results of the prestress force for each BFRP prestressed specimen.

Table 5-2: Prestress force for each prestressed beam

Prestressed BFRP beams	Jacking force	Relative error compared to 20 kips
PB1	18.760 kips	6.2 %
PB2	19.218 kips	3.9 %
PB3	19.196 kips	4.0 %

From Table 5-2, it can be noticed that PB1 failed to stay within 5% of the target prestress force of 20 kips, with a relative error of 6.2 %. However, this difference was still reasonable so it was decided to still exploit the results of PB1 afterward. PB2 and PB3 were inside the 5% margin.

5.4 Transfer Length

5.4.1 Method of measuring strain with DEMEC points

Approximately 24 hours after BFRP prestressed beams were cast, the framework was removed, and DEMEC target points were placed along the side faces of the end regions of the beam immediately. DEMEC point readings were measured before the release of the prestress force. Once the prestress force was released, a series of measurements were effectuated, right after the release of the prestress, then at 24 hours, 7 days, 14 days and 28 days after the prestress release. Each DEMEC point was fixed and numbered from 1 to 9. The invar bar can measure microstrains between 3 DEMEC points, so the strain between target points 1 and 3, then 2 and 4, and following this series until target points 7 and 9 were measured from the dead end and from the live end.

The same operator performed all the measurements, and the gauge was kept as centered as possible when making the readings. The average of three measurements was taken from each reading because the gauge was very sensitive to any vibration or movement. All those steps were done to get consistent results. A total of 756 readings were measured for the 3 prestressed beams. The first readings done before prestress release calibrated set the baseline for subsequent strain values after release of the prestress to the concrete. Those initial readings were subtracted from the DEMEC readings on the given day the measurements were taken. This difference in DEMEC reading was then multiplied by the calibration factor of 7.84 microstrain by division, which can be found in the manufacturer's literature, to convert the DEMEC number into microstrain. Figure 5-4 is a photograph showing the measurement of DEMEC values.

Figure 5-4: DEMEC measurements

5.4.2 95% Average Maximum Strain method

The 95% Average Maximum Strain (AMS) method is a common method used to evaluate the transfer length of prestressing strands (Andrawes, B. et al, 2009). This method was used to evaluate the transfer length for BFRP rod. Relying on the theory of strain compatibility between the rebar and the concrete, the ACI 318-19 Code (2019) describes the transfer length for pretensioned members as the embedded length of the pretensioned strand required to transfer the effective prestress force to concrete by bond. This method used a three point moving average, thus the raw strain profiles can be smoothened to obtain a realistic strain distribution. Where ε_{i-1}, ε_i, and ε_{i+1} are the recorded strains at the i-1-th, i-th and i+1-th gauge, the expression to calculate the average strain at the i-th point is shown in equation (5-1) (Andrawes, B. et al, 2009):

$$\boldsymbol{\varepsilon'_i = \frac{\varepsilon_{i-1} + \varepsilon_i + \varepsilon_{i+1}}{3}} \qquad (\mathbf{5\text{-}1})$$

Afterward, the plot of the microstrain vs. the distance from the end of the beam considered was plotted. The marking line of the 95% maximum average strain was added on the plot, and the first intersection with this line and the graph from the end of the beam was considered as the transfer length. Inconsistent or potentially suspect data was removed from the graph. For instance, in prestressed beam number 2 (PB2), the reading of the strain between target points 5 and 7 remained constant at zero microstrain at all times. This was probably because the two target points were prevented from moving due to the stirrup or some other extraneous factor.

In Appendix H, all the results from the DEMEC points measurements as well as the plot of the strain vs. its position along the beam at different times were plotted. For prestressed beam number 3 (PB3), Figure 5-5a shown its plotted graph without the 95% average smoothing followed by Figure 5-5b with the graph with the 95% average smoothing method. In Figure 5-5b, it can be seen than the strain curve was smoothed with a plateau that was straighter than the raw strain vs. position plot in Figure 5-5a.

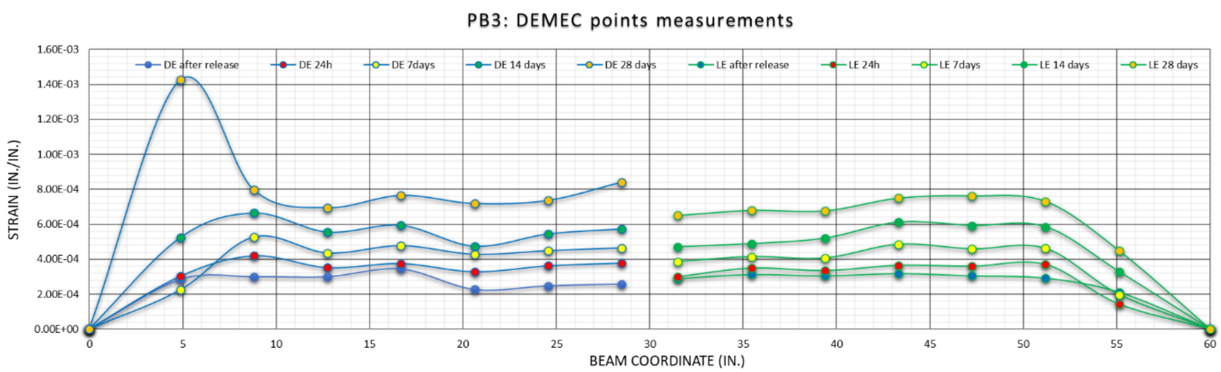

(a)

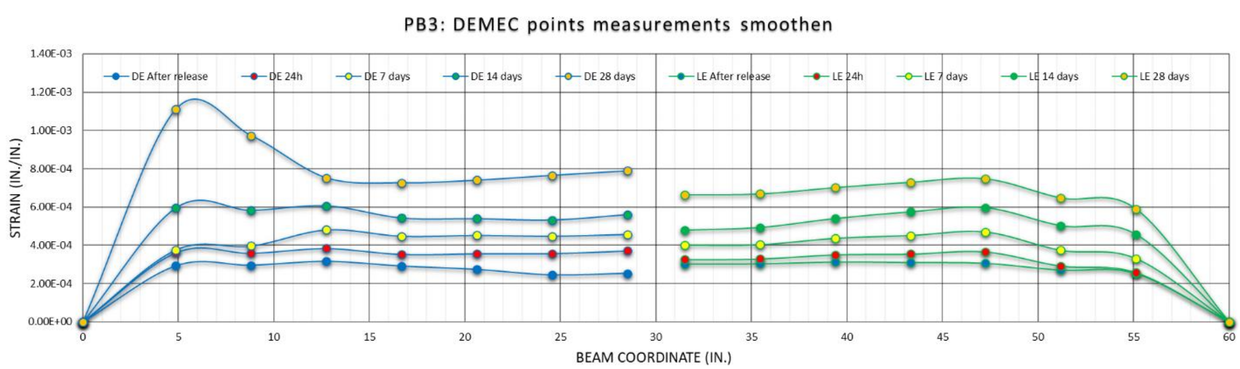

Figure 5-5: Nonsmoothed DEMEC points measurements (a), smoothed DEMEC points measurements (b)

As a consequence, the smoothing procedure was effective. After plotting strain vs. position, the 95% average method was used, and the intersection between the graph and the line representing 95% of the maximum strain in the plateau, corresponded to the transfer length (L_t). This method was used for PB1, PB2, and PB3. Figure 5-6 shows how the procedure to evaluate the transfer length using the 95% average method for PB1 at the dead end was performed. A transfer length of 15.3 in. was found for PB1 after prestress release.

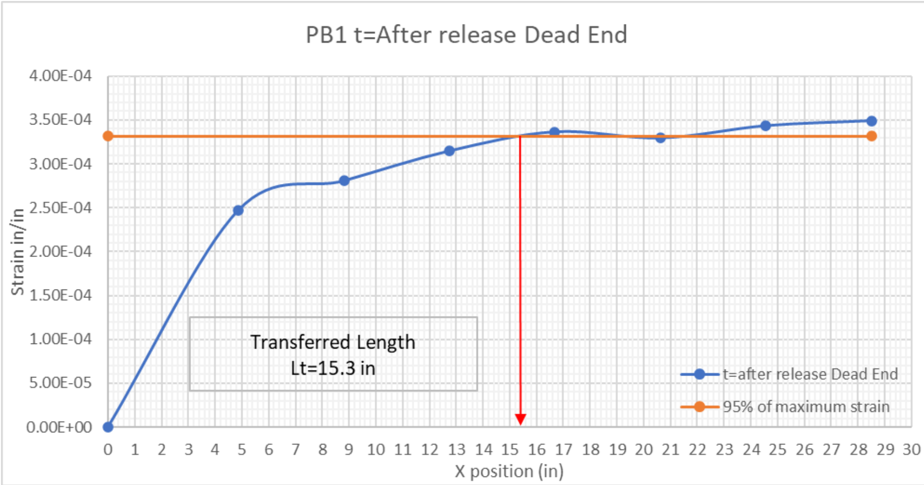

Figure 5-6: 95% average maximum strain method for PB1 from the dead end at the time of prestress release

The results of the transfer length measurements using the plotted data for the 95% average maximum strain method are presented in Table 5-3.

Table 5-3: Transfer length calculated using 95% average maximum strain method

Transfer length (in.)	**PB1**		**PB2**		**PB3**	
Time	Dead End	Live End	Dead End	Live End	Dead End	Live End
After release	15.3	11.2	12.4	4	5	11.5
24 h	18.8	12.6	12	4.2	4.8	11.5
7 days	25.5	20.4	10.5	4.5	5	11.4
14 days	12	4.4	13	4.4	4.6	11.2
28 days	15	4.2	16	4.5	4.5	11
Average	**17.32**	**10.56**	**12.78**	**4.32**	**4.78**	**11.32**

It can be observed that the transfer length results vary from a minimum of 4.32 in. to a maximum of 17.32 in., which indicates that the results were highly variable both between the dead and live ends and between each specimen. The average transfer length regardless of the end considered was 10.18 in. Values of transfer length in Table 5-3 in red seems way more offset from the other values measured, thus they could be attributed to a wrong measurement.

5.4.3 28 day period average strain method

In this research, another method of evaluating the transfer length was proposed. This method is not proposed in the literature and it consisted of averaging all the strain at each different time it was measured to plot the graph of the strain vs. the position. Afterward, a line averaging all the points that formed the plateau of the graph was drawn, and its intersection with the graph from the end of the beam is considered as the transfer length. Since the transfer length found by using the 95% average maximum strain method were fairly constant at each end during time, this new method would provide other results to analyze. This method provided only two curves to analyze, one at the dead end and the other one at the live end. The results of this method proposed in this research were compared with other transfer lengths and the literature in Section 5.4.6. The results of the transfer length using the graph for the 28 day average period for PB3 is shown in Figure 5-7.

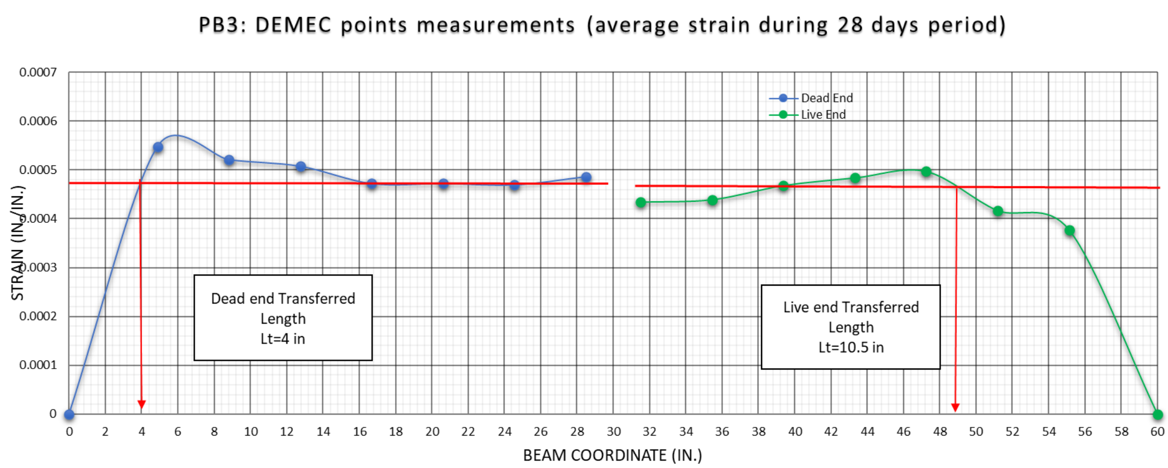

Figure 5-7: Strain vs. position along the beam graph and the transfer length found using the 28 day period average strain method

The graphs for all prestressed beams are presented in Appendix H. All the results of the transfer length measured using the plotted data for the 28 day average strain method are presented in Table 5-4.

Table 5-4: Transfer Length for all Prestressed beams using the 28 day period average

Transfer length (in.)	**PB1**		**PB2**		**PB3**	
Time	Dead End	Live End	Dead End	Live End	Dead End	Live End
28 day period average	**14**	**2**	**12.4**	**2.2**	**4**	**10.5**

It can be noticed in Table 5-4 that the transfer length varies from 2 in. to 14 in. and that the transfer length was not the same at the dead end and at the live end, which means that the dead end and the live end experience different behavior.

5.4.4 End slip method

Another method used to determine the transfer length was the end slip method. This method consists of measuring the elongation of the BFRP rod after releasing the prestress force. This method is based on relating the transfer length of the BFRP rod with the amount of slippage measured upon the release of the prestressing force. The slippage of the BFRP rod was measured using a manual gauge that is inserted inside a fixed metal clamp on the BFRP rod. The BFRP rod draw-in Δ_d is calculated by subtracting the change in the length of the BFRP rod in the stress transfer zone $\delta\varepsilon_b$ to the elastic shortening of the concrete in the stress transfer zone $\delta\varepsilon_c$ due to prestress release. The change of strain in the BFRP rod and in the concrete were assumed linear.

By integrating this difference in strains, the BFRP rod is draw-in Δ_d can be calculated by using the equation (2-6) presented by (Andrawes, B. et al, 2009) where the notations were adjusted for BFRP rod:

$$\boldsymbol{\Delta_d = \int_0^{L_t} (\Delta\varepsilon_b - \Delta\varepsilon_c)dx = \frac{f_{bi}}{\alpha E_b} L_t} \qquad (\mathbf{5\text{-}2})$$

In Equation 5-2, f_{bi} represents the initial stress at prestress release, E_b the Young modulus of BFRP rod, L_t the transfer length and α is the stress distribution constant equal to 2 for a constant stress distribution and 3 in case the stress distribution is linear. In general, the stress distribution is assumed to be 2, but for BFRP rod both possibilities were envisaged. As a result, the transfer length can be expressed as shown in Equation 5-3.

$$\boldsymbol{L_t = \frac{\alpha E_b \Delta_d}{f_{bi}}} \qquad (\mathbf{5\text{-}3})$$

All the calculated transfer length using the end slip method are shown in Table 5-5 and they were computed using Equation (5-3).

Table 5-5: Transfer length calculated using the end slip method

Transfer length (in.)	**PB1**	**PB2**	**PB3**
Time	Dead End	Dead End	Dead End
Jacking force (lb.)	18,760	19,218	19,196
f_{bi} (ksi)	84.13	86.18	86.08
Δd (in.)	0.030	0.035	0.035
Lt with α=2 (in.)	**6.20**	**7.07**	**7.08**
Lt with α=3 (in.)	**9.30**	**10.60**	**10.61**

The transfer length ranged from 6.2 in. to 10.61 in. and a difference of approximately 3 in. for the transfer length can be noted between the constant stress distribution and the linear stress distribution.

5.4.5 Analysis of the transfer lengths results

Six transfer length prediction equations from the literature (ACI committee 318, 2019) (Zia and Mostafa, 1997) (Cousins et al., 1990) (Shahawy, 1992) (Russel end Burns, 1996) (Mitchell et al.,1993) were chosen to be compared with the results found in this research. In Table 5-6, those equations are presented. The notation for the BFRP rod was taken into account instead of the strand for these equations.

Table 5-6: Transfer Length equations proposed by researchers

Source	Equation
Current ACI and AASHTO (2019)	$L_t = \frac{f_{be} d_b}{3}$
Zia and Mostafa (1997)	$L_t = 1.3 \frac{f_{bi} d_b}{f'_{ci}} - 2.3$
Cousins, Johnston and Zia (1990)	$L_t = \frac{0.5 U_t}{B} + \frac{f_{be} A_b}{\pi d_b U_t}$
Shahawy, Issa and Batchelor (1992)	$L_t = \frac{f_{bi} d_b}{3}$
Russell and Burns (1996)	$L_t = \frac{f_{be} d_b}{2}$
Mitchell, Cook, Khan and Tham (1993)	$L_t = \frac{f_{bi} d_b}{3} \sqrt{\frac{3}{f'_{ci}}}$

In Table 5-6, in order to calculate the transfer length based on the Cousins et al. equation (1990), the plastic bond stress, U_t and the slope of the elastic portion in the strain vs. position, B, needed to be determined. The effective prestress stress also needed to be computed, thus it was calculated using the prestress loss results from the DEMEC points at 28 day after prestress release, which can be found in Table 5.12.

To calculate the plastic bond stress, U_t, the 95% average maximum strain method plots were used to determine the different slope of the graph of strain vs. position at 28 day after prestress release. Figure 5-8 indicates the different zones, which are the plastic zone and the elastic zone in the graph of stress vs. distance from the end. These zones needed to be evaluated in order to find the bond stress, U_t, and the bond modulus, B.

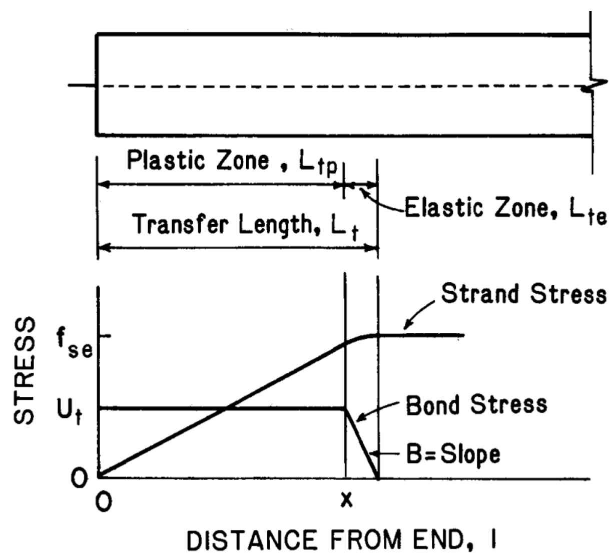

Figure 5-8: Assumptions of transfer length model (Cousins et al. 1990)

To find these parameters, the slope of the plastic zone as well as the elastic zone needed to be evaluated. Equation (5-4) provided by Cousins et al. (1990) was used to calculate the bond modulus once the bond stress, U_t, and the elastic length, L_{te}, were calculated.

$$L_{te} = \frac{U_t}{B} \qquad (5\text{-}4)$$

The DEMEC graphs plotted in Appendix H were used to find those lengths. Because these graphs represented the strain vs. position, by using Hooke's law, the strain was multiplied by the elastic modulus of the BFRP rod, E_b, to obtain a stress. To determine the position of the plastic zone and the elastic zone, points "a", "b" and "c" were used. Point "a" represent the position of the end of the beam which is always equal to zero. Point "b" represent the position corresponding to the end of the plastic zone, and point "c" represent the position of the end of the elastic zone. The plastic bond stress, U_t, and the bond modulus, B, were calculated for all the prestressed beams, and the results are presented in Table 5-7.

Table 5-7: Results of calculations of the plastic bond stress and the bond modulus

Prestressed beams		**PB1**			**PB2**			**PB3**	
Parameters	Position (in.)	Strain (in./in.)	Stress (psi)	Position (in.)	Strain (in./in.)	Stress (psi)	Position (in.)	Strain (in./in.)	Stress (psi)
a	0	0	0	0	0	0	0	0	0
b	4.87	0.00054	4731	4.87	0.00048	4185	5.00	0.00059	5140
c	15	0.00070	6092	16	0.00091	7886	11	0.00071	6187
Elastic length (in.)		10.13			11.13			6.00	
Plastic length (in.)		4.87			4.87			5.00	
Ut (psi)		**970.50**			**858.52**			**1028.02**	
B (psi/in.)		**95.85**			**77.17**			**171.34**	

Only the plot for the dead end for PB1 and PB2 and the live end for PB3 at 28 day after prestress release were used to evaluate the elastic and plastic length. The first reason is because the prestress losses were taken at 28 day after prestress release to calculate the transfer length. The second reason is because the graphs from the live end for PB1 and PB2 and the plot for the dead end for PB3 were unusable because the shape of the graph didn't display clearly the plastic and elastic zone, thus it was not possible to identify parameter "a"," b" and "c". In Table 5-7, the plastic bond stress varies from 858.5 psi to 1,028 psi and the bond modulus varies from 77.17 psi/in. to 171.34 psi/in., thus the results were highly variable.

The average of the prestress losses at each end could have been used to calculate the effective prestress stress but the prestress loss occurring at each end where U_t and B were evaluated was chosen instead. The jacking stress was computed using Table 5-2. By computing the equations shown in Table 5-6, the transfer lengths were calculated and are presented in Table 5-8. All the values of transfer length were compared to each method of calculation used previously. In Table 5-9, the comparison of the 95% average maximum strain method with the transfer length from the literature tabulated in Table 5-8 are shown.

Table 5-8: Transfer length calculated using equations from Table 5-6

Transferred lenght (in.)	**PB1**	**PB2**	**PB3**
Current ACI and AASHTO	14.56	14.61	14.91
Zia and Mostafa	8.12	6.67	7.41
Cousins, Johnston and Zia	5.073	5.574	3.010
Shahawy, Issa and Batchelor	15.70	16.09	16.07
Russel and Burns	21.83	21.92	22.37
Mitchell, Cook, Khan and Tham	11.22	10.53	10.96

Table 5-9: Relative error of the transfer length using the 95% average maximum strain method compared to the transfer length calculated from the literature

Lt (in.)	**PB1**		**PB2**		**PB3**		**Statistics**	
Method	Dead End	Live End	Dead End	Live End	Dead End	Live End	μ Means	σ Standard deviation
95% (ASM)	17.32	10.56	12.78	4.32	4.78	11.32	10.18	4.95
Current ACI and AASHTO	19.0%	27.5%	12.6%	70.4%	67.9%	24.1%	36.9%	26%
Zia and Mostafa	113.4%	67.6%	91.7%	35.2%	35.5%	52.7%	66%	32%
Cousins et al.	241.4%	108.2%	129.3%	22.5%	58.8%	276.1%	139%	100%
Shahawy et al.	10.3%	32.8%	20.6%	73.1%	70.3%	29.6%	39.4%	26%
Russel and Burns	20.7%	51.6%	41.7%	80.3%	78.6%	49.4%	53.7%	23%
Mitchell et al.	54.4%	5.9%	21.3%	59.0%	56.4%	3.3%	33.4%	26%

In Table 5-9, the method which provided the closest result is presented in green text, and the method which provided a transfer length that was the farthest from the results of the tests is presented in red text. It can be noticed that the transfer length suggested by the ACI and AASHTO codes and by Shahawy et al. (1992) were also close to the method shown in green, with means of 36.9 % and 39.4 %.

Table 5-10 displays a comparison of the 28 day period average strain method with the transfer lengths from the literature.

Table 5-10: Relative error of the transfer length using the 28 day period average strain method compared to the transfer length calculated from the literature

Transferred length (in.)	**PB1**		**PB2**		**PB3**		**Statistics**	
Method	Dead End	Live End	Dead End	Live End	Dead End	Live End	μ Means	σ Standard deviation
28 day period average strain method	14	2	12.4	2.2	4	10.5	7.52	5.40
Current ACI and AASHTO	3.8%	86.3%	15.2%	84.9%	73.2%	29.6%	48.8%	37%
Zia and Mostafa	72.5%	75.4%	86.0%	67.0%	46.0%	41.6%	64.8%	17%
Cousins et al.	176.0%	60.6%	122.4%	60.5%	32.9%	248.9%	116.9%	83%
Shahawy et al.	10.8%	87.3%	22.9%	86.3%	75.1%	34.7%	52.9%	34%
Russel and Burns	35.9%	90.8%	43.4%	90.0%	82.1%	53.1%	65.9%	25%
Mitchell et al.	24.8%	82.2%	17.7%	79.1%	63.5%	4.2%	45.2%	34%

It can be observed in Table 5-10 that the transfer length suggested by Mitchell et al. (1993) was the closest in terms of means as it was for the 95% average maximum strain method described previously. The same observation was made for the transfer length suggested by Cousins et al. (1990) where results were farthest from the experimental transfer length's results of the 95% average maximum strain method. Table 5-11 displays the comparison of the end slip method with the transfer lengths from the literature.

Table 5-11: Relative error of the transfer length using the End slip method compared to the transfer length calculated from the literature

Transferred length (in.)	**PB1**		**PB2**		**PB3**		**Statistics**			
Method	Lt with α=2 (in.)	Lt with α=3 (in.)	Lt with α=2 (in.)	Lt with α=3 (in.)	Lt with α=2 (in.)	Lt with α=3 (in.)	μ Means α=2	σ Standard deviation α=2	μ Means α=3	σ Standard deviation α=3
End slip method	6.2	9.3	7.07	10.6	7.08	10.61	6.78	0.51	10.17	0.75
Current ACI and AASHTO	57.4%	36.1%	51.6%	27.5%	52.5%	28.9%	53.9%	3.1%	30.8%	4.6%
Zia and Mostafa	23.6%	14.6%	6.0%	59.0%	4.5%	43.1%	11.4%	10.6%	38.9%	22.5%
Cousins et al.	22.2%	83.3%	26.8%	90.2%	135.2%	252.5%	61.4%	64.0%	142.0%	95.8%
Shahawy et al.	60.5%	40.8%	56.1%	34.1%	55.9%	34.0%	57.5%	2.6%	36.3%	3.9%
Russel and Burns	71.6%	57.4%	67.7%	51.6%	68.4%	52.6%	69.2%	2.1%	53.9%	3.1%
Mitchell et al.	44.7%	17.1%	32.9%	0.6%	35.4%	3.2%	37.7%	6.2%	7.0%	8.9%

From Table 5-11, it can be observed that for the constant stress distribution (α=2), the closest equation in the literature was Zia and Mostafa (1997), and for the linear stress distribution (α=3) the equations suggested by Mitchell et al. (1993) with a 7% relative error was the closest prediction. On the other hand, for the constant stress distribution, the equations suggested by Russel and Burns (1996) were farthest away from the result with a 69.2% relative error. Concerning the linear stress distribution, Cousins et al. (1990) predicted a transfer length farthest from the result with a 142% relative error.

5.4.5 Conclusion

After plotting graphs of the strain vs. position from the DEMEC measurements, the transfer length of the prestressed BFRP concrete beam were evaluated using three different methods. The 95% average maximum strain method enabled the smoothing of the graph as well as achieving a straighter plateau. However, because the transfer length was not varying a lot with time, another method was introduced called the 28 day average strain method, which provided one graph for each prestressed member. The transfer length was evaluated by taking the average of all the points constituting the plateau, and the first intersection between the graph and the plateau, was considered as the transfer length. This method gave only one graph per prestressed beam to analyze. It also smoothed the data giving a straight plateau. The third method was the end slip method. By knowing the slip of the BFRP rod, the transfer length could be evaluated. The results were quite close compared to the results of the two first method, where the transfer length was inconsistent between prestressed beams, and the results were highly variable.

The transfer length was never the same and the results varied considerably regarding the dead or the live end of the prestressed member considered. Thus, each end appears to not behave the same, which means that the mechanism of the transfer of force from the BFRP rod to the concrete may not be the same at each end.

After computing all transfer lengths based on prediction equations proposed in the literature, it can be noticed that the equation suggested by Mitchell et al. (1993) was the most precise in each method of calculation the transfer length. As a consequence, for the BFRP prestressed concrete beams fabricated in this research, the equation suggested by Mitchell et al. (1993) predicted the most accurate transfer length. It also seems that the end slip method achieved the closest results to that expression, however nothing gave the certitude that the end slip method provided the best estimate. Methods using the DEMEC points measurements could have given a better evaluation of the transfer length, however results were too dispersed to come to a solid conclusion. Thus, the anisotropic behavior of the BFRP rod could have been one of the reasons results were dispersed. Errors of measurements using the dial gauge could also have been a possibility.

In general, the end slip method provided more consistent transfer lengths than the DEMEC points measurements, and as a consequence, the end slip method was the more reliable method, and the equations to evaluate the transfer length suggested by Mitchell et al. provided the best estimate.

5.5 Prestress losses

5.5.1 Introduction

Immediately after releasing the prestress force, the BFRP rod shortened because of the elastic shortening of the concrete. There was no anchorage seating loss since it is due to engagement of wedges after release from the jack, which was not in the prestressing setup. Also, since the rams were reacting off of the prestressing steel frame, all elastic shortening of the steel frame was compensated by the rams. When the BFRP rod was cut during prestress release the slippage of the BFRP rod was measured at the dead end and it provided data to calculate the instantaneous prestress losses. The DEMEC measurements also provided enough data to evaluate the prestress losses after prestress release to until 28 days. The prestresses losses after prestress release were compared between each other before noting the differences with the evaluated prestress losses from Zia, Preston et al. (1979).

5.5.2 Measured prestress losses

According to the plots of the strain vs. position, the differences in strain at the level of the BFRP rod were measured. Thanks to this variation of strain, the prestress losses have been calculated. By using Hooke's law, strains were multiplied by the elastic modulus of the BFRP rod of 8,702 ksi to obtain a stress. This elastic modulus was provided by V-ROD's test report. Those stresses calculated at different times after prestress release were the prestress losses. Table 5-12 contains the prestress losses measured from the DEMEC points.

Table 5-12: Measured prestressed losses from DEMEC points

Prestress losses PB1

Time	Dead End		Live End	
	Strain in BFRP rod (in./in.)	Total prestress losses (ksi)	Strain in BFRP rod (in./in.)	Total prestress losses (ksi)
Before prestress release	0	0	0	0
After prestress release	0.00033	2.88	0.00024	2.12
1 day	0.00051	4.41	0.00050	4.38
7 days	0.00079	6.85	0.00057	4.98
14 days	0.00083	7.24	0.00072	6.30
28 days	0.00071	6.15	0.00083	7.26

Table 5-12: (continued)

Prestress losses PB2

Time	Dead End		Live End	
	Strain in BFRP rod (in./in.)	Total prestress losses (ksi)	Strain in BFRP rod (in./in.)	Total prestress losses (ksi)
Before prestress release	0	0	0	0
After prestress release	0.00026	2.30	0.00043	3.78
1 day	0.00042	3.67	0.00055	4.81
7 days	0.00053	4.64	0.00065	5.67
14 days	0.00054	4.68	0.00071	6.18
28 days	0.00091	7.89	0.00080	6.97

Prestress losses PB3

Time	Dead End		Live End	
	Strain in BFRP rod (in./in.)	Total prestress losses (ksi)	Strain in BFRP rod (in./in.)	Total prestress losses (ksi)
Before prestress release	0	0	0	0
After prestress release	0.00030	2.61	0.00030	2.59
1 day	0.00036	3.17	0.00035	3.02
7 days	0.00046	3.98	0.00045	3.88
14 days	0.00058	5.01	0.00057	4.93
28 days	0.00106	9.19	0.00071	6.19

The 95% average maximum strain method plots were used to evaluate the prestress losses in Table 5-12. The strain in the BFRP rod was taken at the plateau representing 95% of the maximum average strain. Prestress losses for all the prestressed BFRP concrete beams did not exceed 9.19 ksi after 28 days. Considering the ideal prestress force of 20 kips creating a stress of approximately 90 ksi, implied a prestress loss of around a maximum of 10% after 28 days following the prestress release. For the calculation of the section strength, the average of the prestress losses at both ends were considered to calculate the effective prestress stress of the BFRP rod f_{be}. As the transfer lengths were not the same at both ends, similarly the prestress losses were different at the live and dead ends as well.

5.5.3 Analysis of prestress losses

The prestress losses were evaluated using the calculation method suggested by Zia et al. (1979), with the calculations revised using the actual jacking stress and the compressive strength of the concrete at prestressed release. Details of the calculations are presented in Appendix I. Table 5-14 presents the estimated prestress losses for each specimen.

Table 5-14: Estimations of the prestressed losses

Prestressed losses for each beam (ksi)	**PB1**	**PB2**	**PB3**
Elastic shortening	2.46	2.33	2.42
Creep	3.9	3.6	3.6
Shrinkage	2.32	2.32	2.32
Relaxation	2.7	2.76	2.75
Total prestress loss	11.36	10.99	11.12

The average total prestress loss for these three prestress BFRP concrete beams was 11.15 ksi, and the results of the calculations were quite similar for each prestressed member. The

Shrinkage and Relaxation calculated according to the Zia et al. method does not consider a specific time. It is considered to be basically the losses over service life of the beam. However, considering it at 56 days is probably reasonable since the losses will more or less flatline over time. Estimation of prestress loss is an important factor for evaluating the serviceability of all types of prestressed members and to calculate the flexural strength of members. Table 5-15 compares the results of the prestressed losses between the actual measured values and the estimated prestress losses at prestress release.

Table 5-15: Comparison of prestress losses at release with the estimation

Prestressed losses (ksi)	**Estimated prestress loss from elastic shortening**	**Prestress loss from DEMEC points at release**
PB1	2.46	2.88
PB2	2.33	2.30
PB3	2.42	2.61
Means μ (ksi)	2.40	2.59
Standard deviation σ (ksi)	0.07	0.29
Relative error ε to the estimated prestress loss		**7.96 %**

From Table 5-15, it can be observed that the prestress loss from the DEMEC points at prestress release were relatively close to the estimated elastic shortening, with a relative error of 7.96 %. Furthermore, the average prestress loss from the DEMEC points of 2.59 ksi was slightly greater than the prestress loss due to the shortening of concrete. Thus DEMEC gauge provided a good estimation of the estimated elastic shortening of the concrete.

Table 5-16 shows the results from the total prestress loss estimated and measured using DEMEC points.

Table 5-16: Comparison of total prestress losses with the estimation

Prestressed losses (ksi)	Estimated total prestress loss	Total averaged prestress loss at 28 days from DEMEC points
PB1	11.36	6.71
PB2	10.99	7.43
PB3	11.12	7.69
Means μ	**11.157**	**7.277**
Standard deviation σ	0.19	0.51
Relative error ε to the estimated prestress loss		**34.78 %**

It can be deduced from Table 5-16 that the estimated total prestress loss was approximately 35% greater than what the DEMEC points measured. The first reason for this difference is that the method to estimate total prestress losses does not consider a specific time. The calculation provides a total prestress loss over a long period of time. The creep and shrinkage losses are typically based on 5 years of service of the prestressed concrete member. The other possible reason is that the prestress losses are based on erroneous data, since the DEMEC points data provided different results for the transfer length. For BFRP material, this will need to be investigated, because the prestress losses might take longer to reach a plateau.

5.5.4 Conclusion

To conclude, in this section, the prestress losses were evaluated using the DEMEC points and the end slip method. The DEMEC points provided prestress losses over time, from the prestress release time to 28 days after. Whereas the end slip method provided the instantaneous prestress loss at prestress release which correspond to the elastic shortening of the concrete. The DEMEC points results provided closer results to the estimated prestress losses at release with a difference of around 8 %. In comparison the end slip method provided a difference of around 42 % which is larger than the estimated elastic shortening of the concrete. It can also be noted that the prestress losses measured using DEMEC points or end slip were in general higher than the estimation. However, the results obtained from the end slip method shown that the instantaneous prestress losses were larger than the elastic shortening of the concrete which means that either other prestress loss are present during prestress release or that the end slip method provided erroneous data.

The total prestressed losses measured at 28 days using the DEMEC points were significantly smaller compared to the estimated total prestress losses, with a difference of approximately 35 %. This implies that either the model of calculation of the prestress losses needs to be revised or that the total prestress losses for BFRP rod would be reached later than 28 days after prestress release as the method considered in this research is based for creep and shrinkage over a long period of time. In addition, the method was modified to take into account the mechanical properties of BFRP and not steel, as a consequence the method might not be suitable for BFRP, as it is a relatively new material. A method to calculate accurately prestress loss for BFRP rod will need to be investigated.

5.6 Testing of prestressed and nonprestressed BFRP concrete beams

5.6.1 Introduction

The testing of the prestressed and nonprestressed BFRP specimens was conducted to evaluate their section strength and observe any differences between the two methods. The testing consisted of three point loading. The goal was to measure the moment capacity of the section in flexure. The beam was over reinforced for shear, so there would be no shear failure. This choice of testing was conducted in order to compare the effectiveness of the use of BFRP for prestressing. The results were also compared to the estimated section capacity. The calculations of the section strength were revised for each beam to take into account the material properties at the time of testing and any slight variations in the span length and load application.

5.6.2 Testing setup

The tests effectuated at Fears Lab were conducted on the MTS machine as shown in Figure 5-9. The setup consisted of placing a W6x20 steel section of 58in. long inside the MTS frame and pushing it from the bottom through a large steel nut welded at midspan. The nut connected the hydraulic cylinder to the steel section, which moved upward pushing the W6x20 beam to apply load to the specimen through two roller supports. A rod attached from the top of the MTS frame had a roller connected to it, preventing the beam from moving upward when the W6x20 beam was loading the specimen from its bottom. By preventing the upward displacement, the concrete beam was subjected to a three point loading arrangement. With two point loads from the bottom at each end of the tested beam representing the support reactions and one point load located at the top at midspan representing the point load creating the bending moment.

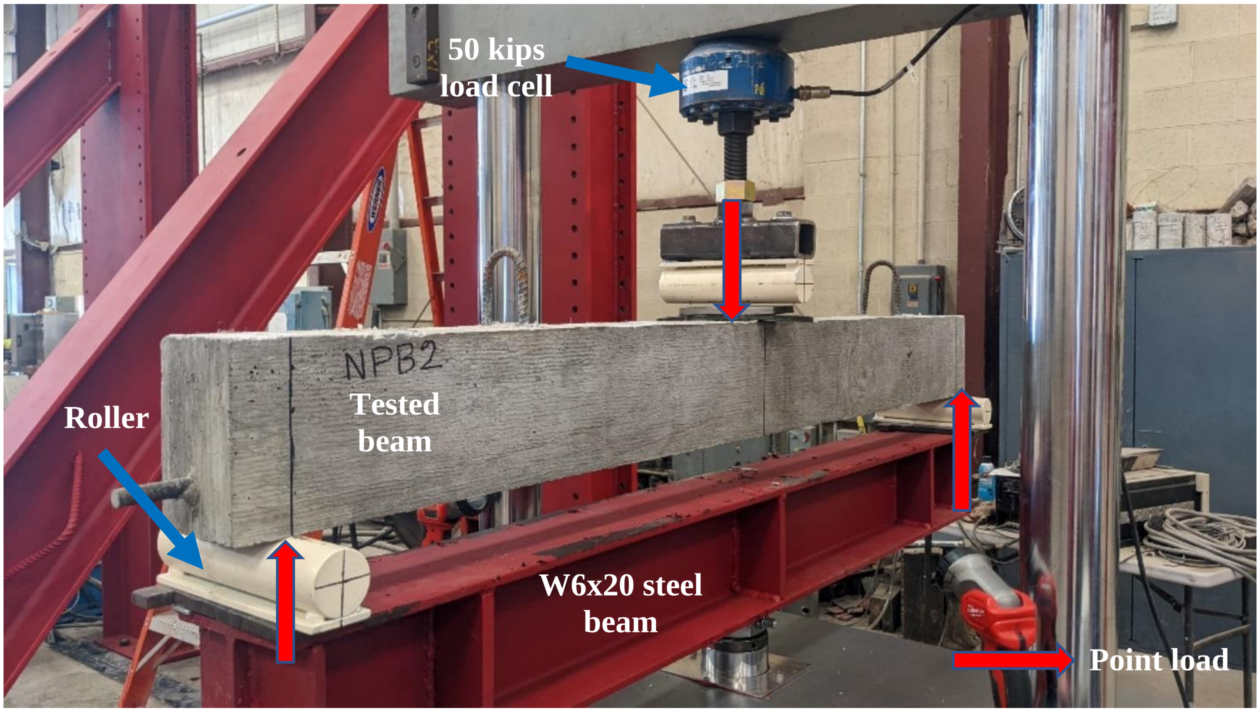

Figure 5-9: Testing setup with the nonprestressed BFRP concrete beam No. 2 ready to be tested in the MTS

After inserting the tested beam on top of the 2 rollers supported by the W6x20 beam, the setup for testing was almost ready. The MTS software was open from a computer and different parameters were chosen. The bending test conducted was controlled by displacement. A rate of 0.04 in./min was chosen in order to not rapidly load the specimen. The 50 kip load cell positioned on top was sufficient since the maximum load was estimated to be around 10 kips.

The outputs chosen were the upward displacement of the setup, which provide an approximation of the deflection of the tested beam, and the force measured by the load cell as well as the time were recorded throughout the testing. It was chosen to record data every 0.1 second in order to have a smooth graph of the load vs. deflection. All the beams were preloaded to 100 lb, and the initial displacement due to the preload was neglected. Then the displacement provided by the MTS was tared to zero, so during the loading the upward displacement of the bottom cylinder from the MTS would display an approximation of the deflection of the tested beam.

Because the rollers used were 2 in. wide, the actual span of the tested beam was reduced to 56 in. since the center of the roller was located at 1 in. from the end of the W6x20 steel beam, which was 58 in. long. Before conducting the test, the tested beam had to be positioned correctly so the second load point could be located directly in the middle span of the tested beam. It was also leveled using steel shims inserted between the steel beam and the roller.

5.6.3 Calculations of the moment capacity

The revised data from the concrete compressive strength as well as the actual prestress losses measured using DEMEC points were used to calculate the section strength more precisely. The prestressed beam and nonprestressed beam were also weighted so the dead load can be adjusted. The measured dead load for each type of beam was very close to the assumed value. The span of the beam was also revised, switching from a span of 60 in. to a span of 56 in., which increased the calculated nominal moment capacity of the section. All details of calculations of the six beams tested are presented in Appendix J. Table 5-17 summarizes the results of the nominal moment capacity of all beams as well as the expected point load at flexural failure.

Table 5-17: Results of strength capacity of all nonprestressed and prestressed BFRP members

Section strength of beam	NPB1	NPB3	NPB3	PB1	PB2	PB3
Nominal moment capacity (kip-in.)	108.63	120.30	119.19	135.55	149.50	147.26
Nominal point load at failure (kip)	7.69	8.53	8.45	9.62	10.62	10.46

The results of the calculations in Table 5-17 show that the nonprestressed BFRP concrete beams have a smaller strength capacity than the prestressed BFRP concrete beam. This implies that the nonprestressed BFRP members will fail at a smaller load than the prestressed BFRP members. Furthermore, it can be noticed that each beam had a different strength capacity due to the actual concrete compressive strength. Also, for the prestressed beams, there were also small variations in the jacking stress and prestress losses, although the capacities were relatively close. In order to verify these observations, the results of the flexural testing are presented in the next section.

5.6.4 Results of the flexural testing

Beams were tested in pairs on the same day, with one prestressed and one nonprestressed BFRP concrete beam corresponding to those that were poured on the same day. During the day of the testing of the set of beams, three concrete cylinders were broken to evaluate the concrete compressive strength at testing day. Those values were used to refine the estimated capacity of each beam.Afterward, each beam was set in the MTS for testing. During the testing, the load application was paused at load increments of approximately 1 kip. After the appearance of the first crack, the testing was paused at intervals of 0.5 kip. Once the load reached a value close to the estimated failure, the load increment was set to 0.2 kip until its failure. The following paragraphs present the testing results of each set of beams. Figure 5-10 presents the load-deflection plots for the first prestressed and nonprestressed BFRP concrete beams.

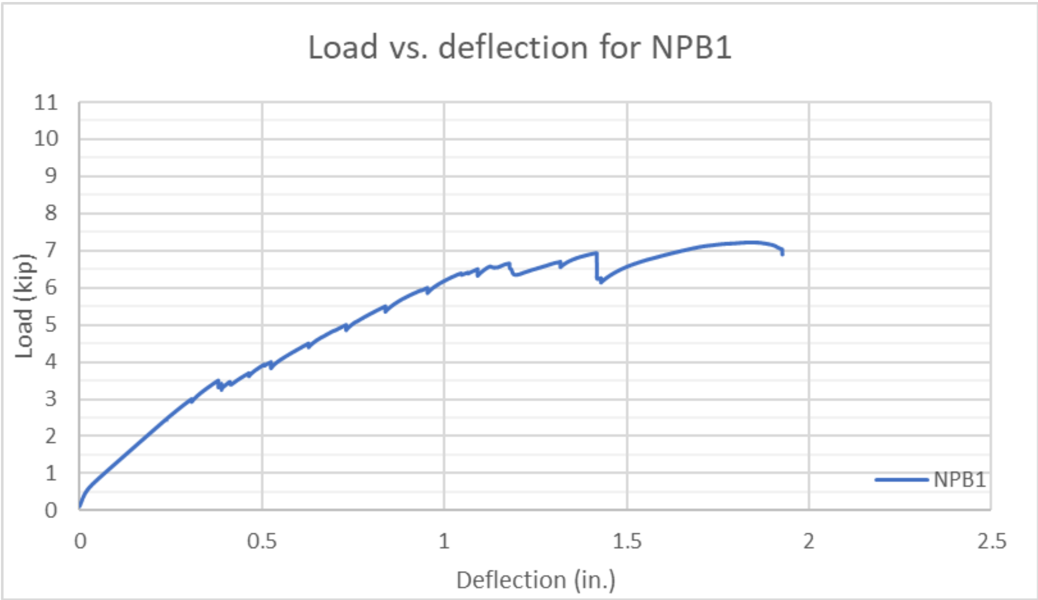

(a)

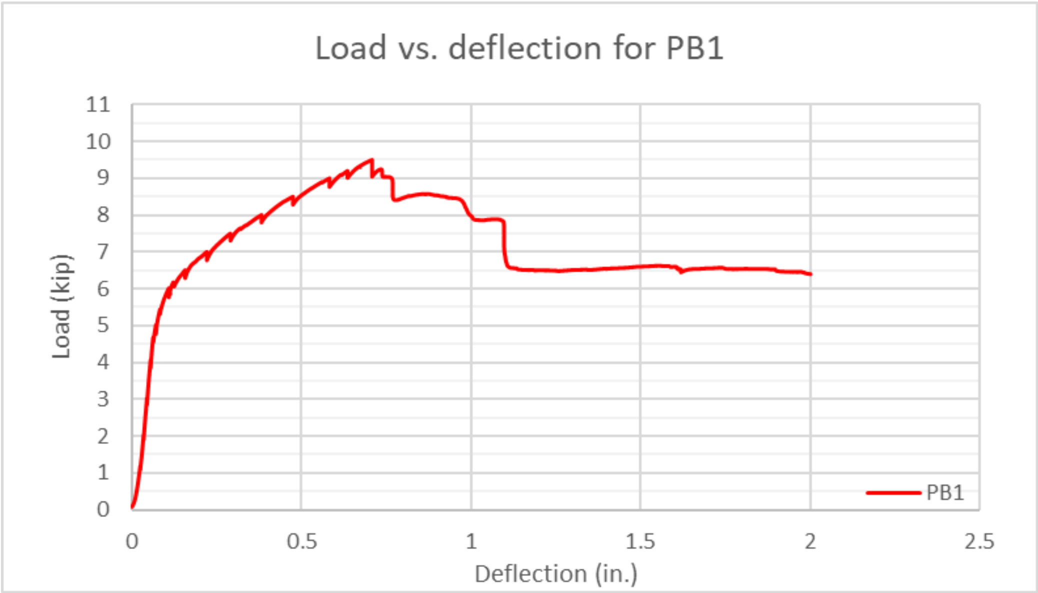

(b)

Figure 5-10: Load vs. deflection graphs for the first set of beams

It can be noticed in Figure 5-10 that the prestressed beam had a greater capacity than the nonprestressed one, consistent with the calculated values. NPB1 failed in flexure suddenly after reaching a maximum capacity of 7.22 kip. Whereas PB1 after reaching a maximum capacity of 9.5 kip, the load dropped slowly until reaching a plateau of 6.5 kip. The test was stopped after reaching a total deflection of 2 in. to avoid damaging the setup. Figure 5-11 presents photographs of NPB1 and PB1 during testing.

(a)

Figure 5-11: Photograph of NPB1 (a) and PB1 (b) during and after testing

From Figure 5-11, it can be observed that NPB1 began to crack around 1 kip, whereas PB1 resisted cracking until a load of 5 kips. This response is consistent with the effect of prestressing concrete in delaying the cracking load. The two beams failed in flexure, and the forms of the cracks located mainly in the middle of the span were flexural cracks, and they were no cracks near the supports. PB1 had significantly fewer cracks than NPB1. Figure 5-12 presents the load-deflection plots for the second prestressed and nonprestressed BFRP concrete beam

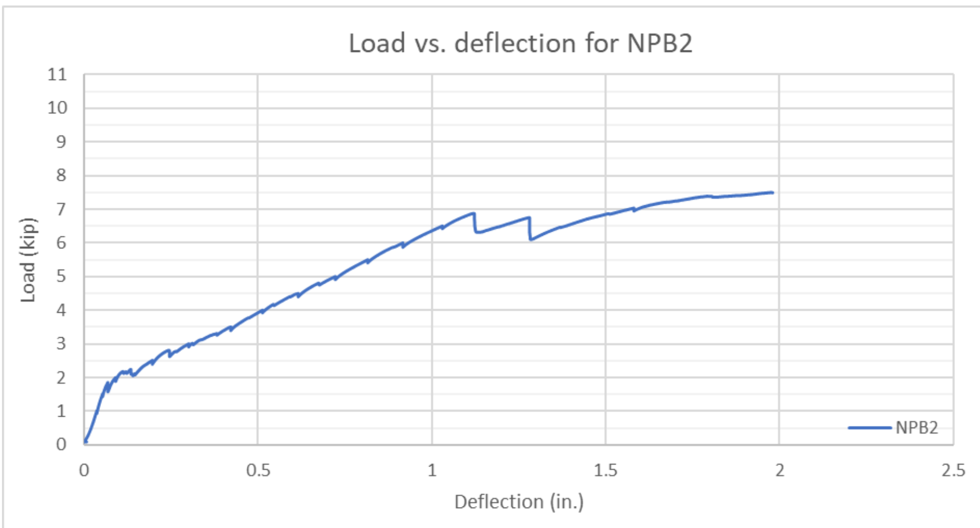

(a)

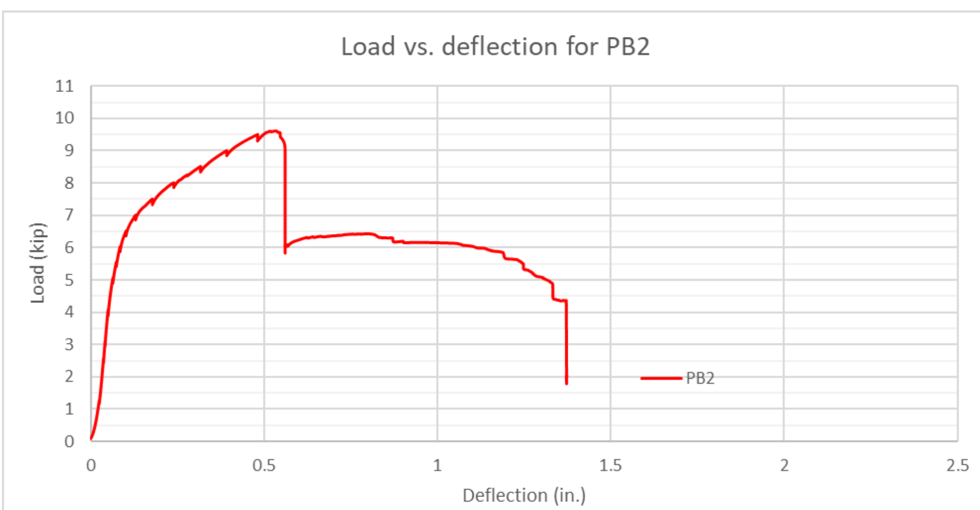

(b)

Figure 5-12: Load vs. deflection graphs for the second set of beams

As with the previous test, from Figure 5-12, it can be observed that the prestressed beam had a greater capacity than the nonprestressed one. NPB2 failed in flexure suddenly after reaching a maximum capacity of 7.5 kip. Whereas PB2 after reaching a maximum capacity of 9.6 kip, the load dropped suddenly to 6 kip where it remained constant. The BFRP rod of PB2 failed after reaching a deflection of 1.38 in. Figure 5-13 presents photographs of NPB2 and PB2 during testing.

(a)

(b)

Figure 5-13: Photograph of NPB2 (a) and PB2 (b) during and after testing

From Figure 5-13, it can be observed that NPB2 began to crack around 1 kip, whereas PB1 resisted cracking until a load of 5 kips. The two beams failed in flexure, and the forms of the cracks located mainly in the middle span were flexural cracks, and they were no cracks near the supports. PB2 had significantly fewer cracks than NPB2. The BFRP rod within specimen PB2 fractures, and the steel located at top of the beam yielded. Figure 5-14 presents load-deflection plots for the third prestressed and nonprestressed BFRP concrete beam.

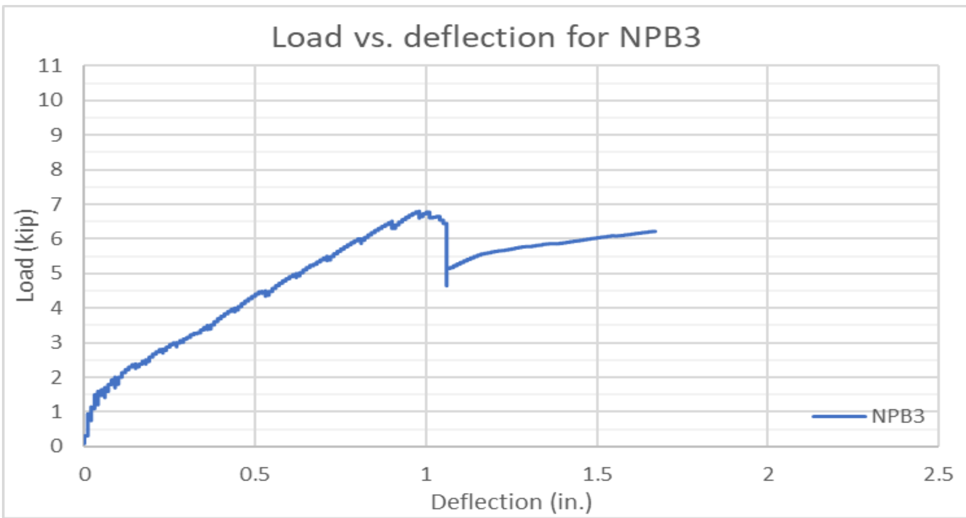

(a)

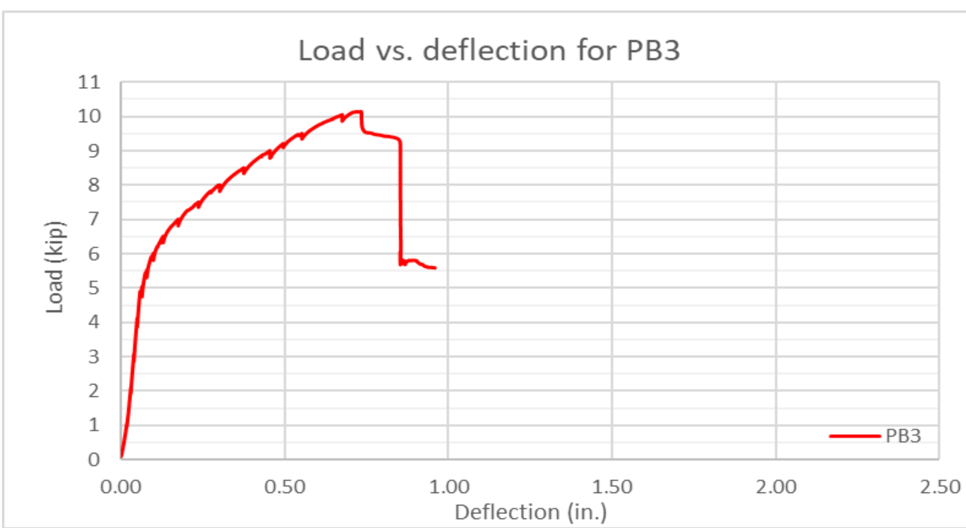

(b)

Figure 5-14: Load vs. deflection graphs for the third set of beams

As with the previous tests, from Figure 5-14, it can be observed that the prestressed beam had a greater capacity than the nonprestressed one. NPB3 failed in flexure suddenly after reaching a maximum capacity of 6.8 kip. Afterward, NPB3 was loaded again until reaching 6.2 kip before failing. The plot doesn't show the sudden drop after 6.2 kip when the beam reached a deflection of 1.63 in. Figure 5-15 presents photographs of NPB3 and PB3 during testing.

(a)

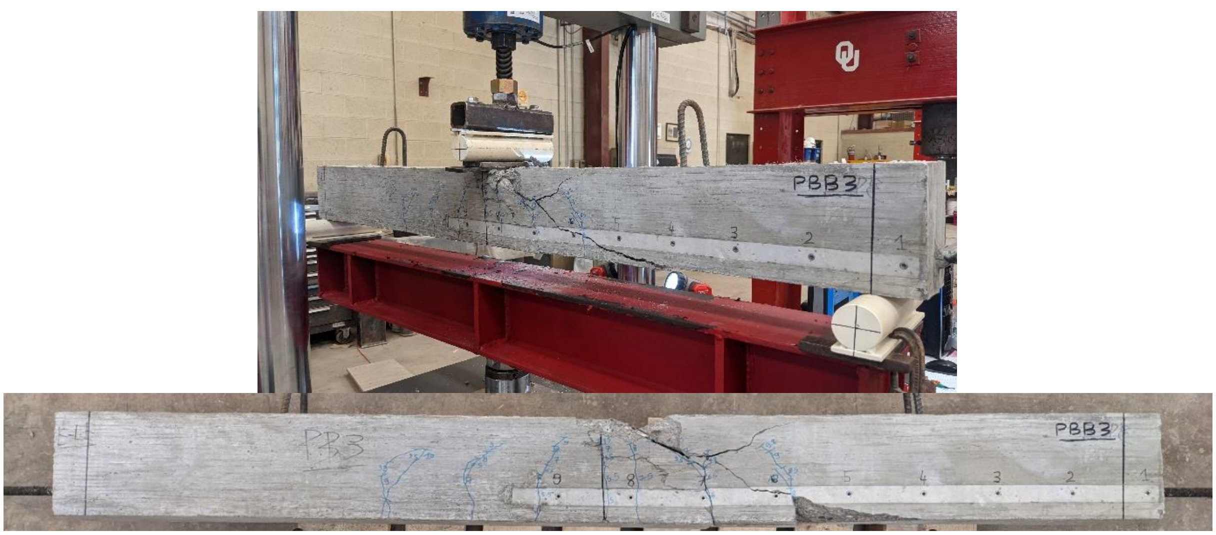

(b)

Figure 5-15: Photograph of NPB3 (a) and PB3 (b) during and after testing

In the other hand PB3 reached a maximum capacity of 10.14 kip before slowly dropping to 9.5 kip until reaching a deflection of 0.86 in. when the load dropped off rapidly to 5.8 kips. The test was then stopped since the loss of 50 % of the capacity occurred and all the concrete on top of the beam was crushed and began falling down.

From Figure 5-15, it can be observed that NPB3 began to crack around 1 kip, whereas PB3 resisted cracking until a load of 5 kips. Usually all of the cracks were symmetric on each half of the beam. The two beams failed in flexure, and the forms of the cracks located mainly in the middle span were flexural cracks, and they were no cracks near the supports. PB3 had significantly fewer cracks than NPB2. Failure occurred due to crushing of the concrete at the top of the beam near at midspan. Table 5-18 summarizes the results of the load and the deflection at failure for each beam.

Table 5-18: Failure of all tested beams

Tested beams	Load at Failure (kip)	Deflection at failure (in.)	Type of failure
NPB1	7.22	1.84	Flexural with concrete crushing
NPB2	7.50	1.97	Flexural with concrete crushing
NPB3	6.80	0.98	Flexural with concrete crushing
PB1	9.50	0.71	Flexural with concrete crushing
PB2	9.60	0.53	Flexural with concrete crushing then BFRP rupture
PB3	10.14	0.73	Flexural with concrete crushing

From Table 5-18, it can be observed that all the beams failed in flexure, which was the predicted and desired failure for this research. Furthermore, the nonprestressed beams failed at loads relatively close to each other, with values of 7.22 kips, 7.50 kips and 6.80 kips for NPB1, NPB2 and NPB3, respectively. By considering the fact that they all have slightly different concrete compressive strengths, the load at failure was very consistent. However, the deflections at failure was very different for NPB3, which reached a value of 0.98 in. for the first significant loss in capacity as evidenced in the plot.

The loads at failure for the prestressed beams were 9.50 kips, 9.60 kips and 10.14 kips for PB1, PB2 and PB3, respectively, which gave a range of values relatively close. By considering the fact that they all have different concrete compressive strength and slightly different prestress force, the loads at failure were very consistent. However, the deflection at failure was very different for PB2 with a value of 0.53 in. compared to PB1 and PB3, which had a relatively close deflection of 0.71 in. and 0.73 in., respectively.

5.6.5 Comparison of calculated and tested section capacities

All the beams failed in flexure, which was the desired failure mode. The measurement of the nominal moment capacities of the beams was calculated based on the load at failure. Table 5-19 provides a comparison of the estimated load at failure to the tested results.

Table 5-19: Comparison of the estimated load at failure to the experiment load obtained

Point load at failure (kip)	Estimated Pu	Experimental Pu	Relative difference ε
NPB1	7.69	7.22	6.2%
NPB2	8.53	7.50	12.1%
NPB3	8.45	6.80	19.5%
PB1	9.62	9.50	1.2%
PB2	10.62	9.60	9.6%
PB3	10.46	10.14	3.0%

From Table 5-19, it can be deduced that the predicted load at failure for the nonprestressed beams was less precise, with a relative error varying from a minimum of 6.2% for NPB1 to a maximum of 19.5% for NPB3, compared to the prestressed BFRP concrete members, which provided results that were much closer to the calculated values at failure. The differences for the prestressed beams ranged from a minimum of 1.2% for PB1 to a maximum of 9.6% for PB2, with PB3 falling in between and closer to PB1 at 3.0%. Both sets of values are very reasonable given the normal variations between theoretical and actual conditions, such as the material properties, support conditions, etc.

For PB2, it is interesting to note that the BFRP rod failed after sustaining a load capacity of around 6 kips. The plateau obtained in the plot can be attributed to the plastic behavior of the steel located on the top of the section. Indeed, the steel yielded preventing the BFRP to fail, until it reached a deflection of 1.38 in. and ruptured the BFRP rod. A photograph of the yielded steel and the failed BFRP rod was taken after removing all the crushed concrete, as shown in Figure 5-16.

Figure 5-16: Photograph of the failed section of PB2

5.6.6 Conclusion

To conclude, three nonprestressed beams as well as three prestressed beams were tested using the MTS set up. A W6x20 steel beam measuring 58 in. was built and designed to transfer the loads to the beam. A load cell attached on the top hold down point measured the load applied to the test specimen. The deflection was obtained from the displacement of the MTS, after offsetting the displacement once the tested beam was preloaded to 100 lb.

After marking the cracks a different load stages, and testing the beams to flexural failure, the results obtained were satisfying. All the beams failed in flexure as predicted, and all the beams failed by the concrete located in the compression zone crushing. After crushing of the concrete, the load usually dropped to around 30% of the maximum value. Afterward, all the beams could sustain a deflection to more than 1 in. and up to 2 in. depending on the type of beam tested. Only PB2 experienced fracture of the BFRP rod prior to crushing of the concrete.

Cracks began to appear through visual observation at approximately 1 kip for all the nonprestressed beam, compared to 5 kips for all the prestressed beams. Moreover, a significantly fewer cracks were observed for the prestressed beams than for the nonprestressed members. As a consequence, the prestressed beams performed better in terms of serviceability. Indeed, by preventing the opening of cracks, water and other aggressive agents would not easily penetrate to the inside of the concrete beams. Thus, the prestressed beams would have a greater expected service life than the nonprestressed beams. Furthermore, by prestressing to around only 50% of the capacity of the BFRP rod, the ultimate load capacity of the prestressed members was increased by roughly 30%, which is very interesting.

6. FINDING, CONCLUSION, AND RECOMMENDATION

6.1 Finding

The following chapter summarizes the findings, conclusions, and recommendations of this research project.

6.1.1 Transfer length

The findings of the different transfer lengths evaluated using the end slip method, the 95% average maximum strain method and the 28 day period average method are presented below:

- The dead end and the live end of each prestressed beam experienced significant differences in transfer length regardless of the measurement method.
- The transfer length increased approximately 35% over time from prestress release to 28 days.
- The 95% average transfer length method resulted in a transfer length that ranged from 4.32 in. to 17.32 in., with an average difference of approximately 54.6% between the dead end and the live end. The average transfer length regardless of the end considered was 10.18 in.
- At release, for the 95% average maximum strain method, for the transfer length, the Mitchell et al. equations (1993) had the closest estimations with a difference of 33.4%, and the Cousins et al. equations (1990) had the farthest estimation with a difference of 139%.
- The 28 day period average method resulted in a transfer length that ranged from 2 in. to 14 in., with an average difference of approximately 72% between the dead end and the live end. The average transfer length regardless of the end considered was 7.35 in.

- For 28 day period average method, the Mitchell et al. equations (1993) had the closest estimations with a difference of 45.2%, and the Cousins et al. equations (1990) had the farthest estimation with a difference of 116.9%.
- For the end slip method, the transfer lengths ranged from 6.2 in. to 10.61 in. with a difference of approximately 3 in. for the transfer length based on whether a constant stress distribution or a linear stress distribution was used. The average transfer length at the dead end was 6.78 in. and 10.17 in. for the constant and linear stress distribution, respectively.
- For the end slip method, the Mitchell et al. equations (1993) and the Zia and Mostafa equations (1997) had the closest estimations with a difference of 7% and 11.4%, respectively. On the other hand, the Cousin et al. equations (1990) had the farthest estimation with a difference of 142%.

6.1.2 Prestress losses

The findings from the prestress losses determined from the DEMEC points measurement and the end slip method are as follows:

- The average prestress losses at release from the DEMEC points measurement provided an instantaneous prestress loss of 2.59 ksi.
- The average total prestress loss at 28 days measured from the DEMEC points provided a calculated value of 7.27 ksi.
- The estimated averaged elastic shortening of the concrete using the Zia et. al method (1979) provided a calculated value of 2.40 ksi.
- The estimated total prestress losses using the Zia et al. method (1979) provided a

calculated value of 11.15 ksi.

6.1.3 Testing results

The findings from the beam load test results are as follows:

- The average concrete strength of the three set of beams at 28 days was 10,570 psi.
- The average concrete strength of the three set of beams at testing day was 10,870 psi.
- The average point load at failure for the nonprestressed BFRP concrete beams was 8.22 kips.
- The average point load at failure for the prestressed BFRP concrete beams was 10.23 kips.
- All the specimens tested failed in flexure.
- The nonprestressed BFRP concrete beams showed the appearance of flexural cracks around a load of 1 kip.
- The prestressed BFRP concrete beams showed the appearance of flexural cracks around a load of 5 kips.
- The load-deflection plot and visual observations of the nonprestressed BFRP concrete beams indicated a brittle failure after crushing of the top fibers of the concrete and a loss of capacity greater than 50%.
- The load-deflection plot and visual observations of the prestressed BFRP concrete beams indicated a brittle failure after crushing of the top fibers of the concrete and an average loss of capacity of 30%.
- Specimen PB2 failed first by concrete crushing. After maintaining the loading, the BFRP rod broke and the No. 4 steel rebar along the top of the specimen yielded.

- The nonprestressed BFRP concrete beams had an average deflection at failure of 1.60 in.
- The prestressed BFRP concrete beams had an average deflection at failure of approximately 0.66 in.

6.2 Conclusions

Based on the previously stated findings, several conclusions can be made concerning the development of the prestressing anchor system, the transfer length, the prestress losses, and finally the results of the flexural testing.

- The anchoring system fabricated with a 1/4-in.-thick and 11.5-in.-long steel pipe filled with an expansive mortar was successful in sustaining the required prestress force of 20 kips. This anchoring system had reserve capacity beyond the required 20 kips that would probably allow a higher level of prestressing. By pouring the expansive mortar from a hole drilled along the top of the steel tube, the anchor could be placed without moving the prestressing fame.
- All the methods used to evaluate the transfer length in this research resulted in significant differences in transfer length between the live and dead ends.
- The Mitchell et al. equations (1993) provided a good estimation of the transfer length for BFRP prestressing rods.
- The Zia et al. method (1979) provided a reasonable estimation of the prestress loss, however this method is only applicable after several years of service, which means it was an approximation of prestress losses at 28 days.
- All prestressed BFRP concrete beams were evaluated to lose 10% of their jacking stress

at 28 days, which is consistent with beams prestressed with steel strand.

- All nonprestressed and prestressed BFRP concrete beams failed in flexure as designed.
- The calculated failure loads were very close to the values that resulted from testing, with an average precision of 12.6% and 4.6% for the nonprestressed and prestressed members, respectively, which means that the section strength was more accurately predicted for the prestressed members.
- Prestressed BFRP concrete beams were around 20% stronger than nonprestressed BFRP concrete beams.
- Prestressed BFRP concrete beams fail at smaller deflections than nonprestressed BFRP concrete beams, most likely due to the enhanced stiffness caused by the prestressing.
- Prestressed BFRP concrete beams can sustain a load 5 times larger than nonprestressed BFRP concrete beam without the appearance of flexural cracks, thus a greater expected service life is attributed to prestress members.
- Prestressing BFRP concrete beams is viable and worth it in terms of strength and durability.

6.3 Recommendations

The goal of this research project was to determine whether BFRP rods could be used to prestress concrete. The findings and conclusions drawn from this research have led to the following recommendations for future study:

- Determine an optimal length for the steel anchor. Fabricating shorter anchors will prevent buckling, but if the anchor is too short, slip may occur if the confinement and friction of the mortar are less than the tensioning force.

- Develop a reusable anchor for the BFRP rods.
- The stirrup used in this research did not meet the code specification for the bending diameter, since the beam section was small. As a consequence, another solution that could have been used would consist of using welded wire for shear reinforcement. This way will save time for fabrication and space within the beam, since welded wire has a higher yield strength, which will increase the shear capacity.
- Develop a splice to allow longer BFRP rods in the field as the stiffness of the rods prevents coiling prior to shipping.
- Fabricate longer prestressed BFRP concrete beams in order to evaluate the development length of prestressed BFRP rods.
- Develop a method to measure slip of the BFRP rods from both ends to increase the accuracy of the estimation of the transfer length from the end slip method.

APPENDICES

Appendix A: Calculations of moment capacity for nonprestressed BFRP beams

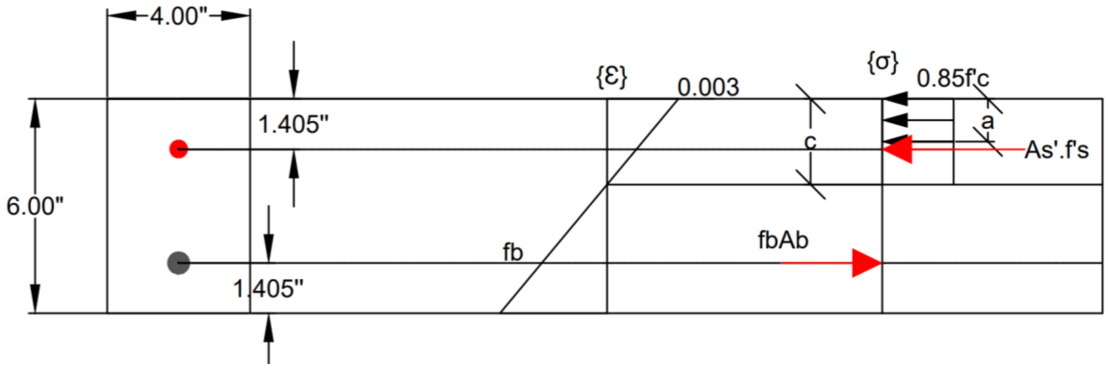

Width of the section:	b=4 in
Hight of the section:	h=6 in
Beam length:	L=60 in
Compressive strength of concrete at 28days:	f'_c=10 ksi
Yield strength of steel:	f_y=60 ksi
Young modulus of concrete ACI 318-19 19.2.2.1(b):	$\mathrm{Ec} = 57{,}000\sqrt{\mathrm{f'c}} = 5700\ \mathrm{ksi}$
Young modulus of steel:	$E_{s=}$ 29,000 ksi
Young modulus of BFRP (V-ROD):	E_b =8,702 ksi
BFRP to concrete ratio：	$\mathrm{n1} = \dfrac{\mathrm{Eb}}{\mathrm{Ec}} = 1.53$
Steel to concrete ratio：	$\mathrm{n2} = \dfrac{\mathrm{Es}}{\mathrm{Ec}} = 5.09$
Steel section of No.4 bar:	A_s'=0.2in^2
BFRP section of No.4 bar:	A_b =0.223in^2
Concrete section:	A0=bh- A_s'- A_b =23.58 in^2

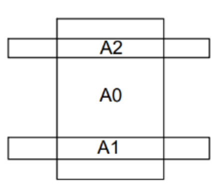

Equivalent area of BFRP: $A1 = n1 x A_b = 0.34 \text{ in}^2$

Equivalent area of steel: $A2 = n2 x A_s' = 1.01 \text{ in}^2$

Gross section: $Ag = bh = 24 \text{ in}^2$

Transformed section: $A_{tr} = A0 + A1 + A2 = 24.93 \text{ in}^2$

Distance from bottom fiber to BFRP centroid: $y_{Gb} = 1.405$ in

Distance from bottom fiber to Steel centroid: $y_{Gs} = 4.595$ in

Distance from bottom fiber to gross section centroid: $y_{Gc} = 3$ in

Centroid of transformed section: $y_{tr} = \frac{\sum_{i=0}^{3} \text{yi.Ai}}{\text{Atr}} = 2.94 \text{ in}$

Eccentricity: $e = y_{tr} - y_{Gb} = 1.53$ in

Quadratic moment of inertia of gross section: $I = \frac{bh^3}{12} = 72\ in^4$

Quadratic moment of inertia of transformed section: $Itr = I + A_g(\text{yGc} - \text{ytr})^2 = 72.1\ in^4$

Strain compatibility method:

Iteration: i=1

Assumption of the distance from the top fiber to the centroid: c=2 in

ACI 318-19 (Table 22.2.2.4.3) f'c=10 ksi>8 ksi => β1=0.65

Equivalent rectangular compression zone a=β1.c=1.3

Strain at the steel bar using similar triangle (bar in the compression area) :

$$\varepsilon_{ps} = \frac{0.003(\text{c} - (\text{h} - y_{Gs}))}{c} = 0.0009\ in/in$$

Stress at the steel bar: $f's = E_s \varepsilon_{ps} = 25.88$ ksi

Strain at the BFRP bar using similar triangle (bar in the tension area):

$$\varepsilon_{pb} = \frac{0.003(\mathrm{h} - \mathrm{c} - y_{Gb})}{c} = 0.00389\ in/in$$

Stress at the BFRP bar: $f_b = E_b \varepsilon_{pb} = 33.8\ ksi$

Sum of compression force: $\mathrm{C} = 0.85 f'_c \mathrm{ab} + f'_s A'_s = 49.37$ kips

Sum of tension force: $T = f_b A_b = 7.55\ kips$

$$\% = \frac{|T - C|}{T} = 554\% \ \rightarrow T \neq C$$

Iteration: i=2

Assumption of the distance from the top fiber to the centroid: c=0.77 in

ACI318-19 (Table 22.2.2.4.3) f'_c=10 ksi >8 ksi => β1=0.65

Equivalent rectangular compression zone a=β1.c=0.5

Strain at the steel bar using similar triangle (bar in the tension area):

$$\varepsilon_{ps} = \frac{0.003(\mathrm{h} - \mathrm{c} - y_{Gs}))}{c} = 0.0025\ in/in$$

Stress at the steel bar: $f'_s = E_s \varepsilon_{ps}$ >60 ksi so the steel yield and f'_s=60ksi.

Strain at the BFRP bar using similar triangle (bar in the tension area):

$$\varepsilon_{pb} = \frac{0.003(\mathrm{h} - \mathrm{c} - y_{Gb})}{c} = 0.015\ in/in$$

Stress at the BFRP bar: $f_b = E_b \varepsilon_{pb} = 129.7\ ksi$

Sum of compression force: $\mathrm{C} = 0.85 f'_c \mathrm{ab} + f'_s A'_s = 29$ kips

Sum of tension force: $T = f_b A_b = 28.9\ kips$

$$\% = \frac{|T - C|}{T} = 0.34\% \ \rightarrow T \approx C \ \rightarrow Good\ enough$$

Nominal moment calculated from the centroid of the equivalent rectangular compression zone axis: $M_n = f_b A_b\,(h - y_{Gb} - 0.5a) - f'_s A'_s (h - y_{Gs} - 0.5a) =$ **111.8 kip.in**

Appendix B Calculations of moment capacity for prestressed BFRP beam

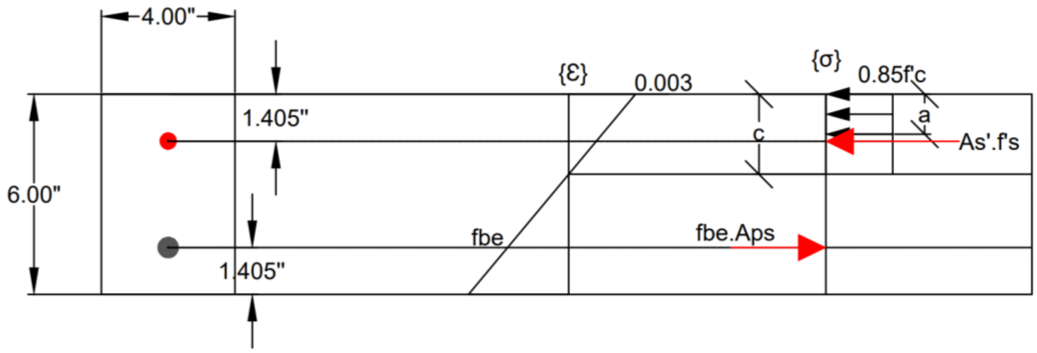

Width of the section:	$b=4$ in
Hight of the section:	$h=6$ in
Beam length:	$L=60$ in
Compressive strength of concrete at 28days:	$f'_c=10$ ksi
Yield strength of steel:	$f_y=60$ ksi
Young modulus of concrete ACI 318-19 19.2.2.1(b):	$Ec = 57{,}000\sqrt{f'c} = 5700$ ksi
Young modulus of steel:	$E_{s=}$ 29,000 ksi
Young modulus of BFRP (V-ROD):	$E_b = 8{,}702$ ksi
BFRP to concrete ratio：	$n1 = \frac{Eb}{Ec} = 1.53$
Steel to concrete ratio：	$n2 = \frac{Es}{Ec} = 5.09$
Steel section of No.4 bar:	$A_s' = 0.2 in^2$
BFRP section of No.4 bar:	$A_b = 0.223 in^2$
Concrete section:	$A0 = bh - A_s' - A_b = 23.58\ in^2$
Equivalent area of BFRP:	$A1 = n1 x A_b = 0.34\ in^2$

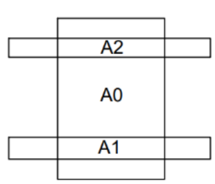

Equivalent area of steel: $A2 = n2x\ A_s' = 1.01\ in^2$

Gross section: $Ag = bh = 24\ in^2$

Transformed section: $A_{tr} = A0 + A1 + A2 = 24.93\ in^2$

Distance from bottom fiber to BFRP centroid: $y_{Gb} = 1.405$ in

Distance from bottom fiber to Steel centroid: $y_{Gs} = 4.595$ in

Distance from bottom fiber to gross section centroid: $y_{Gc} = 3$ in

Centroid of transformed section: $y_{tr} = \frac{\sum_{i=0}^{3} \text{yi.Ai}}{\text{Atr}} = 2.94 \text{ in}$

Eccentricity: $e = y_{tr} - y_{Gb} = 1.53$ in

Quadratic moment of inertia of gross section: $I = \frac{bh^3}{12} = 72\ in^4$

Quadratic moment of inertia of transformed section: $Itr = I + A_g(\text{yGc} - \text{ytr})^2 = 72.1\ in^4$

Prestressed force: $P_i = 20$kips

Age of concrete at prestressed release: $f'_{ci} = 0.6f'_c = 6\ ksi$

Initial prestressed force corresponding to the jacking stress: $f_j = \frac{P_i}{A_b} = 89.7\ ksi$

Prestress losses:

Calculations were based on **(Zia et al. 1979)**

<u>Elastic shortening of concrete:</u>

For pretensioned members: $K_{es} = 1$ and $K_{cir} = 0.9$

Stress in concrete at centroid of BFRP rod due to weight of the beam at time prestress is applied: $f_g = \frac{M_0 e}{I} = 0.94\ ksi$

Net compressive stress in concrete at centroid of BFRP rod immediately after prestress has been applied: $f_{cir} = K_{cir} f_{cpi} - f_g = 1.32\ ksi$

In the expression of the elastic shortening the equation was modified, it was used the modulus of BFRP instead of the steel according to the ACI 440-4R.

$$ES = K_{es} E_b \frac{f_{cir}}{E_{ci}} = 2.59\ ksi$$

Creep:

K_{cr}=2 for pretensioned members

Stress due to the superimposed dead load f_{cds}=0 since no superimposed dead load.

$$CR = K_{cr} \frac{E_b}{E_c} (f_{cir} - f_{cds}) = 4\ ksi$$

Shrinkage:

Volume to surface ratio: $\frac{V}{S} = \frac{A}{P} = \frac{24 in^2}{20 in} = 1.2$

Average relative humidity in Oklahoma: RH=65%

K_{sh}=1 for pretensioned members

$$SH = 8.2 \times 10^{-6} K_{sh} E_b \left(1 - 0.06 \frac{V}{S}\right)(100 - RH) = 2.32\ ksi$$

Relaxation:

The relaxation is complicated to evaluate for BFRP rod, in section 3.10 of ACI 440-4R 04, they gives an estimations of "Relaxation losses (REL) in FRP tendons results from three sources: relaxation of polymer Rp; straightening of fibers Rs; and relaxation of fibers Rf ."

Volume fraction of fibers in the BFRP bar (Assumed using ACI 440-4R 04 section 3.10):

$$\nu_f \sim 37\%$$

Volume fraction of resin: $\nu_r = 1 - \nu_f = 63\%$

They estimated it to be around 1.2% in general ACI 440-4R 04 : $R_p = n_r \nu_r \approx 1.2\%$

They also estimated that R_s=2% and it was chosen to take R_f=0% since there is no information for BFRP available. Thus, the relaxation can be estimated to be 3.2% of the initial prestress force.

$$REL = R_p + R_s + R_f \sim 3.2\% f_j = 2.87\ ksi$$

Total losses=ES+CR+SH+REL=11.8 ksi

Effective prestress stress: f_{se}=f_j-Total losses=78 ksi

Effective prestress force: $P_e = \frac{fse}{A_b} = 17.37\ kips$

Stresses

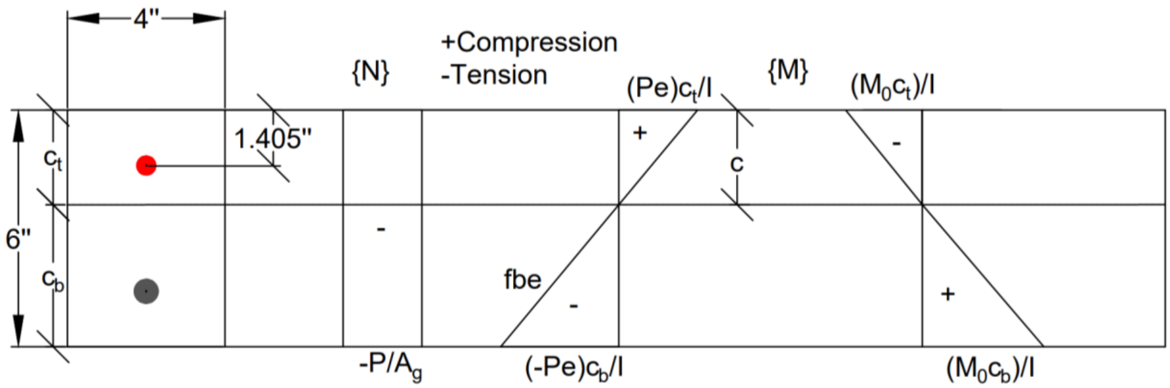

c_b= y_{tr}=2.94 in

c_t =h-y_{tr}=3.06 in

Concrete flexural stress for top fiber at support during prestressed release

$$f^t = \frac{-P}{A_g} + \frac{Pec_t}{I} = 0.47\ ksi$$

Concrete flexural stress for bottom fiber at support during prestressed release

$$f_b = \frac{-P}{A_g} - \frac{Pec_b}{I} = -2.08\ ksi$$

Concrete flexural stress for top fiber at midspan during prestressed release

$$f^t = \frac{-P}{A_g} + \frac{Pec_t}{I} - \frac{M_0 c_t}{I} = 0.430\ ksi$$

Concrete flexural stress for bottom fiber at midspan during prestressed release

$$f_b = \frac{-P}{A_g} - \frac{Pec_b}{I} + \frac{M_0 c_b}{I} = -2.045\ ksi$$

Concrete flexural stress for top fiber at midspan under final conditions

$$f^t = \frac{-P_e}{A_g} + \frac{P_e ec_t}{I} - \frac{M_0 c_t}{I} = 0.368\ ksi$$

Concrete flexural stress for bottom fiber at midspan under final conditions

$$f_b = \frac{-P_e}{A_g} - \frac{P_e ec_b}{I} + \frac{M_0 c_b}{I} = 0.323\ ksi$$

ACI limits

Those limits can be found in Table 24.5.3.1 and Table 24.5.3.2 ACI 318-19.

Concrete compressive stress limits immediately after transfer of prestress:

$$f_{cia} = 0.6f'_{ci} = -3.6\ ksi$$

Concrete tensile stress limits immediately after transfer of prestress at the end support and all other location respectively: $f_{tia} = 6\sqrt{f'_{ci}} = 0.465\ ksi$ $\quad f_{tia} = 3\sqrt{f'_{ci}} = 0.232\ ksi$

F_{cia} is greater than the stress at the bottom fiber that is compressed.

And F_{tia} is not greater for stress at midspan 0.232 ksi $< f_t = 0.430$ ksi thus a steel bar will need to be used at the top in order to resist to the tension stresses.

Loads

Assumed density of beam: w_c=150 lb/ft^3

Self-weight: $w_0 = w_c A_g = 0.025\ kip/ft$

Moment due to self-weight: $M_0 = \frac{w_0 L^2}{8} = 0.94\ kip.in$

Strain compatibility method:

Iteration: i=1

Assumption of the distance from the top fiber to the centroid: c=2 in

ACI 318-19 (Table 22.2.2.4.3) f'c=10 ksi>8 ksi => β1=0.65

Equivalent rectangular compression zone a=β1.c=1.3

Strain at the steel bar using similar triangle (bar in the compression area) :

$$\varepsilon_{ps} = \frac{0.003(\mathrm{c} - (\mathrm{h} - y_{Gs}))}{c} = 0.000893\ in/in$$

Stress at the steel bar: $f'_s = E_s \varepsilon_{ps}$ =25.88 ksi

$$\varepsilon_1 = \frac{f_{se}}{E_b} = 0.0895\ in/in$$

$$\varepsilon_2 = \left(\frac{P_e}{A_{tr}} + \frac{P_e e^2}{I_{tr}}\right)\frac{1}{E_c} = 0.000221\ in/in$$

$$\varepsilon_3 = \frac{0.003e}{c} = 0.00389\ in/in$$

Total Strain at the BFRP bar:

$$\varepsilon_{pb} = \varepsilon_1 + \varepsilon_2 + \varepsilon_3 = 0.013\ in/in$$

Sum of compression force: $\mathrm{C} = 0.85 f'_c \mathrm{ab} + f'_s A'_s = 49.37$ kips

Sum of tension force: $T = f_b A_b = 25.35\ kips$

$$\% = \frac{|T - C|}{T} = 95\% \ \rightarrow T \neq C$$

Iteration: i=2

Assumption of the distance from the top fiber to the centroid: c=1.1 in

ACI 318-19 (Table 22.2.2.4.3) f'c=10 ksi>8 ksi => β1=0.65

Equivalent rectangular compression zone a=β1.c=0.715

Strain at the steel bar using similar triangles (bar in the compression area) :

$$\varepsilon_{ps} = \frac{0.003(\mathrm{c} - (\mathrm{h} - y_{Gs}))}{c} = 0.00095\ in/in$$

Stress at the steel bar: $f'_s = E_s \varepsilon_{ps}$ >60 ksi => Steel yield so f'_s=60 ksi

$$\varepsilon_1 = \frac{f_{se}}{E_b} = 0.0895\ in/in$$

$$\varepsilon_2 = \left(\frac{P_e}{A_{tr}} + \frac{P_e e^2}{I_{tr}}\right)\frac{1}{E_c} = 0.000221\ in/in$$

$$\varepsilon_3 = \frac{0.003e}{c} = 0.0095\ in/in$$

Total Strain at the BFRP bar:

$$\varepsilon_{pb} = \varepsilon_1 + \varepsilon_2 + \varepsilon_3 = 0.0187\ in/in$$

Sum of compression force: $\mathrm{C} = 0.85 f'_c \mathrm{ab} + f'_s A'_s = 36.31$ kips

Sum of tension force: $T = f_b A_b = 36.29\ kips$

$$\% = \frac{|T - C|}{T} = 0.04\% \ \rightarrow T \approx C \ \rightarrow Good\ enough$$

Nominal moment calculated from the centroid of the equivalent rectangular compression zone axis: $M_n = f_b A_b\,(h - y_{Gb} - 0.5a) - f'_s A'_s(h - y_{Gs} - 0.5a) =$ **141.24 kip.in**

Appendix C: Calculations of shear reinforcement for nonprestressed BFRP beam

No.3 Steel was used for shear reinforcement.
Uniform load is $q = w_c A_g = 0.0028\ kip/in$

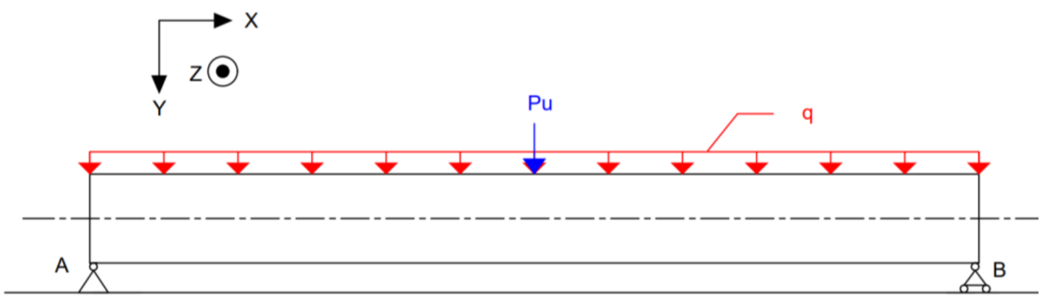

Using the fundamental principle of the static to the {beam}:

$$\begin{cases} R_A + R_B + P_u + qL = 0 \\ \dfrac{qL^2}{2} + \dfrac{P_u L}{2} + R_B L = 0 \end{cases} \xrightarrow{yields} R_A = R_B = -\left(\frac{qL}{2} + \frac{P_u}{2}\right)$$

$$For\ x \in [0; \tfrac{L}{2}] : \begin{cases} V(x) = R_A + qx \\ M(x) = \frac{-qx^2}{2} - R_A x \end{cases} \xrightarrow{yields} \begin{array}{l} V(x) = qx - (\frac{qL}{2} + \frac{P_u}{2}) \\ M(x) = \frac{-qx^2}{2} + (\frac{qL}{2} + \frac{P_u}{2})x \end{array}$$

$$M^{MAX} = M\left(\frac{L}{2}\right) = \frac{-qL^2}{8} + \frac{P_u L}{4}$$

To find the load Pu that will lead to the nominal moment, this equation needs to be solved:

$$\frac{-qL^2}{8} + \frac{P_u L}{4} = Mn$$

$$P_u = \frac{4Mn}{L} - \frac{qL}{2} = 7.4\ kips$$

$$V_{u,max} = \frac{-dM(x)}{dx} = \left(\frac{qL}{2} + \frac{P_u}{2}\right) = 3.76\ kips$$

Fiber reinforced polymer reinforcement ratio: $\rho_f = \frac{A_b}{A_g} = 0.0093$ and $n_f = n_1$

$k = \sqrt{2\rho_f n_f + (\rho_f n_f)^2} - \rho_f n_f = 0.15$ 7.3.2.2b ACI 440 1R 15 and $\phi = 0.75$

$$V_c = \frac{5}{2}k\left(2\sqrt{f'_c}b_w d\right) = 1.17\ kips$$

$$V_s = \frac{V_{u,max}}{\phi} - V_c = 3.74\ kips$$

One legged No.3 stirrup Av=0.11 in^2

Spacing $s = \frac{A_v f_{yt} d}{V_s} = 8.11\ in$

$$\frac{A_v}{s} = max\begin{cases} 0.75\dfrac{\sqrt{f'_c}b_w}{f_{yt}} \\ \dfrac{50b_w}{f_{yt}} \end{cases} = 0.005\ in$$

$$s_{max} = \frac{A_v}{0.005} = 22 in\ this\ is\ too\ much\ check\ maximum\ spacing\ allowed$$

ACI 318-19 table 9.7.6.2.2 : $s_{min} = min\begin{cases} \frac{d}{2} \\ 24in \end{cases} = 2.29in$

The spacing of **2.25 in** was chosen to facilitate the construction of the beam.

Appendix D Calculations of shear reinforcement for prestressed BFRP beam

No.3 Steel was used for shear reinforcement.
Uniform load is $q = w_c A_g = 0.0028\ kip/in$

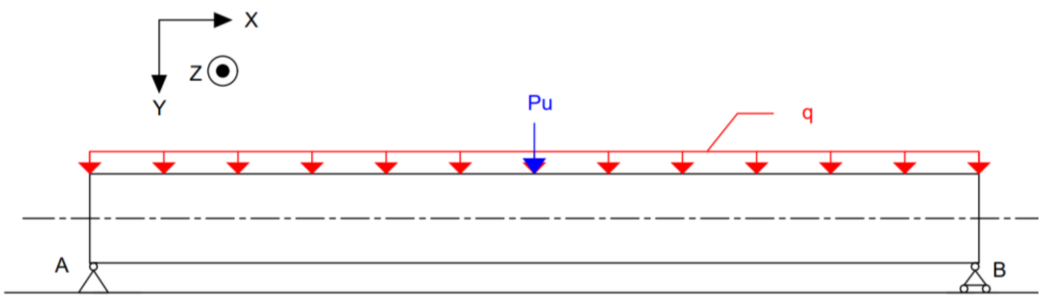

Using the fundamental principle of the static to the (Thorhallsson and Jonsson):

$$\begin{cases} R_A + R_B + P_u + qL = 0 \\ \dfrac{qL^2}{2} + \dfrac{P_u L}{2} + R_B L = 0 \end{cases} \xrightarrow{yields} R_A = R_B = -\left(\frac{qL}{2} + \frac{P_u}{2}\right)$$

$$For\ x \in [0; \tfrac{L}{2}]: \begin{cases} V(x) = R_A + qx \\ M(x) = \frac{-qx^2}{2} - R_A x \end{cases} \xrightarrow{yields} \begin{matrix} V(x) = qx - (\frac{qL}{2} + \frac{P_u}{2}) \\ M(x) = \frac{-qx^2}{2} + (\frac{qL}{2} + \frac{P_u}{2})x \end{matrix}$$

$$M^{MAX} = M\left(\frac{L}{2}\right) = \frac{-qL^2}{8} + \frac{P_u L}{4}$$

To find the load Pu that will lead to the nominal moment, this equation needs to be solved:

$$\frac{-qL^2}{8} + \frac{P_u L}{4} = Mn$$

$$P_u = \frac{4Mn}{L} - \frac{qL}{2} = 9.35\ kips$$

$$V_{u,max} = \frac{-dM(x)}{dx} = \left(\frac{qL}{2} + \frac{P_u}{2}\right) = 4.74\ kips$$

Fiber reinforced polymer reinforcement ratio : $\rho_f = \frac{A_b}{A_g} = 0.0093$ and $n_f = n_1$

$k = \sqrt{2\rho_f n_f + (\rho_f n_f)^2} - \rho_f n_f = 0.15$ 7.3.2.2b ACI 440 1R 15

$$V_c = \frac{5}{2}k\left(2\sqrt{f'_c}b_w d\right) = 1.17\ kips$$

$$V_s = \frac{V_{u,max}}{\phi} - V_c = 5.05\ kips$$

One legged No.3 stirrup Av=0.11 in^2

Spacing $s = \frac{A_v f_{yt} d}{V_s} = 6.01\ in$

$$\frac{A_v}{s} = max\begin{cases} 0.75\frac{\sqrt{f'_c}b_w}{f_{yt}} \\ \frac{50b_w}{f_{yt}} \end{cases} = 0.005\ in$$

$$s_{max} = \frac{A_v}{0.005} = 22in\ this\ is\ too\ much\ check\ maximum\ spacing\ allowed$$

ACI 318-19 table 9.7.6.2.2 : $s_{min} = min\begin{cases} \frac{3d}{4} \\ 24in \end{cases} = 4.5\ in$

The spacing of **4.5 in** was chosen to facilitate the construction of the beam.

Appendix E: Calculations for Anchors buckling load

Robot structural from the Autodesk suite, was used to calculate the section properties for the 1/8 in and 1/4 in wall thickness.

The section properties of the 1/8 in wall thickness section was calculated below:

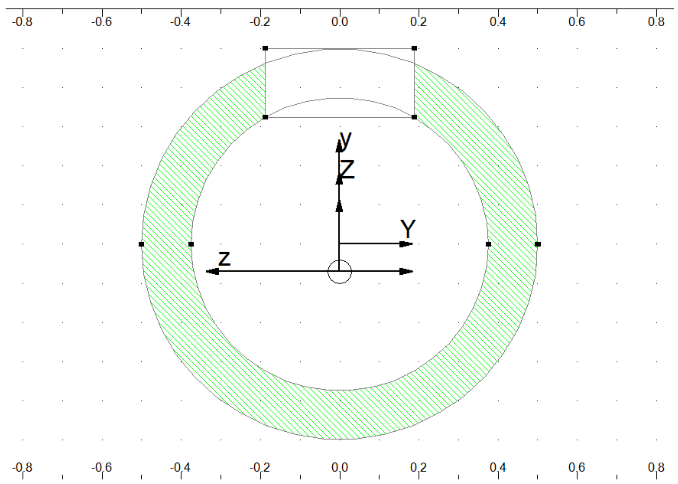

Cross section area:	A	$= 0.295\ in^2$
Center of gravity:	Y_c	$= -0.000$ in
	Z_c	$= -0.070$ in
Young modulus of steel:	E	$= 29{,}000$ ksi
Steel yield strength	Fy	$= 35$ ksi

Calculation made relative to the principal axis:

Quadratic moments:

	I_x	$= 0.001\ in^4$
	I_y	$= 0.033\ in^4$ (This quadratic moment will be used)
	I_z	$= 0.023\ in^4$

Radius of giration:

	r_y	$= 0.334$ in
	r_z	$= 0.281$ in

The 14th edition of the steel construction manual table 4-22, was used for the calculation (American Institute of Steel 2017) of the available critical stress for compression members for a slenderness ratio of : $\frac{kL}{r_y} = \frac{2*11.5}{0.281} \approx 82$

Giving,

ASD: $\frac{F_{cr}}{\Omega_c} = 14.9ksi \rightarrow 4.39\ kips\ \ < 20\ kips\ on\ the\ steel\ pipe$

LRFD: $\phi F_{cr} = 22.3\ ksi$ →6.57 kips < 20 kips on the steel pipe

If the wall thickness is now ¼ in, so two times bigger, the same software (Robot Structural) gave these results:

Cross section area: A = 1.18 in^2

Quadratic moments:

I_y = 0.182 in^4

I_z = 0.231 in^4 (This quadratic moment will be used)

Radius of giration:

r_y = 0.393 in

r_z = 0.442 in

The 14th edition of the steel construction manual table 4-22, was used for the calculation (American Institute of Steel 2017) of the available critical stress for compression members for a slenderness ratio of : $\frac{kL}{r_y} = \frac{2*11.5}{0.393} \approx 59$

Giving

ASD: $\frac{F_{cr}}{\Omega_c} = 17.26\ ksi \rightarrow 20.36\ kips\ \ > 20\ kips\ on\ the\ steel\ pipe$

LRFD: $\phi F_{cr} = 26.5\ ksi$ →31.27 kips > 20 kips on the steel pipe

Appendix F: Jacking load on prestressed beams

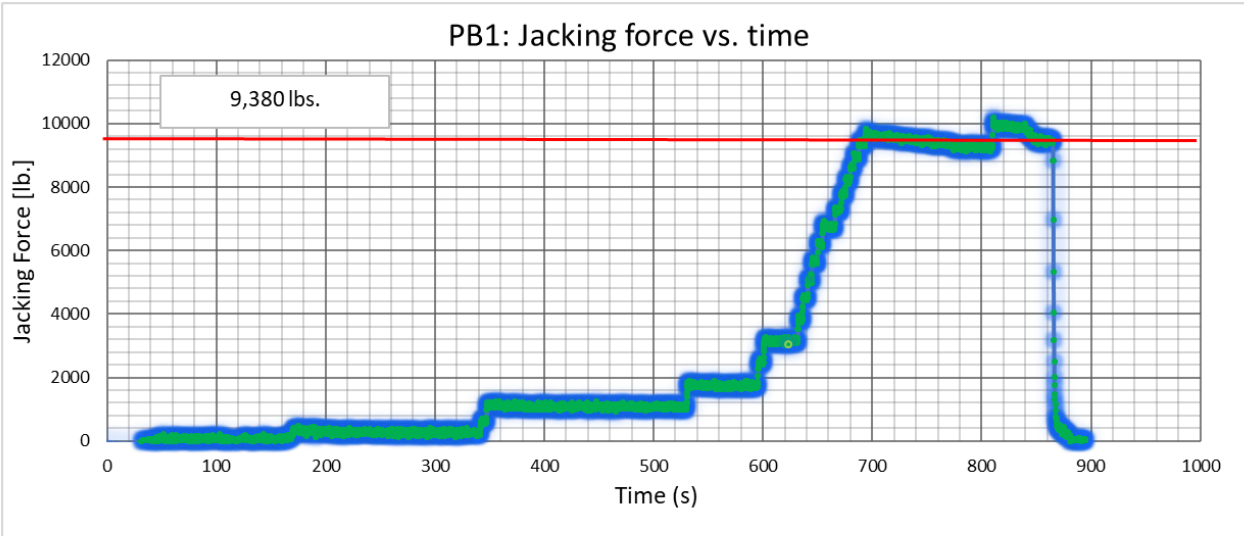

Figure F1: Jacking force vs. time for PB1

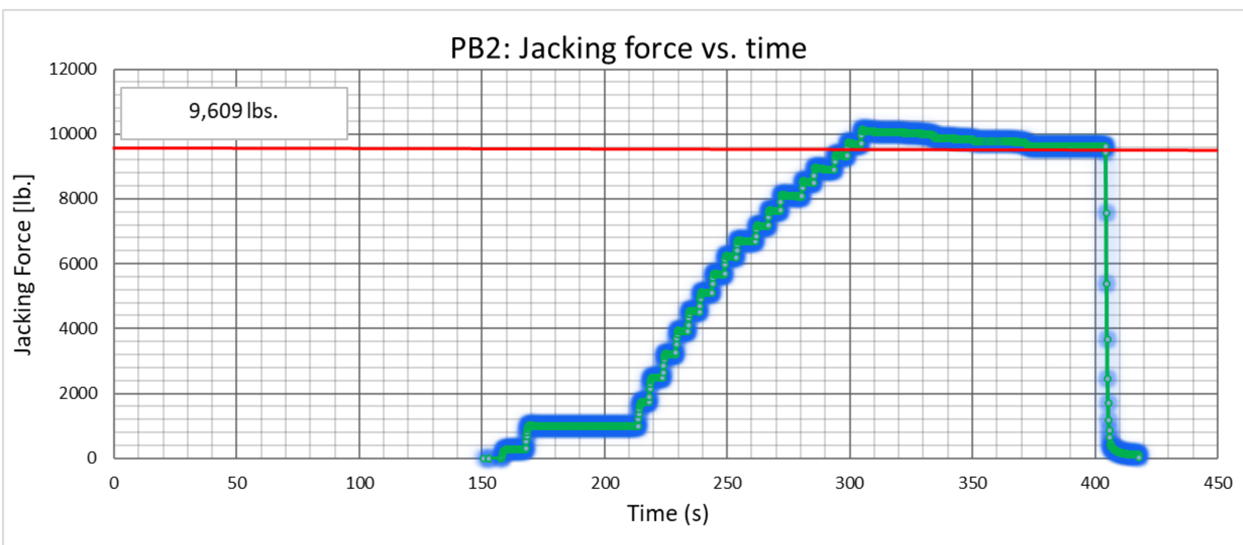

Figure F2: Jacking force vs. time for PB2

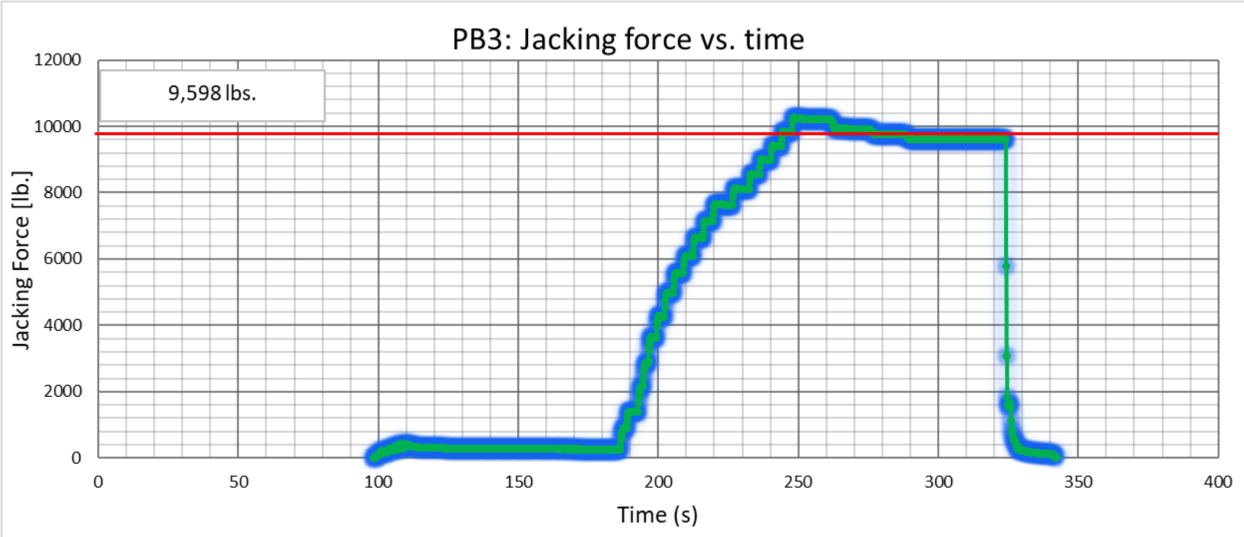

Figure F3: Jacking force vs. time for PB3

Appendix G: Concrete compressive strength

Table G1: Testing Concrete Mix

1 day					
4X8	Compressive force		Stress at failure		Average
C1	58,785	lb	4678	psi	**4548**
C2	56,889	lb	4527	psi	
C3	55,772	lb	4438	psi	
2 days					
4x8	Compressive force		Stress at failure		Average
C1	89,010	lb	7083	psi	**7157**
C2	90,859	lb	7230	psi	
C3	91,904		7313	psi	
3 days					
4X8	Compressive force		Stress at failure		Average
C1	105,403	lb	8388	psi	**8281**
C2	102,720	lb	8174	psi	
7 days					
4x8	Compressive force		Stress at failure		Average
C1	113,441	lb	9027	psi	**9098**
C2	119,271	lb	9491	psi	
C3	110,278	lb	8776	psi	
14 days					
4x8	Compressive force		Stress at failure		Average
C1	103,600	lb	8244	psi	**9184**
C2	118,606	lb	9438	psi	
C3	124,007	lb	9868	psi	
28 days					
4x8	Compressive force		Stress at failure		Average
C1	127,925	lb	10180	psi	**10085**
C2	127,088	lb	10113	psi	
C3	125,182	lb	9962	psi	

Table G2: 1st Concrete Mix

24h					
4X8	Compressive force		Stress at failure		Average
C1	66,509	lb	5293	psi	5337
C2	66,398	lb	5284	psi	
C3	68,282	lb	5434	psi	
At release = 28h					
4x8	Compressive force		Stress at failure		Average
C1	73,802	lb	5873	psi	5880
C2	73,982	lb	5887	psi	
C3	78,390	lb	6238	psi	
72h					
4X8	Compressive force		Stress at failure		Average
C1	88,513	lb	7044	psi	7405
C2	93,420	lb	7434	psi	
C3	97,241	lb	7738	psi	
7 days					
4x8	Compressive force		Stress at failure		Average
C1	103,445	lb	8232	psi	8363
C2	106,744	lb	8494	psi	
C3		lb	0	psi	
14 days					
4x8	Compressive force		Stress at failure		Average
C1	112,852	lb	8980	psi	8974
C2	111,448	lb	8869	psi	
C3	113,998	lb	9072	psi	
28 days					
4x8	Compressive force		Stress at failure		Average
C1	111,534	lb	8892	psi	9039
C2	117,271	lb	9332	psi	
C3	111,743	lb	8892	psi	
Testing day=72 days					
4x8	Compressive force		Stress at failure		Average
C1	126,773	lb	9295	psi	9396
C2	120,606	lb	9598	psi	
C3	116,809	lb	9295	psi	

Table G3: 2^{nd} Concrete Mix

19h18min					
4X8	Compressive force		Stress at failure		Average
C1	84,862	lb	6753	psi	6892
C2	89,120	lb	7092	psi	
C3	85,836	lb	6831	psi	
At release= 21h21min					
4x8	Compressive force		Stress at failure		Average
C1	87,836	lb	6990	psi	6996
C2	87,999	lb	7003	psi	
C3	82,854	lb	6593	psi	
48h					
4X8	Compressive force		Stress at failure		Average
C1	115,974	lb	9229	psi	9245
C2	116,705	lb	9287	psi	
C3	115,862	lb	9220	psi	
7 days					
4x8	Compressive force		Stress at failure		Average
C1	118,359	lb	9419	psi	10249
C2	139,216	lb	11078	psi	
C3	94,392	lb	7511	psi	
14 days					
4x8	Compressive force		Stress at failure		Average
C1	133,185	lb	10599	psi	10847
C2	144,470	lb	11497	psi	
C3	131,257	lb	10445	psi	
28 days					
4x8	Compressive force		Stress at failure		Average
C1	148,519	lb	11819	psi	11605
C2	143,795	lb	11443	psi	
C3	145,182	lb	11553	psi	
Testing day=58 days					
4x8	Compressive force		Stress at failure		Average
C1	158,898	lb	11631	psi	11749
C2	150,599	lb	11984	psi	
C3	146,156	lb	11631	psi	

Table G4: 3rd Concrete Mix

17h 45 min					
4X8	Compressive force		Stress at failure		Average
C1	56,793	lb	4519	psi	4673
C2	58,827	lb	4681	psi	
C3	60,542	lb	4818	psi	
20 h					
4x8	Compressive force		Stress at failure		Average
C1	58,397	lb	4647	psi	5518
C2	70,140	lb	5582	psi	
C3	68,530	lb	5453	psi	
At release= 23 h					
4X8	Compressive force		Stress at failure		Average
C1	78,140	lb	6218	psi	6452
C2	79,264	lb	6308	psi	
C3	85,845	lb	6831	psi	
7 days					
4x8	Compressive force		Stress at failure		Average
C1	116,735	lb	9289	psi	9540
C2	123,255	lb	9808	psi	
C3	119,645	lb	9521	psi	
14 days					
4x8	Compressive force		Stress at failure		Average
C1	133,055	lb	10588	psi	10188
C2	119,057	lb	9474	psi	
C3	131,948	lb	10500	psi	
28 days					
4x8	Compressive force		Stress at failure		Average
C1	140,046	lb	11145	psi	11080
C2	139,304	lb	11085	psi	
C3	138,370	lb	11011	psi	
Testing day= 49 days					
4x8	Compressive force		Stress at failure		Average
C1	139,356	lb	11568	psi	11456
C2	141,163	lb	11233	psi	
C3	145,368	lb	11568	psi	

Appendix H: DEMEC MEASUREMENTS

Table H1: DEMEC points measurements for PB1

Dead End											Live End									
Di	Di+1	R1	R2	R3	Average	ε		ε,avg			Di	Di+1	R1	R2	R3	Average	ε		ε,avg	
1	3	12.20	12.20	12.20	12.20	ε 1-3=	0.0095648	ε avg1=	8.51E-03	t=0- Before releasing prestress	1	3	10.55	10.54	10.56	10.55	ε 1-3=	0.0082712	ε avg1=	7.92E-03
2	4	9.50	9.50	9.50	9.50	ε 2-4=	0.0074480	ε avg2=	8.23E-03		2	4	9.65	9.66	9.67	9.66	ε 2-4=	0.0075734	ε avg2=	6.86E-03
3	5	9.81	9.79	9.81	9.80	ε 3-5=	0.0076858	ε avg3=	7.41E-03		3	5	6.02	6.03	6.04	6.03	ε 3-5=	0.0047275	ε avg3=	6.32E-03
4	6	9.07	9.07	9.07	9.07	ε 4-6=	0.0071109	ε avg4=	6.87E-03		4	6	8.5	8.49	8.51	8.50	ε 4-6=	0.0066640	ε avg4=	6.75E-03
5	7	7.39	7.40	7.40	7.40	ε 5-7=	0.0057990	ε avg5=	6.42E-03		5	7	11.3	11.30	11.31	11.30	ε 5-7=	0.0088618	ε avg5=	7.62E-03
6	8	8.08	8.09	8.10	8.09	ε 6-8=	0.0063426	ε avg6=	6.29E-03		6	8	9.34	9.35	9.35	9.35	ε 6-8=	0.0073278	ε avg6=	8.65E-03
7	9	8.58	8.56	8.57	8.57	ε 7-9=	0.0067189	ε avg7=	6.53E-03		7	9	12.46	12.45	12.44	12.45	ε 7-9=	0.0097608	ε avg7=	8.54E-03

Dead End											Live End									
Di	Di+1	R1	R2	R3	Average	ε		ε,avg			Di	Di+1	R1	R2	R3	Average	ε		ε,avg	
1	3	11.87	11.93	11.93	11.91	ε 1-3=	0.0093374	ε avg1=	8.26E-03	t=0+ After releasing prestress	1	3	10.34	10.33	10.33	10.33	ε 1-3=	0.0081013	ε avg1=	7.70E-03
2	4	9.15	9.16	9.17	9.16	ε 2-4=	0.0071814	ε avg2=	7.95E-03		2	4	9.30	9.30	9.30	9.30	ε 2-4=	0.0072912	ε avg2=	6.64E-03
3	5	9.35	9.36	9.37	9.36	ε 3-5=	0.0073382	ε avg3=	7.10E-03		3	5	5.72	5.80	5.80	5.77	ε 3-5=	0.0045263	ε avg3=	6.07E-03
4	6	8.65	8.66	8.64	8.65	ε 4-6=	0.0067816	ε avg4=	6.53E-03		4	6	8.13	8.14	8.14	8.14	ε 4-6=	0.0063791	ε avg4=	6.50E-03
5	7	6.98	6.97	6.97	6.97	ε 5-7=	0.0054671	ε avg5=	6.09E-03		5	7	10.96	10.97	10.98	10.97	ε 5-7=	0.0086005	ε avg5=	7.43E-03
6	8	7.68	7.67	7.67	7.67	ε 6-8=	0.0060159	ε avg6=	5.94E-03		6	8	9.98	8.97	8.97	9.31	ε 6-8=	0.0072964	ε avg6=	8.47E-03
7	9	8.10	8.10	8.09	8.10	ε 7-9=	0.0063478	ε avg7=	6.18E-03		7	9	12.15	12.12	12.13	12.13	ε 7-9=	0.0095125	ε avg7=	8.40E-03

Dead End											Live End									
Di	Di+1	R1	R2	R3	Average	ε		ε,avg			Di	Di+1	R1	R2	R3	Average	ε		ε,avg	
1	3	11.73	11.75	11.74	11.74	ε 1-3=	0.0092042	ε avg1=	8.08E-03	t=24h After releasing prestress	1	3	10.20	10.17	10.20	10.19	ε 1-3=	0.0079890	ε avg1=	7.57E-03
2	4	8.92	8.88	8.85	8.88	ε 2-4=	0.0069645	ε avg2=	7.84E-03		2	4	9.15	9.13	9.11	9.13	ε 2-4=	0.0071579	ε avg2=	6.50E-03
3	5	9.98	9.00	9.10	9.36	ε 3-5=	0.0073382	ε avg3=	6.95E-03		3	5	5.54	5.56	5.57	5.56	ε 3-5=	0.0043564	ε avg3=	5.81E-03
4	6	8.4	8.33	8.35	8.36	ε 4-6=	0.0065542	ε avg4=	6.39E-03		4	6	7.58	7.55	7.56	7.56	ε 4-6=	0.0059297	ε avg4=	6.24E-03
5	7	6.73	6.74	6.73	6.73	ε 5-7=	0.0052789	ε avg5=	5.89E-03		5	7	10.78	10.76	10.75	10.76	ε 5-7=	0.0084385	ε avg5=	7.09E-03
6	8	7.42	7.47	7.42	7.44	ε 6-8=	0.0058303	ε avg6=	5.76E-03		6	8	8.80	8.78	8.81	8.80	ε 6-8=	0.0068966	ε avg6=	8.22E-03
7	9	7.86	7.87	7.86	7.86	ε 7-9=	0.0061649	ε avg7=	6.00E-03		7	9	11.87	11.87	11.89	11.88	ε 7-9=	0.0093113	ε avg7=	8.10E-03

Dead End											Live End									
Di	Di+1	R1	R2	R3	Average	ε		ε,avg			Di	Di+1	R1	R2	R3	Average	ε		ε,avg	
1	3	11.6	11.59	11.61	11.60	ε 1-3=	0.0090944	ε avg1=	7.95E-03	t=7 daysAfter releasing prestress	1	3	9.97	9.99	9.98	9.98	ε 1-3=	0.0078243	ε avg1=	7.41E-03
2	4	8.65	8.68	8.72	8.68	ε 2-4=	0.0068077	ε avg2=	7.63E-03		2	4	8.93	8.91	8.90	8.91	ε 2-4=	0.0069881	ε avg2=	6.59E-03
3	5	8.90	8.92	8.92	8.91	ε 3-5=	0.0069881	ε avg3=	6.78E-03		3	5	6.31	6.32	6.33	6.32	ε 3-5=	0.0049549	ε avg3=	6.02E-03
4	6	8.35	8.33	8.36	8.35	ε 4-6=	0.0065438	ε avg4=	6.24E-03		4	6	7.80	7.79	7.78	7.79	ε 4-6=	0.0061074	ε avg4=	6.45E-03
5	7	6.61	6.62	6.62	6.62	ε 5-7=	0.0051875	ε avg5=	5.80E-03		5	7	10.56	10.58	10.55	10.56	ε 5-7=	0.0082817	ε avg5=	7.04E-03
6	8	7.22	7.23	7.23	7.23	ε 6-8=	0.0056657	ε avg6=	5.53E-03		6	8	8.59	8.60	8.57	8.59	ε 6-8=	0.0067319	ε avg6=	8.06E-03
7	9	7.66	6.65	7.65	7.32	ε 7-9=	0.0057389	ε avg7=	5.70E-03		7	9	11.68	11.68	11.66	11.67	ε 7-9=	0.0091519	ε avg7=	7.94E-03

Dead End											Live End									
Di	Di+1	R1	R2	R3	Average	ε		ε,avg			Di	Di+1	R1	R2	R3	Average	ε		ε,avg	
1	3	11.44	11.45	11.44	11.44	ε 1-3=	0.0089716	ε avg1=	7.80E-03	t=14 days after releasing prestress	1	3	9.88	8.86	9.86	9.53	ε 1-3=	0.0074741	ε avg1=	7.16E-03
2	4	8.43	8.45	8.46	8.45	ε 2-4=	0.0066222	ε avg2=	7.45E-03		2	4	8.74	8.73	8.73	8.73	ε 2-4=	0.0068469	ε avg2=	6.10E-03
3	5	8.64	8.63	8.63	8.63	ε 3-5=	0.0067685	ε avg3=	6.57E-03		3	5	5.07	5.07	5.06	5.07	ε 3-5=	0.0039723	ε avg3=	5.58E-03
4	6	8.05	8.07	8.08	8.07	ε 4-6=	0.0063243	ε avg4=	6.02E-03		4	6	7.57	7.56	7.58	7.57	ε 4-6=	0.0059349	ε avg4=	6.01E-03
5	7	6.33	6.34	6.31	6.33	ε 5-7=	0.0049601	ε avg5=	5.59E-03		5	7	10.36	10.37	10.36	10.36	ε 5-7=	0.0081249	ε avg5=	6.88E-03
6	8	7	6.99	6.99	6.99	ε 6-8=	0.0054828	ε avg6=	5.42E-03		6	8	8.41	8.40	8.42	8.41	ε 6-8=	0.0065934	ε avg6=	7.90E-03
7	9	7.43	7.44	7.43	7.43	ε 7-9=	0.0058277	ε avg7=	5.66E-03		7	9	11.46	11.47	11.48	11.47	ε 7-9=	0.0089925	ε avg7=	7.79E-03

Dead End											Live End									
Di	Di+1	R1	R2	R3	Average	ε		ε,avg			Di	Di+1	R1	R2	R3	Average	ε		ε,avg	
1	3	11.65	11.66	11.66	11.66	ε 1-3=	0.0091388	ε avg1=	7.96E-03	t=28 days after releasing prestress	1	3	9.05	9.08	9.08	9.07	ε 1-3=	0.0071096	ε avg1=	7.04E-03
2	4	8.65	8.62	8.70	8.66	ε 2-4=	0.0067868	ε avg2=	7.61E-03		2	4	8.93	8.87	8.90	8.90	ε 2-4=	0.0069776	ε avg2=	6.33E-03
3	5	8.81	8.82	8.82	8.82	ε 3-5=	0.0069123	ε avg3=	6.72E-03		3	5	6.25	6.27	6.26	6.26	ε 3-5=	0.0049078	ε avg3=	5.98E-03
4	6	8.22	8.25	8.23	8.23	ε 4-6=	0.0064549	ε avg4=	6.16E-03		4	6	7.73	7.75	7.73	7.74	ε 4-6=	0.0060655	ε avg4=	6.40E-03
5	7	6.5	6.55	6.52	6.52	ε 5-7=	0.0051143	ε avg5=	5.73E-03		5	7	10.50	10.53	10.48	10.50	ε 5-7=	0.0082346	ε avg5=	7.01E-03
6	8	7.15	7.16	7.15	7.15	ε 6-8=	0.0056082	ε avg6=	5.56E-03		6	8	8.57	8.58	8.56	8.57	ε 6-8=	0.0067189	ε avg6=	8.03E-03
7	9	7.6	7.62	7.61	7.61	ε 7-9=	0.0059662	ε avg7=	5.79E-03		7	9	11.62	11.65	11.68	11.65	ε 7-9=	0.0091336	ε avg7=	7.93E-03

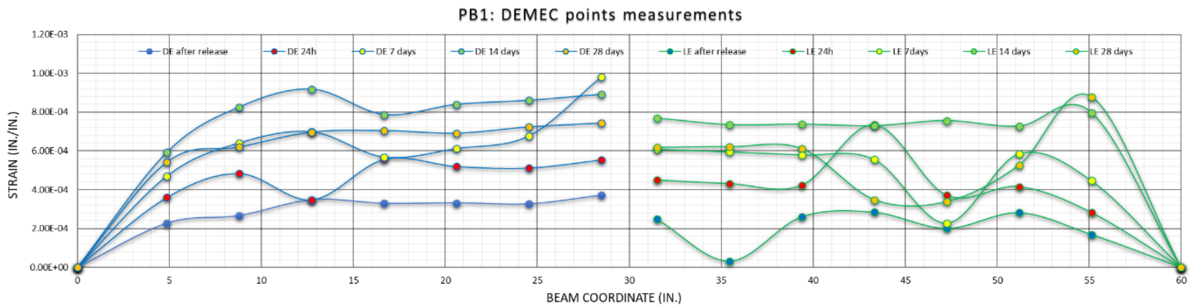

Figure H1: DEMEC points measurements for PB1

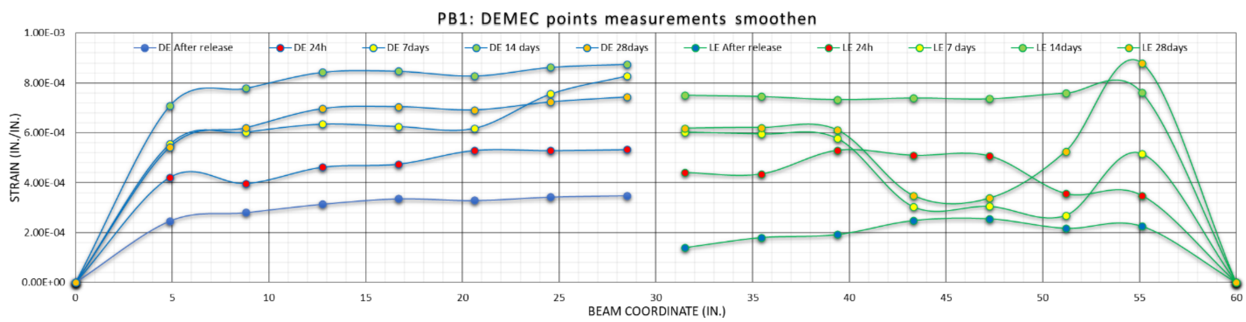

Figure H2: DEMEC points measurements smoothen for PB1 (95% average maximum strain method)

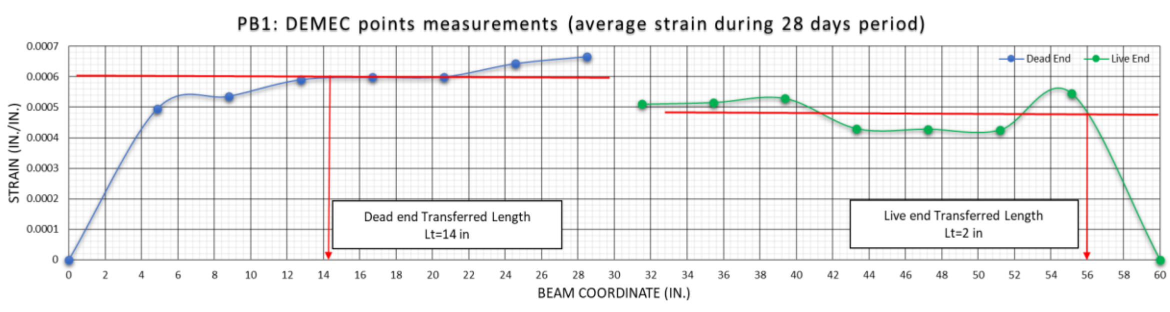

Figure H3: DEMEC points measurements for PB1 (average strain during 28 days period)

The following figures show how the transfer length was evaluated using 95% average maximum strain method:

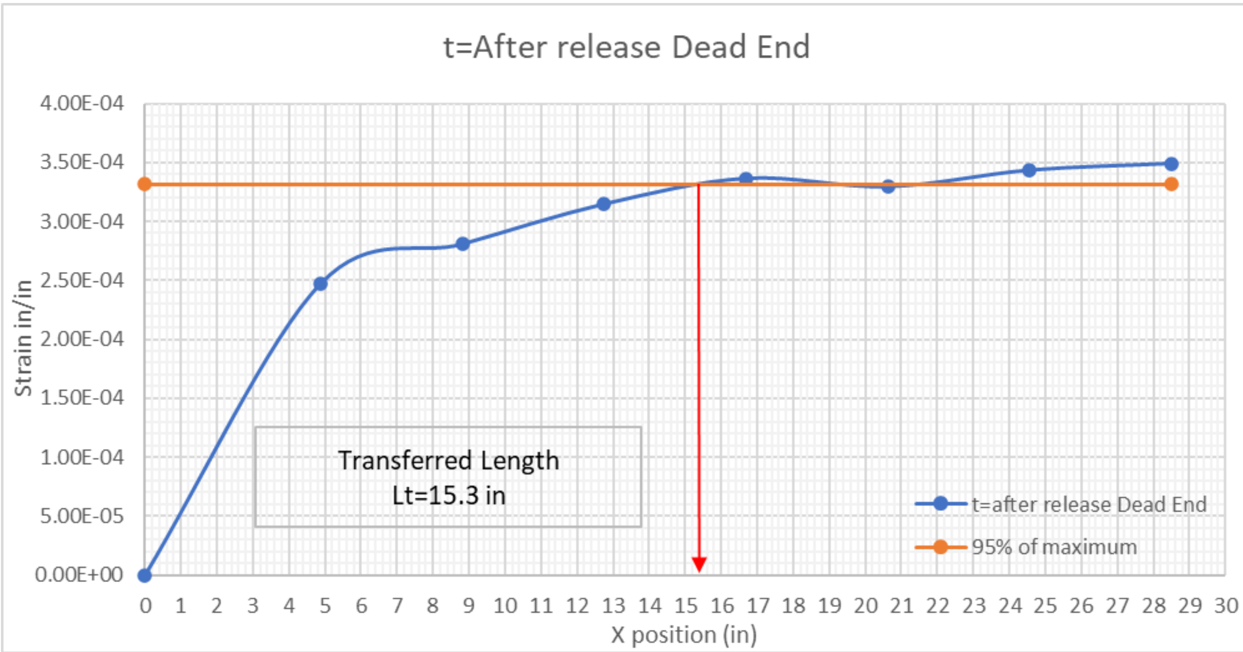

Figure H4: Evaluation of transfer length at the time of prestress release (Dead End)

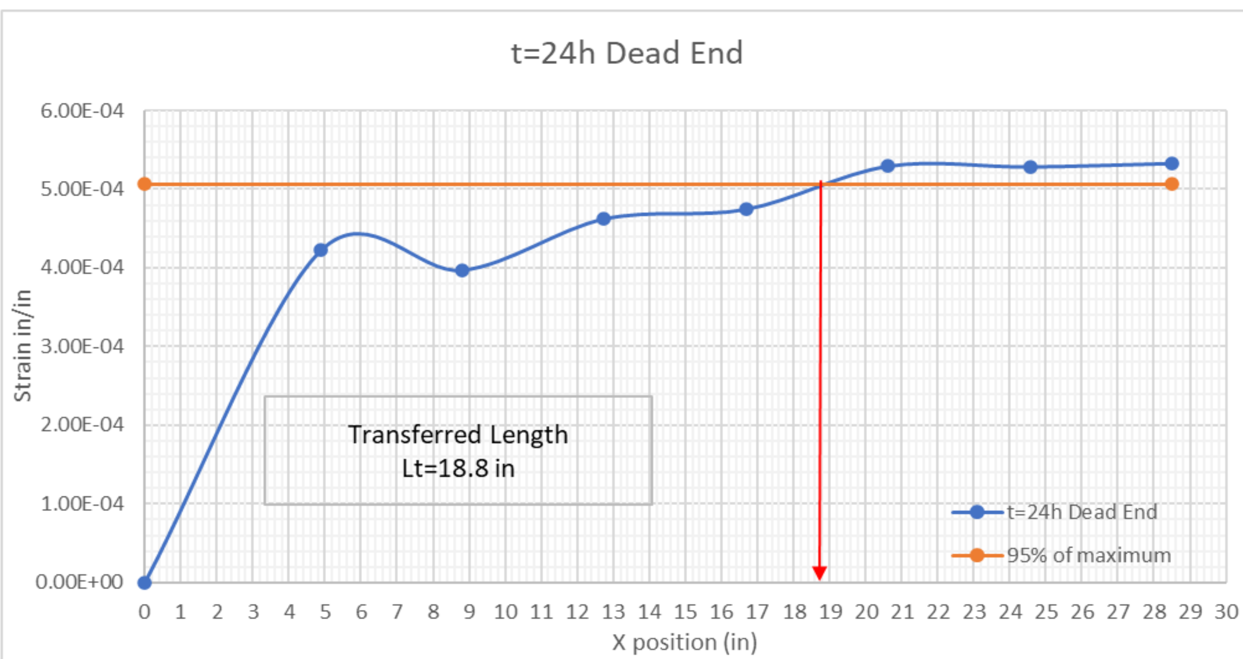

Figure H5: Evaluation of transfer length 24 hours after prestress release (Dead End)

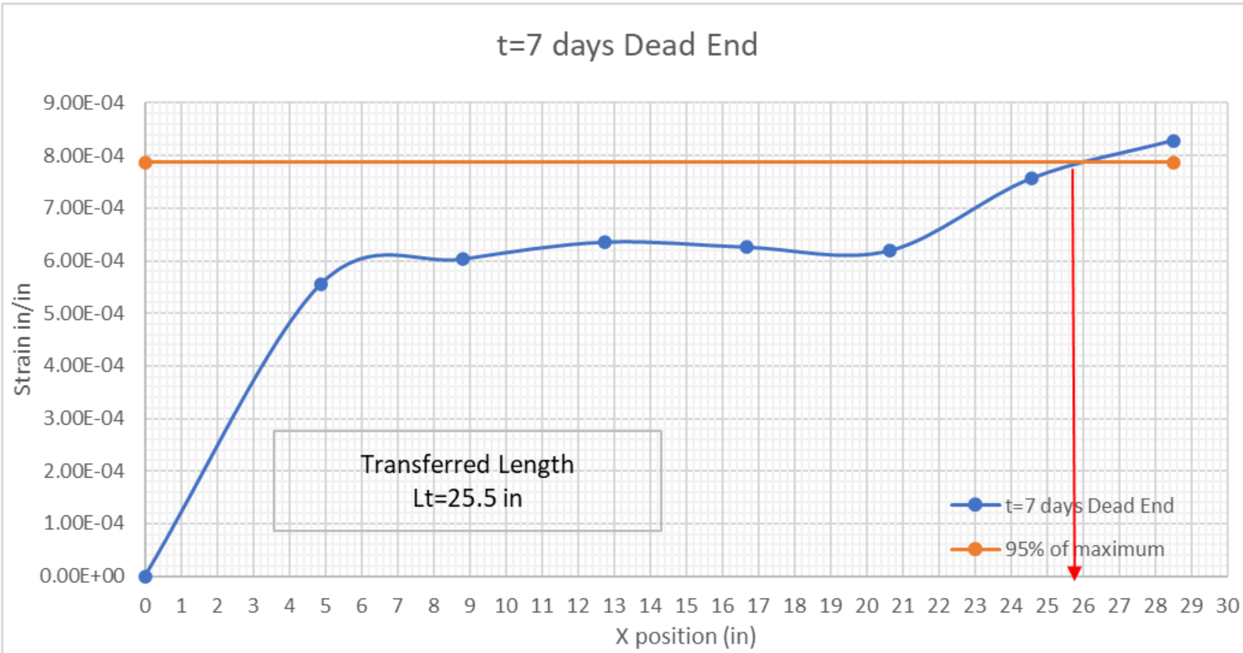

Figure H6: Evaluation of transfer length 7 days after prestress release (Dead End)

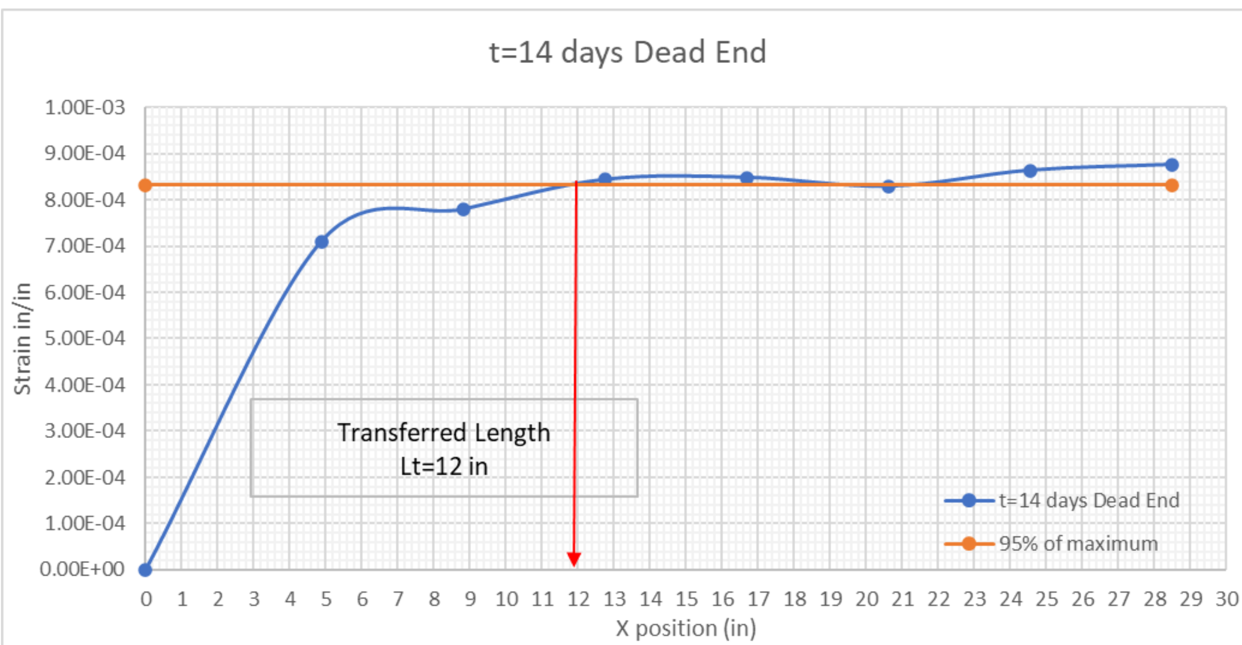

Figure H7: Evaluation of transfer length 14 days after prestress release (Dead End)

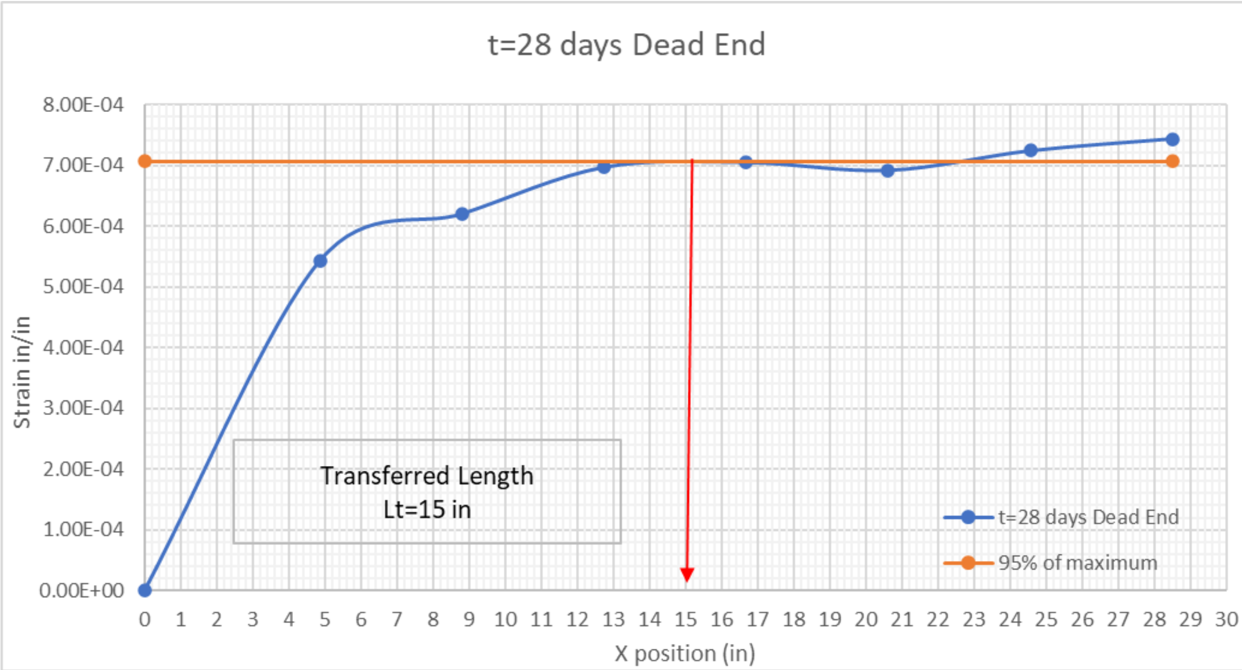

Figure H8: Evaluation of transfer length 28 days after prestress release (Dead End)

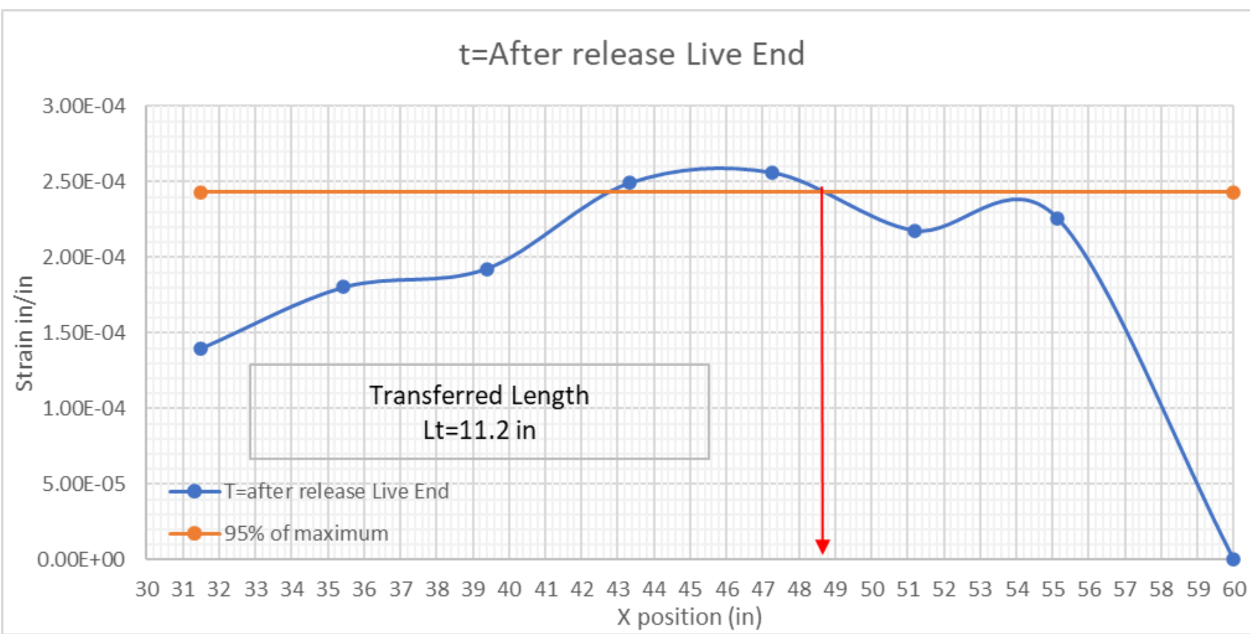

Figure H9: Evaluation of transfer length at the time of prestress release (Live End)

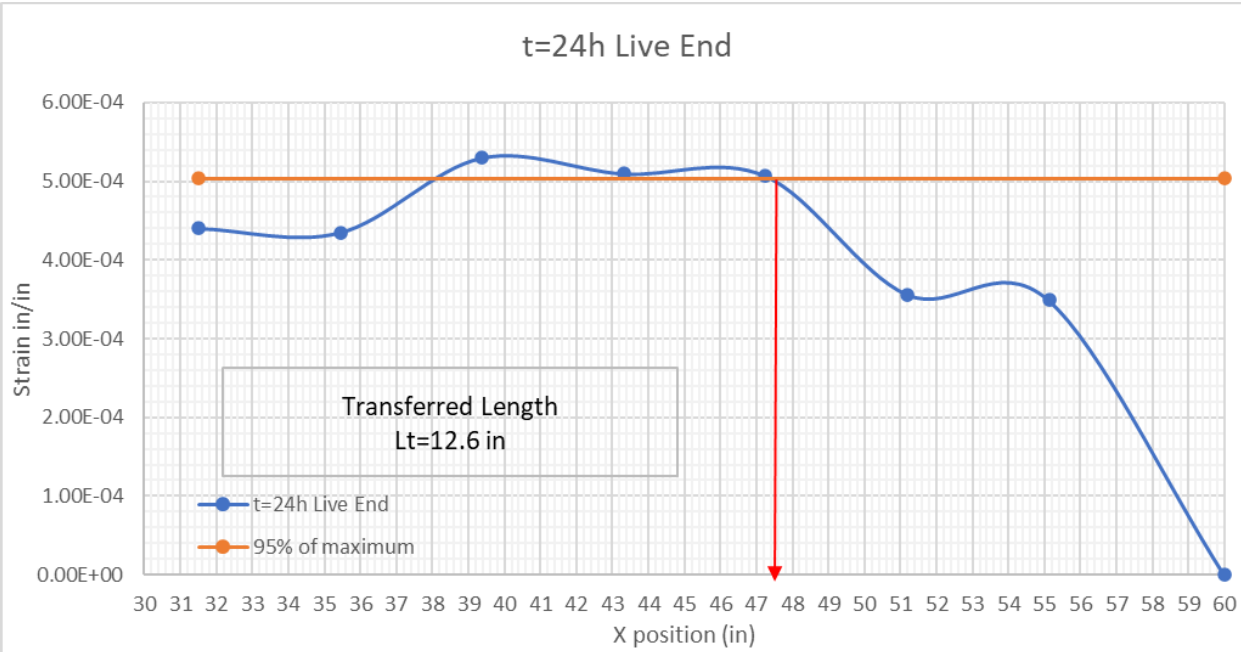

Figure H10: Evaluation of transfer length 24 hours after prestress release (Live End)

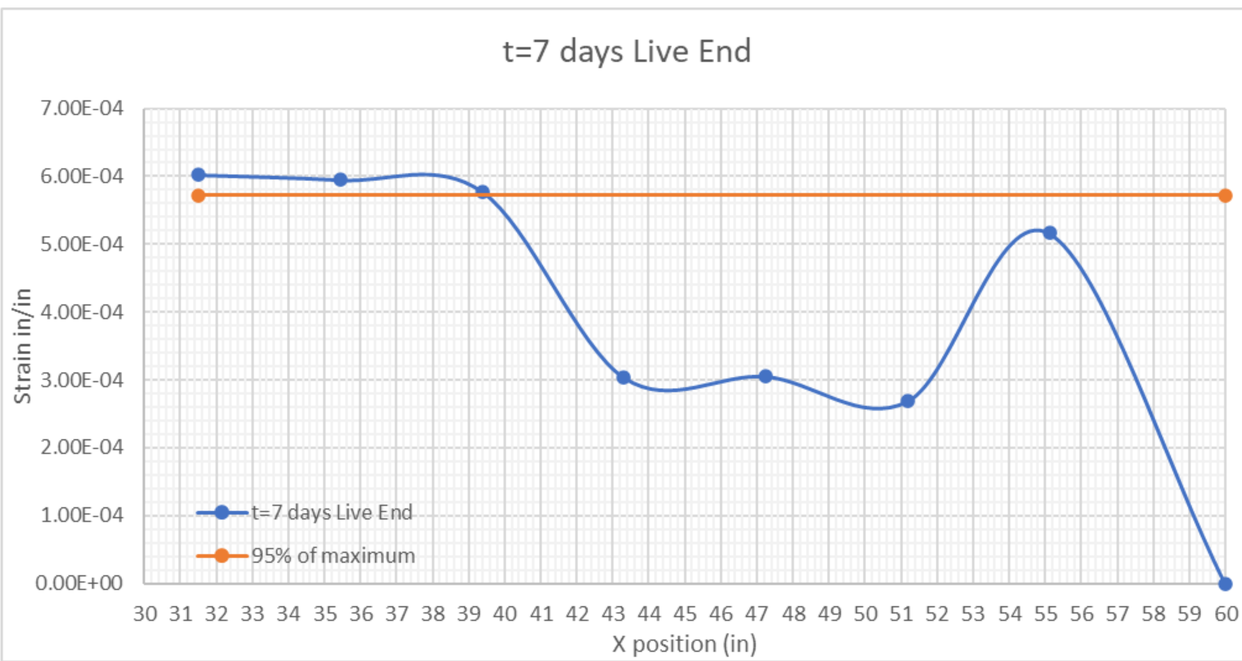

Figure H11: Evaluation of transfer length 7 days after prestress release (Live End)

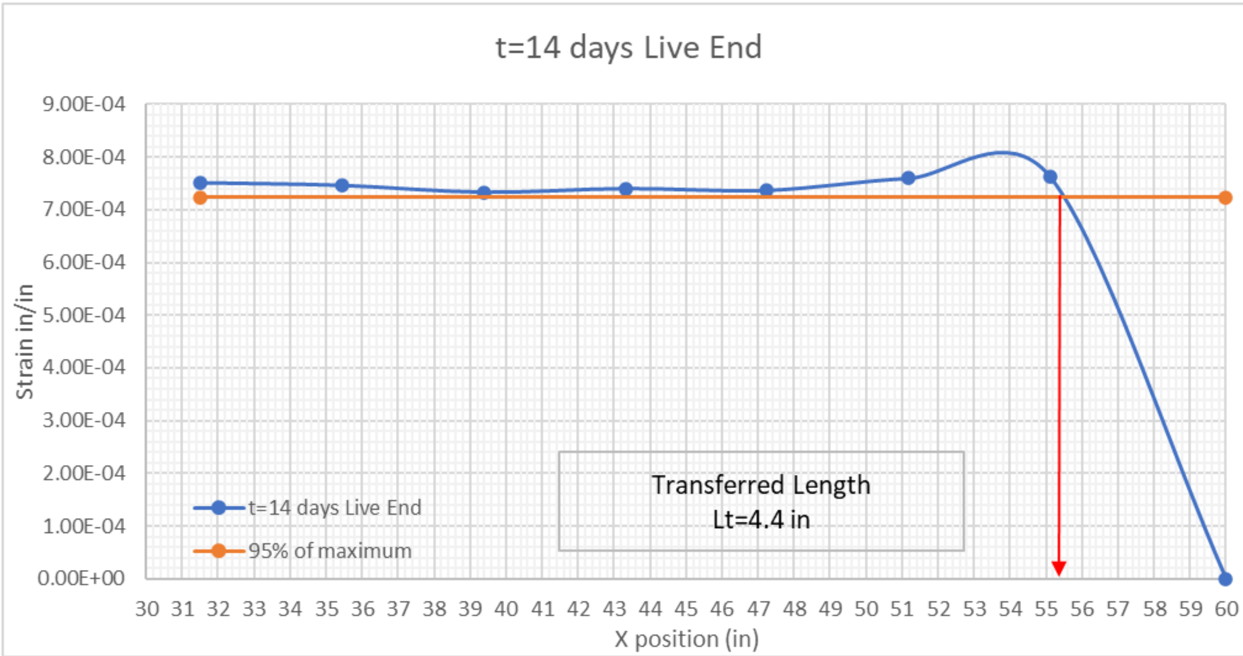

Figure H12: Evaluation of transfer length 14 days after prestress release (Live End)

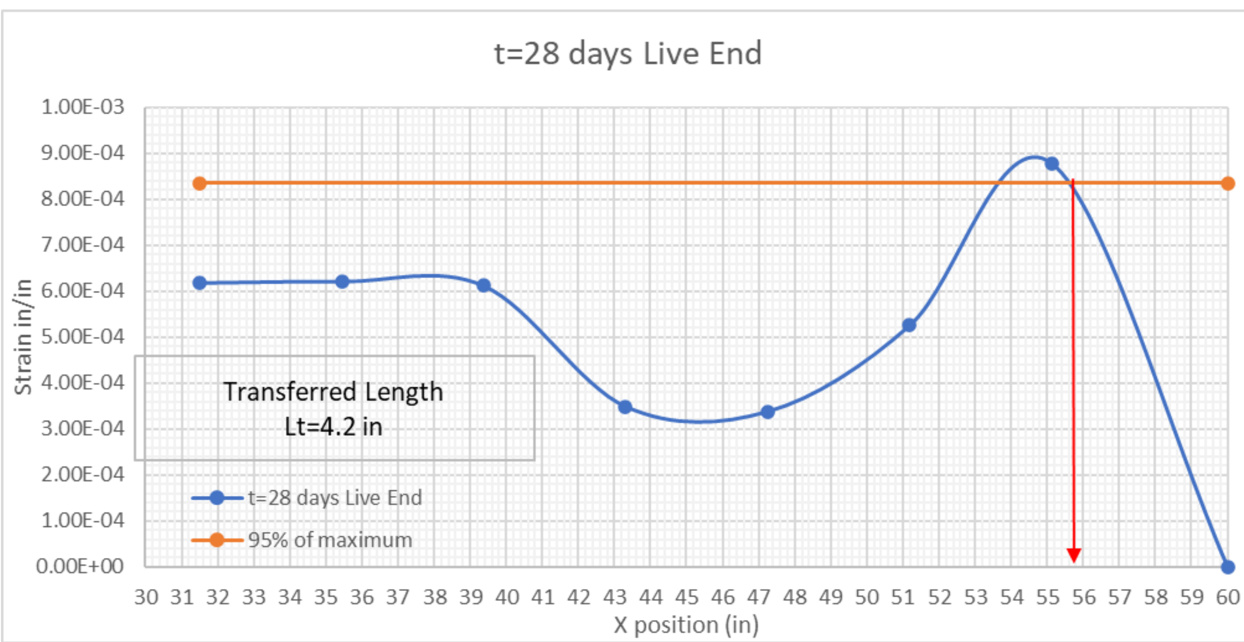

Figure H13: Evaluation of transfer length 28 after prestress release (Live End)

Table H2: DEMEC points measurements for PB2

PB2: DEMEC MEASUREMENTS

Dead End											Live End									
Di	Di+1	R1	R2	R3	Average	ε		ε,avg			Di	Di+1	R1	R2	R3	Average	ε		ε,avg	
1	3	10.89	10.88	10.88	10.88	**ε 1-3=**	0.008533	**ε avg1=**	0.007864	t=0- Before releasing prestress	1	3	9.97	9.97	9.97	9.97	**ε 1-3=**	0.00781648	**ε avg1=**	0.00724547
2	4	9.18	9.17	9.18	9.18	**ε 2-4=**	0.007195	**ε avg2=**	0.006721		2	4	8.52	8.51	8.51	8.51	**ε 2-4=**	0.00667445	**ε avg2=**	0.00850379
3	5	5.65	5.67	5.65	5.66	**ε 3-5=**	0.004435	**ε avg3=**	0.005958		3	5	14.07	14.05	14.05	14.06	**ε 3-5=**	0.01102043	**ε avg3=**	0.00902210
4	6	7.96	7.98	7.95	7.96	**ε 4-6=**	0.006243	**ε avg4=**	0.007187		4	6	11.96	11.95	11.95	11.95	**ε 4-6=**	0.00937141	**ε avg4=**	0.00828862
5	7	13.88	13.88	13.88	13.88	**ε 5-7=**	0.010882	**ε avg5=**	0.008322		5	7	0	0.00	0.00	0.00	**ε 5-7=**		**ε avg5=**	
6	8	10.00	10.00	10.00	10.00	**ε 6-8=**	0.007840	**ε avg6=**	0.009147		6	8	5.7	5.71	5.71	5.71	**ε 6-8=**	0.00447403	**ε avg6=**	0.00760480
7	9	11.14	11.10	11.12	11.12	**ε 7-9=**	0.008718	**ε avg7=**	0.008279		7	9	11.44	11.44	11.44	11.44	**ε 7-9=**	0.00896896	**ε avg7=**	0.00672149

Dead End											Live End									
Di	Di+1	R1	R2	R3	Average	ε		ε,avg			Di	Di+1	R1	R2	R3	Average	ε		ε,avg	
1	3	10.65	10.67	10.67	10.66	**ε 1-3=**	0.008360	**ε avg1=**	0.007652	t=0+ After releasing prestress	1	3	8.91	8.90	8.89	8.90	**ε 1-3=**	0.00697760	**ε avg1=**	0.00678813
2	4	8.85	8.87	8.85	8.86	**ε 2-4=**	0.006944	**ε avg2=**	0.006489		2	4	8.40	8.42	8.43	8.42	**ε 2-4=**	0.00659867	**ε avg2=**	0.00843148
3	5	5.30	5.31	5.32	5.31	**ε 3-5=**	0.004163	**ε avg3=**	0.005691		3	5	14.95	14.92	14.97	14.95	**ε 3-5=**	0.01171819	**ε avg3=**	0.00915189
4	6	7.61	7.62	7.60	7.61	**ε 4-6=**	0.005966	**ε avg4=**	0.006911		4	6	11.65	11.66	11.66	11.66	**ε 4-6=**	0.00913883	**ε avg4=**	0.00837835
5	7	13.52	13.55	13.50	13.52	**ε 5-7=**	0.010602	**ε avg5=**	0.008019		5	7	0	0.00	0.00	0.00	**ε 5-7=**		**ε avg5=**	
6	8	9.55	9.60	9.50	9.55	**ε 6-8=**	0.007487	**ε avg6=**	0.008869		6	8	5.45	5.46	5.46	5.46	**ε 6-8=**	0.00427803	**ε avg6=**	0.00738354
7	9	10.84	10.85	10.90	10.86	**ε 7-9=**	0.008517	**ε avg7=**	0.008002		7	9	11.14	11.14	11.14	11.14	**ε 7-9=**	0.00873376	**ε avg7=**	0.00650589

Dead End											Live End									
Di	Di+1	R1	R2	R3	Average	ε		ε,avg			Di	Di+1	R1	R2	R3	Average	ε		ε,avg	
1	3	10.52	10.54	10.54	10.53	**ε 1-3=**	0.008258	**ε avg1=**	0.00752	t=24h after prestress releasing	1	3	8.80	8.79	8.79	8.79	**ε 1-3=**	0.00689397	**ε avg1=**	0.00666400
2	4	8.65	8.64	8.64	8.64	**ε 2-4=**	0.006776	**ε avg2=**	0.00635		2	4	8.22	8.20	8.20	8.21	**ε 2-4=**	0.00643403	**ε avg2=**	0.00830256
3	5	5.12	5.14	5.14	5.13	**ε 3-5=**	0.004025	**ε avg3=**	0.00553		3	5	14.75	14.76	14.80	14.77	**ε 3-5=**	0.01157968	**ε avg3=**	0.00899509
4	6	7.38	7.39	7.39	7.39	**ε 4-6=**	0.005791	**ε avg4=**	0.00677		4	6	11.45	11.44	11.44	11.44	**ε 4-6=**	0.00897157	**ε avg4=**	0.00819193
5	7	13.4	13.38	13.40	13.39	**ε 5-7=**	0.010500	**ε avg5=**	0.00788		5	7	0.00	0.00	0.00	0.00	**ε 5-7=**		**ε avg5=**	
6	8	9.43	9.32	9.35	9.37	**ε 6-8=**	0.007343	**ε avg6=**	0.00873		6	8	5.15	5.10	5.15	5.13	**ε 6-8=**	0.00402453	**ε avg6=**	0.00719015
7	9	10.64	10.66	10.67	10.66	**ε 7-9=**	0.008355	**ε avg7=**	0.00785		7	9	10.93	10.94	10.94	10.94	**ε 7-9=**	0.00857435	**ε avg7=**	0.00629944

Dead End											Live End									
Di	Di+1	R1	R2	R3	Average	ε		ε,avg			Di	Di+1	R1	R2	R3	Average	ε		ε,avg	
1	3	10.38	10.4	10.36	10.38	**ε 1-3=**	0.008138	**ε avg1=**	0.00738136	t=7 days after prestress releasing	1	3	8.68	8.67	8.68	8.68	**ε 1-3=**	0.00680251	**ε avg1=**	0.00655947
2	4	8.46	8.44	8.45	8.45	**ε 2-4=**	0.006625	**ε avg2=**	0.00621015		2	4	8.06	8.05	8.06	8.06	**ε 2-4=**	0.00631643	**ε avg2=**	0.00792624
3	5	4.94	4.93	4.93	4.93	**ε 3-5=**	0.003868	**ε avg3=**	0.00539653		3	5	13.59	13.58	13.62	13.60	**ε 3-5=**	0.01065979	**ε avg3=**	0.00861355
4	6	7.28	7.25	7.27	7.27	**ε 4-6=**	0.005697	**ε avg4=**	0.00665180		4	6	11.33	11.30	11.29	11.31	**ε 4-6=**	0.00886443	**ε avg4=**	0.00782868
5	7	13.25	13.23	13.28	13.25	**ε 5-7=**	0.010391	**ε avg5=**	0.00777728		5	7	0.00	0.00	0.00	0.00	**ε 5-7=**		**ε avg5=**	
6	8	9.25	9.24	9.23	9.24	**ε 6-8=**	0.007244	**ε avg6=**	0.00864142		6	8	5.04	5.05	5.07	5.05	**ε 6-8=**	0.00396181	**ε avg6=**	0.00712308
7	9	10.55	10.60	10.57	10.57	**ε 7-9=**	0.008289	**ε avg7=**	0.00776683		7	9	10.91	10.90	10.88	10.90	**ε 7-9=**	0.00854299	**ε avg7=**	0.00625240

Dead End											Live End									
Di	Di+1	R1	R2	R3	Average	ε		ε,avg			Di	Di+1	R1	R2	R3	Average	ε		ε,avg	
1	3	11.43	11.45	11.45	11.44	**ε 1-3=**	0.008972	**ε avg1=**	0.00782432	t=14 days after prestress releasing	1	3	8.67	8.70	8.08	8.48	**ε 1-3=**	0.00665093	**ε avg1=**	0.00649805
2	4	8.52	8.49	8.54	8.52	**ε 2-4=**	0.006677	**ε avg2=**	0.00651243		2	4	8.10	8.08	8.10	8.09	**ε 2-4=**	0.00634517	**ε avg2=**	0.00788356
3	5	4.96	4.94	4.98	4.96	**ε 3-5=**	0.003889	**ε avg3=**	0.00542702		3	5	13.60	13.58	13.59	13.59	**ε 3-5=**	0.01065456	**ε avg3=**	0.00863184
4	6	7.28	7.29	7.30	7.29	**ε 4-6=**	0.005715	**ε avg4=**	0.00665093		4	6	11.35	11.34	11.35	11.35	**ε 4-6=**	0.00889579	**ε avg4=**	0.00813008
5	7	13.22	13.18	13.20	13.20	**ε 5-7=**	0.010349	**ε avg5=**	0.00775550		5	7	0.00	0.00	0.00	0.00	**ε 5-7=**		**ε avg5=**	
6	8	9.17	9.20	9.19	9.19	**ε 6-8=**	0.007202	**ε avg6=**	0.00861442		6	8	6.15	6.20	6.17	6.17	**ε 6-8=**	0.00483989	**ε avg6=**	0.00744016
7	9	10.63	10.53	10.57	10.58	**ε 7-9=**	0.008292	**ε avg7=**	0.00774723		7	9	10.94	10.96	10.95	10.95	**ε 7-9=**	0.00858480	**ε avg7=**	0.00671235

Dead End											Live End									
Di	Di+1	R1	R2	R3	Average	ε		ε,avg			Di	Di+1	R1	R2	R3	Average	ε		ε,avg	
1	3	10.28	10.26	10.27	10.27	**ε 1-3=**	0.008052	**ε avg1=**	0.00728989	t=28 days after prestress releasing	1	3	8.42	8.48	8.50	8.47	**ε 1-3=**	0.00663787	**ε avg1=**	0.00640267
2	4	8.32	8.33	8.33	8.33	**ε 2-4=**	0.006528	**ε avg2=**	0.00610736		2	4	7.86	7.87	7.87	7.87	**ε 2-4=**	0.00616747	**ε avg2=**	0.00777902
3	5	4.76	4.78	4.78	4.77	**ε 3-5=**	0.003742	**ε avg3=**	0.00528242		3	5	13.44	13.43	13.43	13.43	**ε 3-5=**	0.01053173	**ε avg3=**	0.00848898
4	6	7.1	7.12	7.12	7.11	**ε 4-6=**	0.005577	**ε avg4=**	0.00625109		4	6	11.17	11.19	11.19	11.18	**ε 4-6=**	0.00876773	**ε avg4=**	0.00772240
5	7	12.04	12.03	12.03	12.03	**ε 5-7=**	0.009434	**ε avg5=**	0.00736786		5	7	0.00	0.00	0.00	0.00	**ε 5-7=**		**ε avg5=**	
6	8	9.04	9.05	9.05	9.05	**ε 6-8=**	0.007093	**ε avg6=**	0.00822503		6	8	4.91	4.94	4.95	4.93	**ε 6-8=**	0.00386773	**ε avg6=**	0.00700460
7	9	10.42	10.38	10.38	10.39	**ε 7-9=**	0.008148	**ε avg7=**	0.00762048		7	9	10.70	10.68	10.68	10.69	**ε 7-9=**	0.00837835	**ε avg7=**	0.00612304

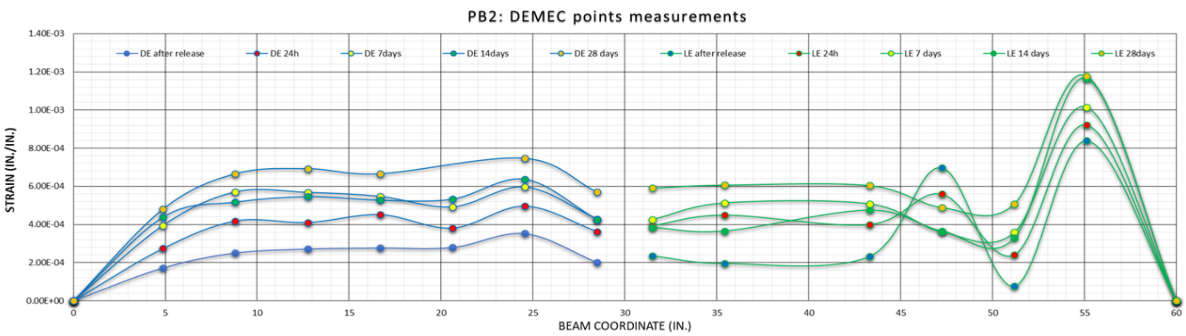

Figure H14: DEMEC points measurements for PB2

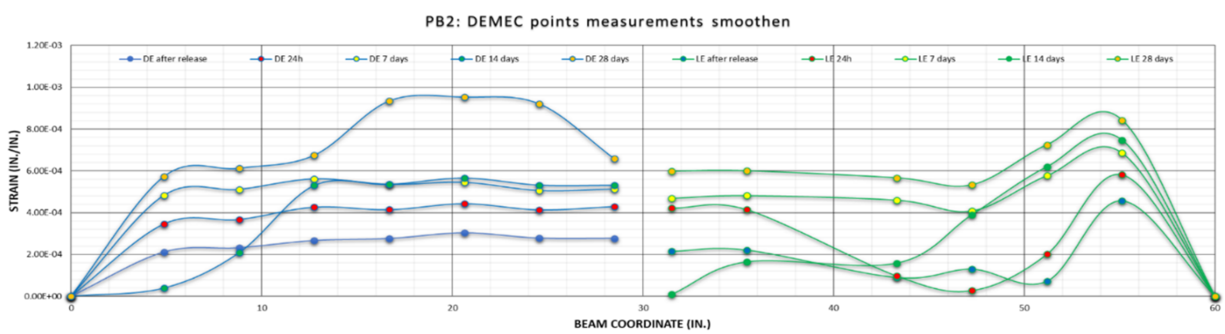

Figure H15: DEMEC points measurements smoothen for PB2 (95% average maximum strain

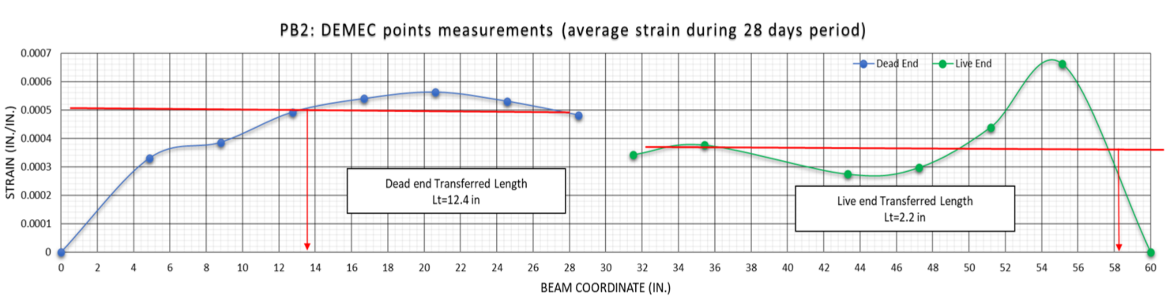

Figure H16: DEMEC points measurements for PB2 (average strain during 28 days period)

The following figures show how the transfer length was evaluated using 95% average maximum strain method:

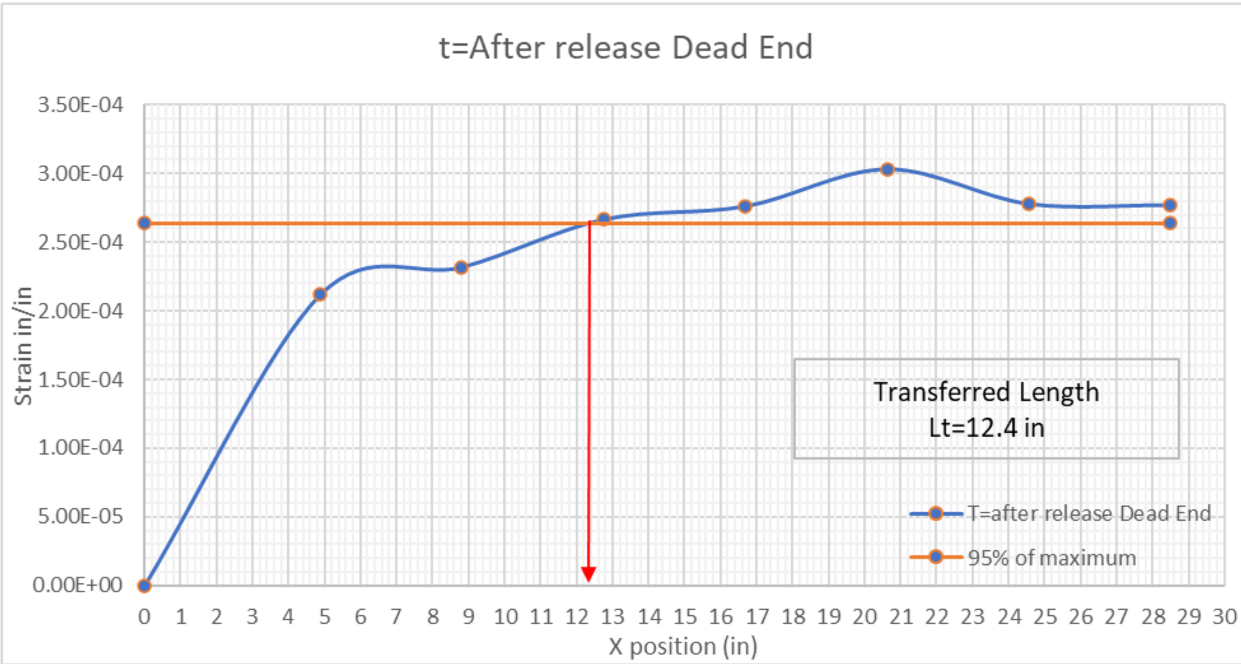

Figure H17: Evaluation of transfer length at the time of prestress release (Dead End)

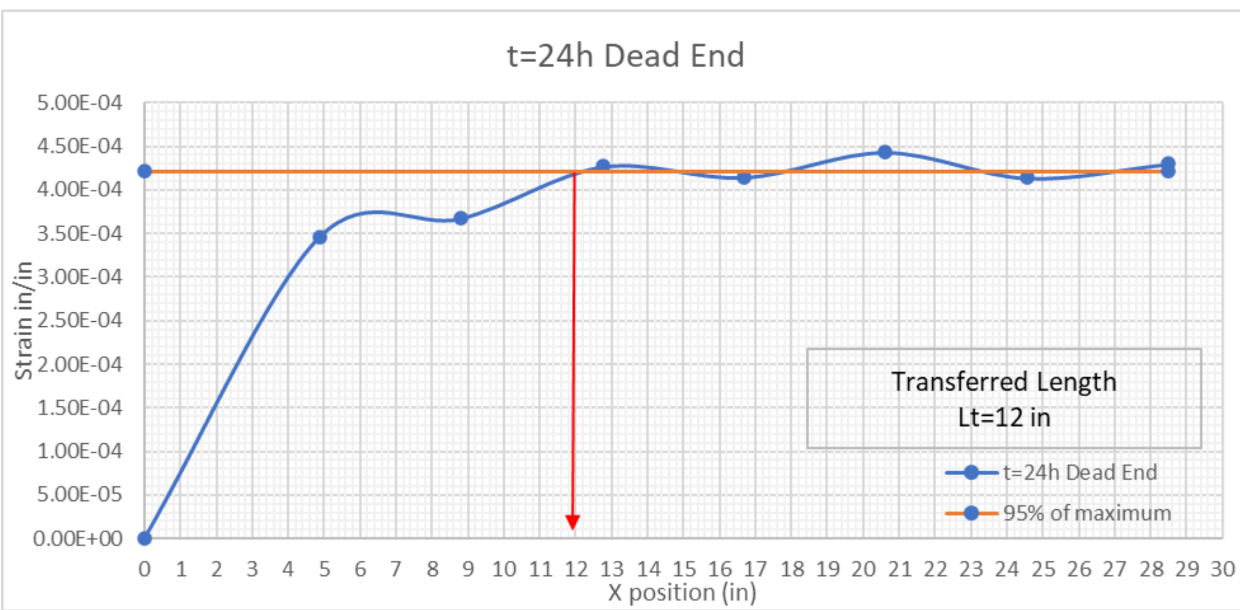

Figure H18: Evaluation of transfer length 24 hours after prestress release (Dead End)

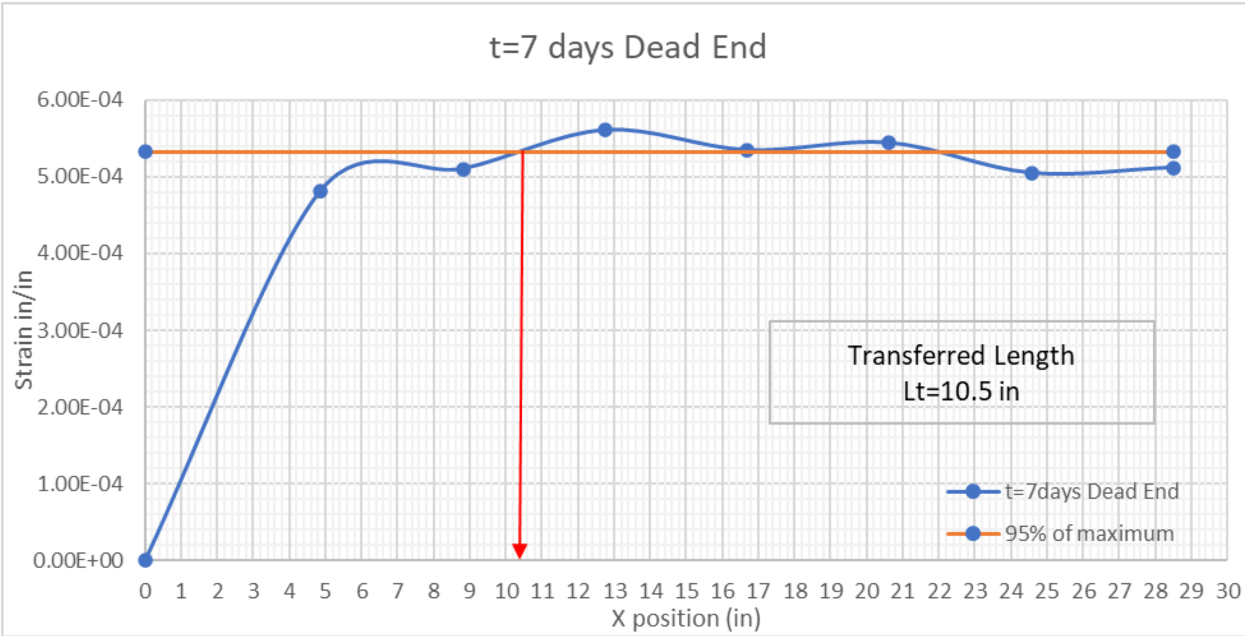

Figure H19: Evaluation of transfer length 7 days after prestress release (Dead End)

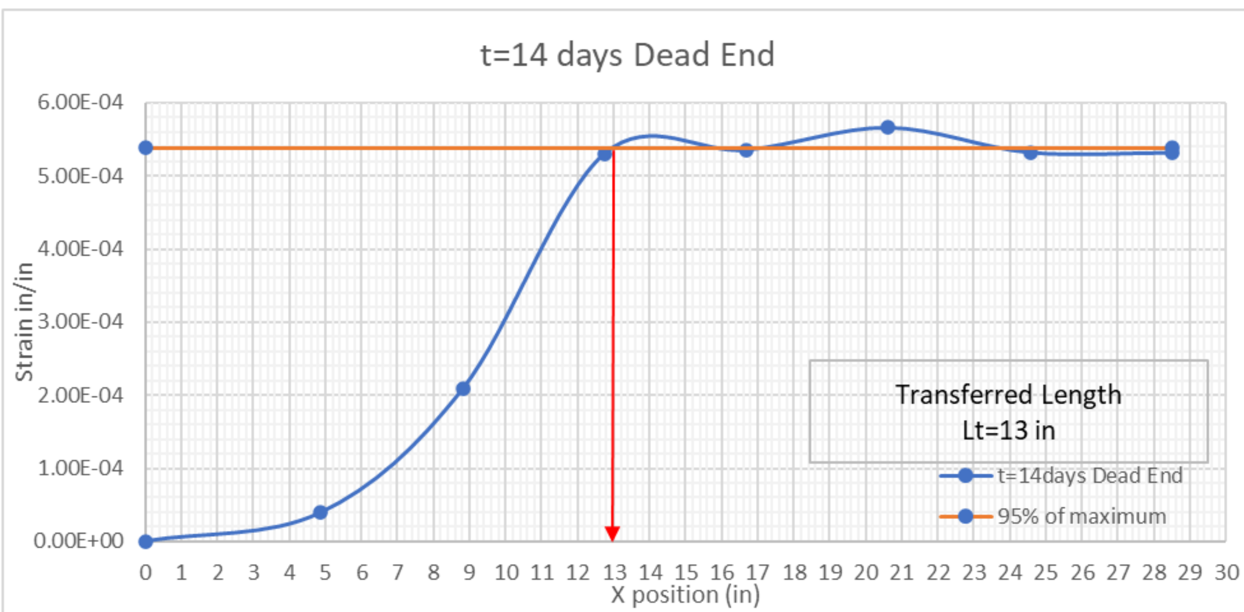

Figure H20: Evaluation of transfer length 14 days after prestress release (Dead End)

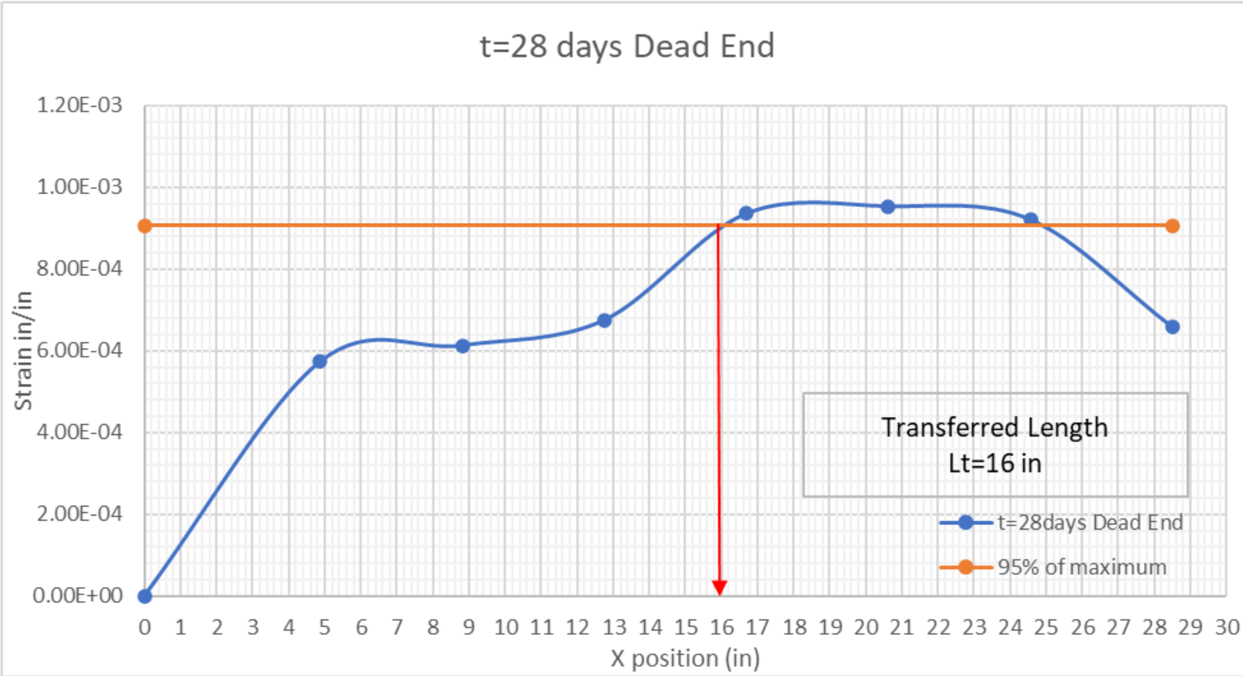

Figure H21: Evaluation of transfer length 28 days after prestress release (Dead End)

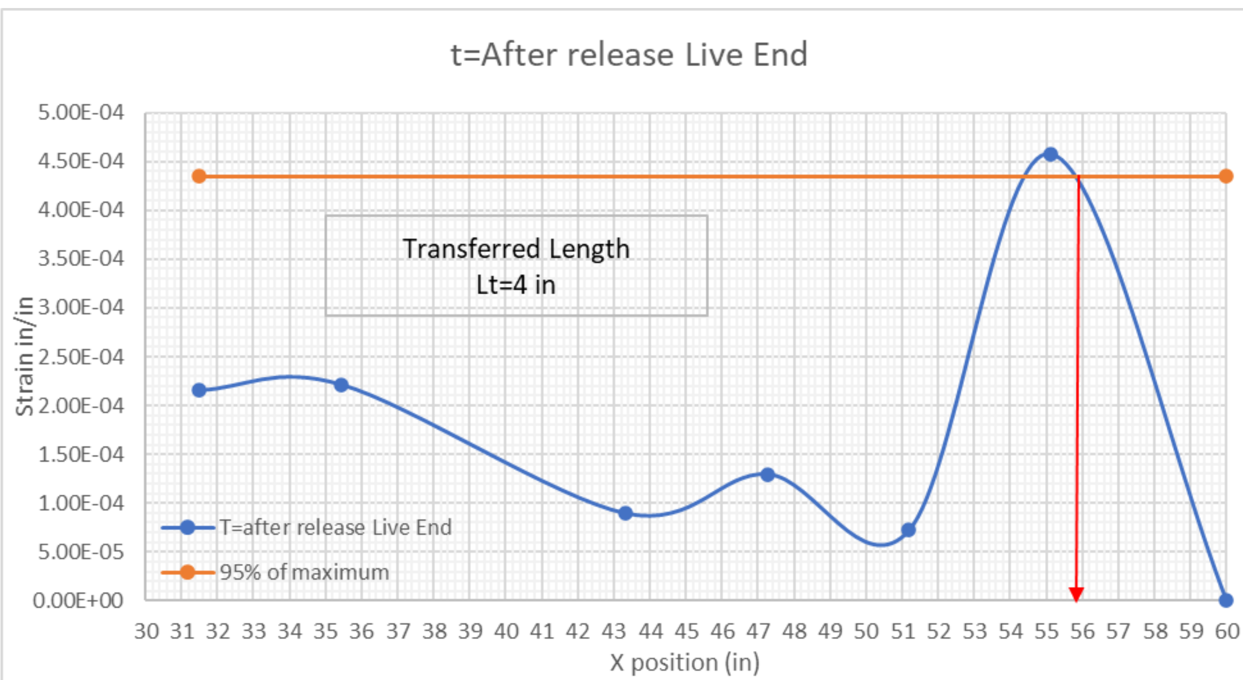

Figure H22: Evaluation of transfer length at the time of prestress release (Live End)

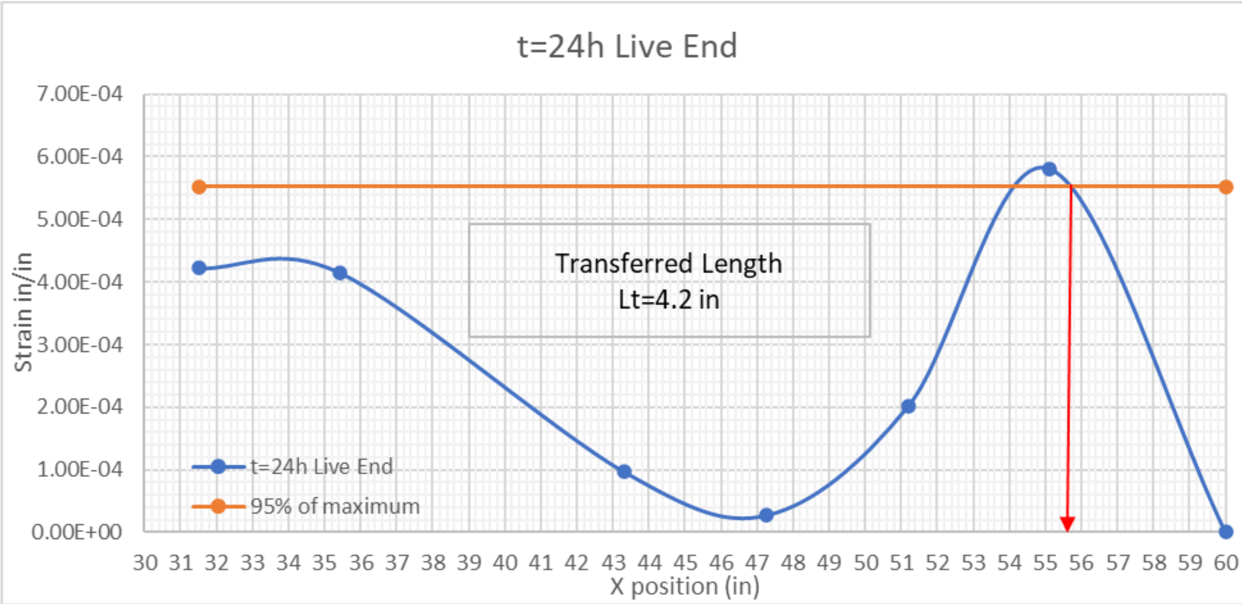

Figure H23: Evaluation of transfer length 24 hours after prestress release (Live End)

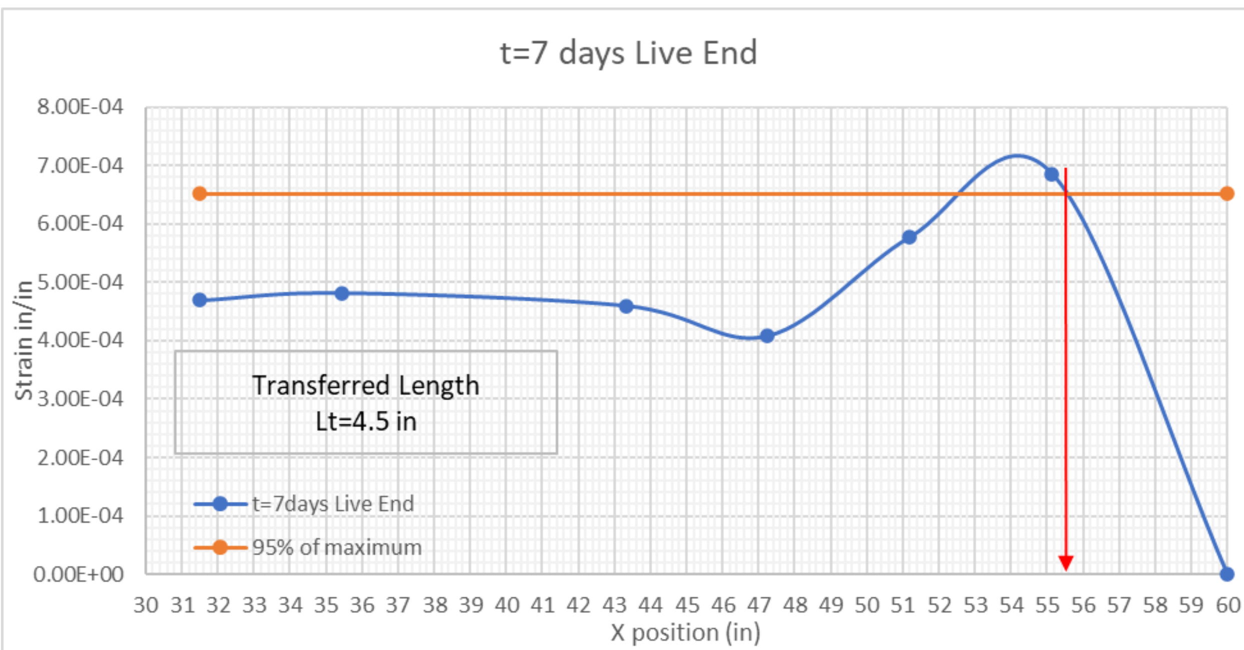

Figure H24: Evaluation of transfer length 7 days after prestress release (Live End)

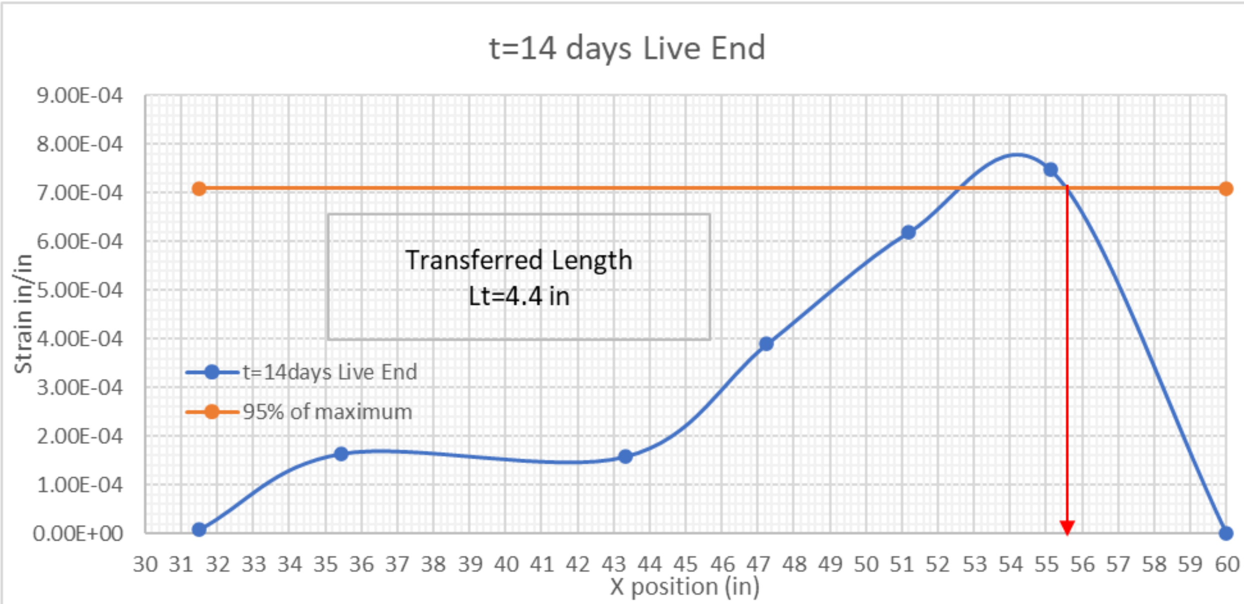

Figure H25: Evaluation of transfer length 14 days after prestress release (Live End)

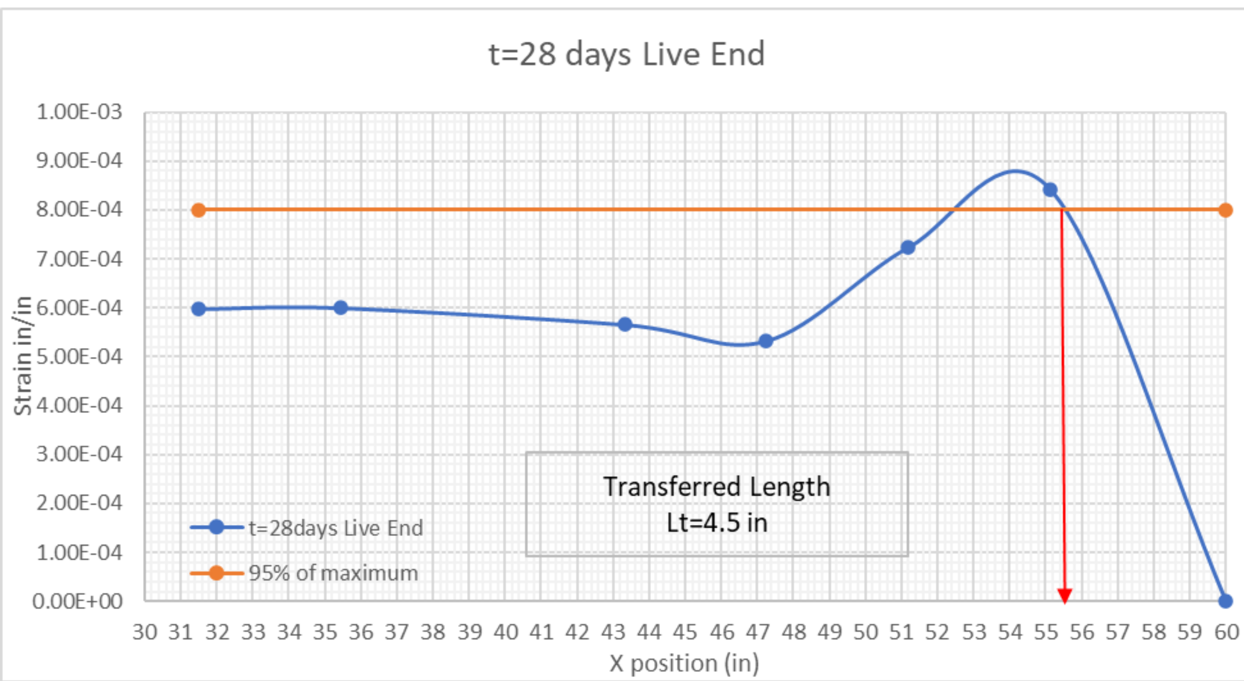

Figure H26: Evaluation of transfer length 28 days after prestress release (Live End)

Table H3: DEMEC points measurements for PB3

PB3: DEMEC MEASUREMENTS

t=0- Before releasing prestress

Dead End									
Di	Di+1	R1	R2	R3	Average	ε		ε,avg	
1	3	12.82	12.80	12.81	12.81	ε 1-3=	0.0100430	ε avg1=	0.0080491
2	4	7.70	7.75	7.72	7.72	ε 2-4=	0.0060551	ε avg2=	0.0077703
3	5	9.20	9.22	9.18	9.20	ε 3-5=	0.0072128	ε avg3=	0.0075673
4	6	12.04	12.03	12.03	12.03	ε 4-6=	0.0094341	ε avg4=	0.0065647
5	7	3.89	3.87	3.90	3.89	ε 5-7=	0.0030471	ε avg5=	0.0056274
6	8	5.62	5.60	5.62	5.61	ε 6-8=	0.0044009	ε avg6=	0.0055559
7	9	11.75	11.76	11.77	11.76	ε 7-9=	0.0092198	ε avg7=	0.00681035

Live End									
Di	Di+1	R1	R2	R3	Average	ε		ε,avg	
1	3	9.65	9.67	9.70	9.67	ε 1-3=	0.0075839	ε avg1=	0.0070273
2	4	8.25	8.26	8.25	8.25	ε 2-4=	0.0064706	ε avg2=	0.0061196
3	5	5.48	5.50	5.49	5.49	ε 3-5=	0.0043042	ε avg3=	0.0059854
4	6	9.17	9.15	9.16	9.16	ε 4-6=	0.0071814	ε avg4=	0.0069288
5	7	11.88	11.86	11.85	11.86	ε 5-7=	0.0093009	ε avg5=	0.0082546
6	8	10.55	10.56	10.58	10.56	ε 6-8=	0.0082817	ε avg6=	0.0096327
7	9	14.45	14.42	14.43	14.43	ε 7-9=	0.0113157	ε avg7=	0.00979869

t=0+ After releasing prestress

Dead End									
Di	Di+1	R1	R2	R3	Average	ε		ε,avg	
1	3	12.45	12.43	12.46	12.45	ε 1-3=	0.0097582	ε avg1=	0.0077564
2	4	7.35	7.33	7.34	7.34	ε 2-4=	0.0057546	ε avg2=	0.0074750
3	5	8.80	8.83	8.82	8.82	ε 3-5=	0.0069123	ε avg3=	0.0072520
4	6	11.58	11.60	11.60	11.59	ε 4-6=	0.0090892	ε avg4=	0.0062737
5	7	3.60	3.61	3.58	3.60	ε 5-7=	0.0028198	ε avg5=	0.0053538
6	8	5.30	5.29	5.30	5.30	ε 6-8=	0.0041526	ε avg6=	0.0053112
7	9	11.42	11.44	11.43	11.43	ε 7-9=	0.0089611	ε avg7=	0.00655685

Live End									
Di	Di+1	R1	R2	R3	Average	ε		ε,avg	
1	3	9.40	9.41	9.40	9.40	ε 1-3=	0.0073722	ε avg1=	0.0067751
2	4	7.88	7.88	7.88	7.88	ε 2-4=	0.0061779	ε avg2=	0.0058495
3	5	5.10	5.10	5.10	5.10	ε 3-5=	0.0039984	ε avg3=	0.0056796
4	6	8.76	8.75	8.75	8.75	ε 4-6=	0.0068626	ε avg4=	0.0066187
5	7	11.46	11.48	11.48	11.47	ε 5-7=	0.0089951	ε avg5=	0.0079419
6	8	10.15	10.16	10.18	10.16	ε 6-8=	0.0079681	ε avg6=	0.0093296
7	9	14.05	14.07	14.07	14.06	ε 7-9=	0.0110257	ε avg7=	0.00949685

t=24h after prestressed released

Dead End									
Di	Di+1	R1	R2	R3	Average	ε		ε,avg	
1	3	12.42	12.43	12.42	12.42	ε 1-3=	0.0097399	ε avg1=	0.0076871
2	4	7.18	7.20	7.18	7.19	ε 2-4=	0.0056343	ε avg2=	0.0074114
3	5	8.74	8.75	8.76	8.75	ε 3-5=	0.0068600	ε avg3=	0.0071841
4	6	11.56	11.55	11.55	11.55	ε 4-6=	0.0090578	ε avg4=	0.0062119
5	7	3.42	3.45	3.53	3.47	ε 5-7=	0.0027179	ε avg5=	0.0052711
6	8	5.15	5.16	5.14	5.15	ε 6-8=	0.0040376	ε avg6=	0.0051988
7	9	11.25	11.28	11.30	11.28	ε 7-9=	0.0088409	ε avg7=	0.00643925

Live End									
Di	Di+1	R1	R2	R3	Average	ε		ε,avg	
1	3	9.48	9.49	9.50	9.49	ε 1-3=	0.0074402	ε avg1=	0.0067698
2	4	7.82	7.75	7.77	7.78	ε 2-4=	0.0060995	ε avg2=	0.0058277
3	5	5.05	5.04	5.00	5.03	ε 3-5=	0.0039435	ε avg3=	0.0056195
4	6	8.68	8.70	8.70	8.69	ε 4-6=	0.0068156	ε avg4=	0.0065747
5	7	11.43	11.46	11.42	11.44	ε 5-7=	0.0089650	ε avg5=	0.0079040
6	8	10.12	10.10	10.13	10.12	ε 6-8=	0.0079315	ε avg6=	0.0093039
7	9	14.05	14.03	14.07	14.05	ε 7-9=	0.0110152	ε avg7=	0.00947333

t=7 daysAfter releasing prestress

Dead End									
Di	Di+1	R1	R2	R3	Average	ε		ε,avg	
1	3	12.29	12.30	12.98	12.52	ε 1-3=	0.0098183	ε avg1=	0.0076727
2	4	7.04	7.06	7.05	7.05	ε 2-4=	0.0055272	ε avg2=	0.0073740
3	5	8.62	8.65	8.66	8.64	ε 3-5=	0.0067764	ε avg3=	0.0070865
4	6	11.42	11.43	11.42	11.42	ε 4-6=	0.0089559	ε avg4=	0.0061169
5	7	3.38	3.30	3.34	3.34	ε 5-7=	0.0026186	ε avg5=	0.0051753
6	8	5.03	5.04	5.05	5.04	ε 6-8=	0.0039514	ε avg6=	0.0051082
7	9	11.17	11.16	11.17	11.17	ε 7-9=	0.0087547	ε avg7=	0.00635301

Live End									
Di	Di+1	R1	R2	R3	Average	ε		ε,avg	
1	3	9.4	9.44	9.42	9.42	ε 1-3=	0.0073853	ε avg1=	0.0066967
2	4	7.66	7.68	7.65	7.66	ε 2-4=	0.0060081	ε avg2=	0.0057458
3	5	4.90	4.89	4.92	4.90	ε 3-5=	0.0038442	ε avg3=	0.0055159
4	6	8.55	8.54	8.53	8.54	ε 4-6=	0.0066954	ε avg4=	0.0064776
5	7	11.35	11.34	11.34	11.34	ε 5-7=	0.0088932	ε avg5=	0.0078182
6	8	10.02	10.05	10.03	10.03	ε 6-8=	0.0078661	ε avg6=	0.0092294
7	9	13.93	13.94	13.95	13.94	ε 7-9=	0.0109290	ε avg7=	0.00939755

t=14 days after releasing prestress

Dead End									
Di	Di+1	R1	R2	R3	Average	ε		ε,avg	
1	3	12.12	12.15	12.15	12.14	ε 1-3=	0.0095178	ε avg1=	0.0074532
2	4	6.88	6.87	6.87	6.87	ε 2-4=	0.0053887	ε avg2=	0.0071875
3	5	8.49	8.49	8.49	8.49	ε 3-5=	0.0066562	ε avg3=	0.0069610
4	6	11.28	11.27	11.27	11.27	ε 4-6=	0.0088383	ε avg4=	0.0060220
5	7	3.3	3.27	3.27	3.28	ε 5-7=	0.0025715	ε avg5=	0.0050882
6	8	4.87	5.00	4.88	4.92	ε 6-8=	0.0038547	ε avg6=	0.0050237
7	9	11.04	11.02	11.02	11.03	ε 7-9=	0.0086449	ε avg7=	0.00624979

Live End									
Di	Di+1	R1	R2	R3	Average	ε		ε,avg	
1	3	9.25	9.26	9.25	9.25	ε 1-3=	0.0072546	ε avg1=	0.0065699
2	4	7.50	7.51	7.51	7.51	ε 2-4=	0.0058852	ε avg2=	0.0056169
3	5	4.72	4.74	4.74	4.73	ε 3-5=	0.0037109	ε avg3=	0.0053887
4	6	8.38	8.38	8.38	8.38	ε 4-6=	0.0065699	ε avg4=	0.0063539
5	7	11.20	11.20	11.20	11.20	ε 5-7=	0.0087808	ε avg5=	0.0077146
6	8	9.92	9.95	9.95	9.94	ε 6-8=	0.0077930	ε avg6=	0.0091397
7	9	13.80	13.85	13.85	13.83	ε 7-9=	0.0108453	ε avg7=	0.00931915

t=28 days after releasing prestress

Dead End									
Di	Di+1	R1	R2	R3	Average	ε		ε,avg	
1	3	11	10.99	10.98	10.99	ε 1-3=	0.0086162	ε avg1=	0.0069371
2	4	6.71	6.70	6.71	6.71	ε 2-4=	0.0052580	ε avg2=	0.0067973
3	5	8.33	8.30	8.31	8.31	ε 3-5=	0.0065177	ε avg3=	0.0068147
4	6	11.05	11.06	11.06	11.06	ε 4-6=	0.0086684	ε avg4=	0.0058382
5	7	2.93	2.98	3.00	2.97	ε 5-7=	0.0023285	ε avg5=	0.0048869
6	8	4.66	4.68	4.68	4.67	ε 6-8=	0.0036639	ε avg6=	0.0047902
7	9	10.68	10.68	10.70	10.69	ε 7-9=	0.0083783	ε avg7=	0.00602112

Live End									
Di	Di+1	R1	R2	R3	Average	ε		ε,avg	
1	3	9.09	9.10	9.11	9.10	ε 1-3=	0.0071344	ε avg1=	0.0064366
2	4	7.33	7.30	7.33	7.32	ε 2-4=	0.0057389	ε avg2=	0.0054714
3	5	4.52	4.53	4.50	4.52	ε 3-5=	0.0035411	ε avg3=	0.0052371
4	6	8.19	8.21	8.21	8.20	ε 4-6=	0.0064314	ε avg4=	0.0061988
5	7	11.00	11.00	11.00	11.00	ε 5-7=	0.0086240	ε avg5=	0.0075525
6	8	9.72	9.69	9.68	9.70	ε 6-8=	0.0076022	ε avg6=	0.0089637
7	9	13.61	13.60	13.60	13.60	ε 7-9=	0.0106650	ε avg7=	0.00913360

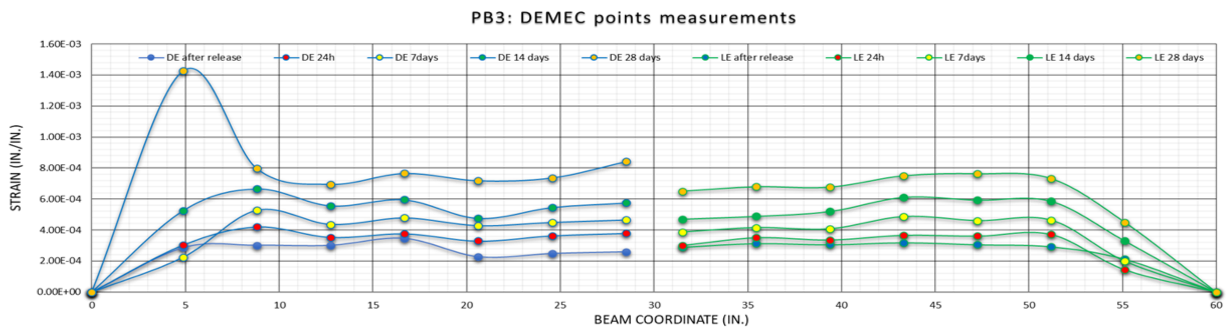

Figure H27: DEMEC points measurements for PB3

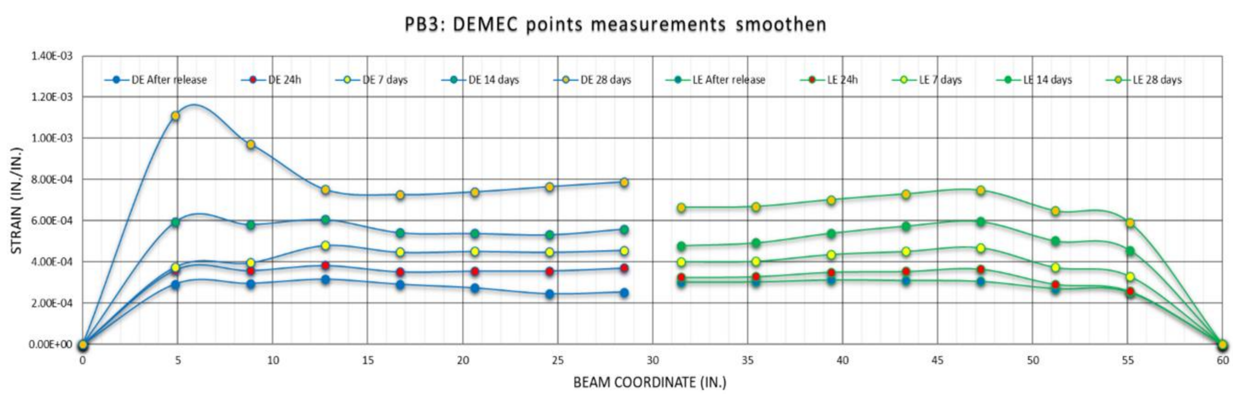

Figure H28: DEMEC points measurements smoothen for PB3 (95% average maximum strain method)

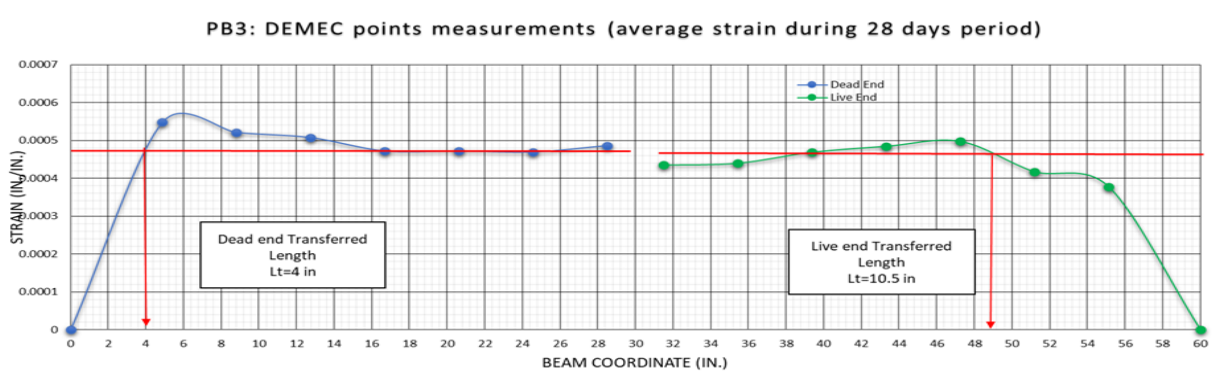

Figure H29: DEMEC points measurements for PB3 (average strain during 28 days period)

The following figures show how the transfer length was evaluated using 95% average maximum strain method:

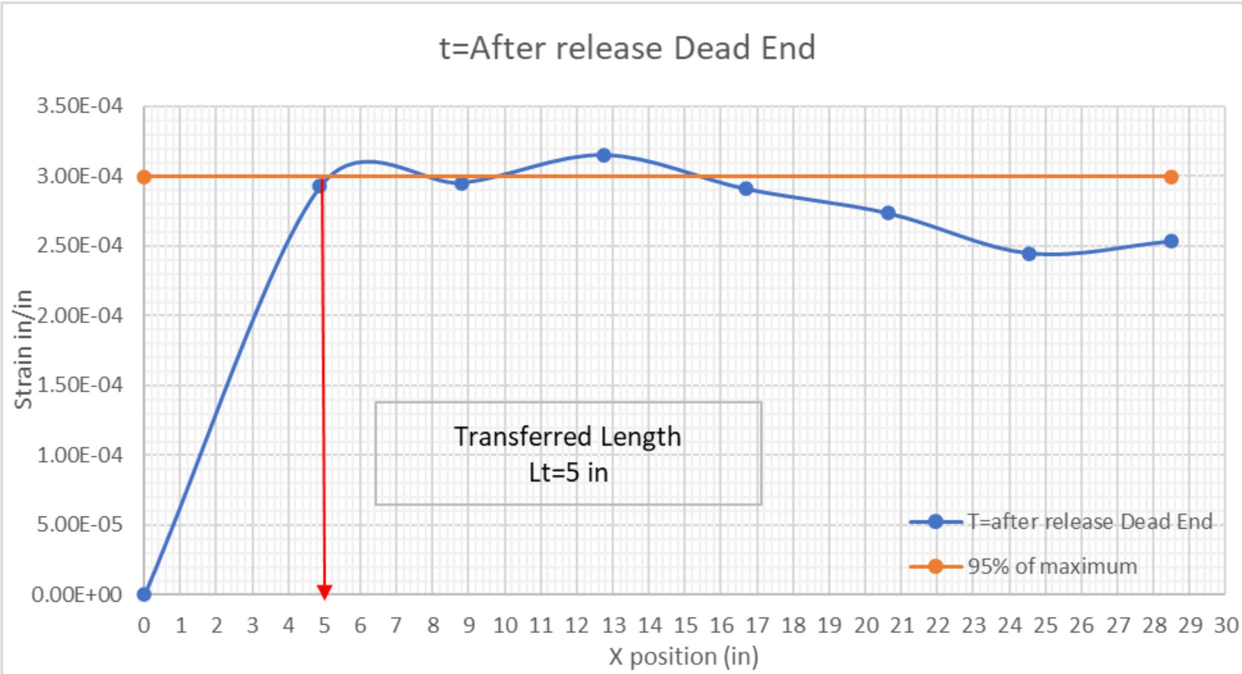

Figure H30: Evaluation of transfer length at the time of prestress release (Dead End)

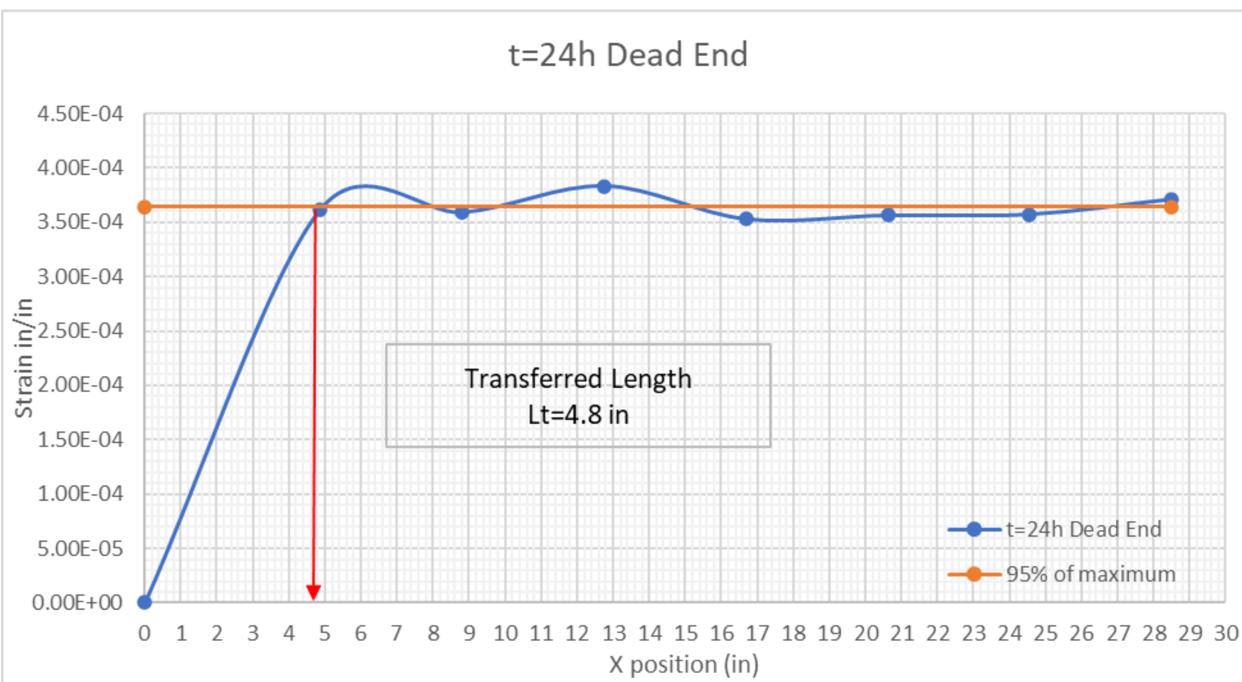

Figure H31: Evaluation of transfer length 24 hours after prestress release (Dead End)

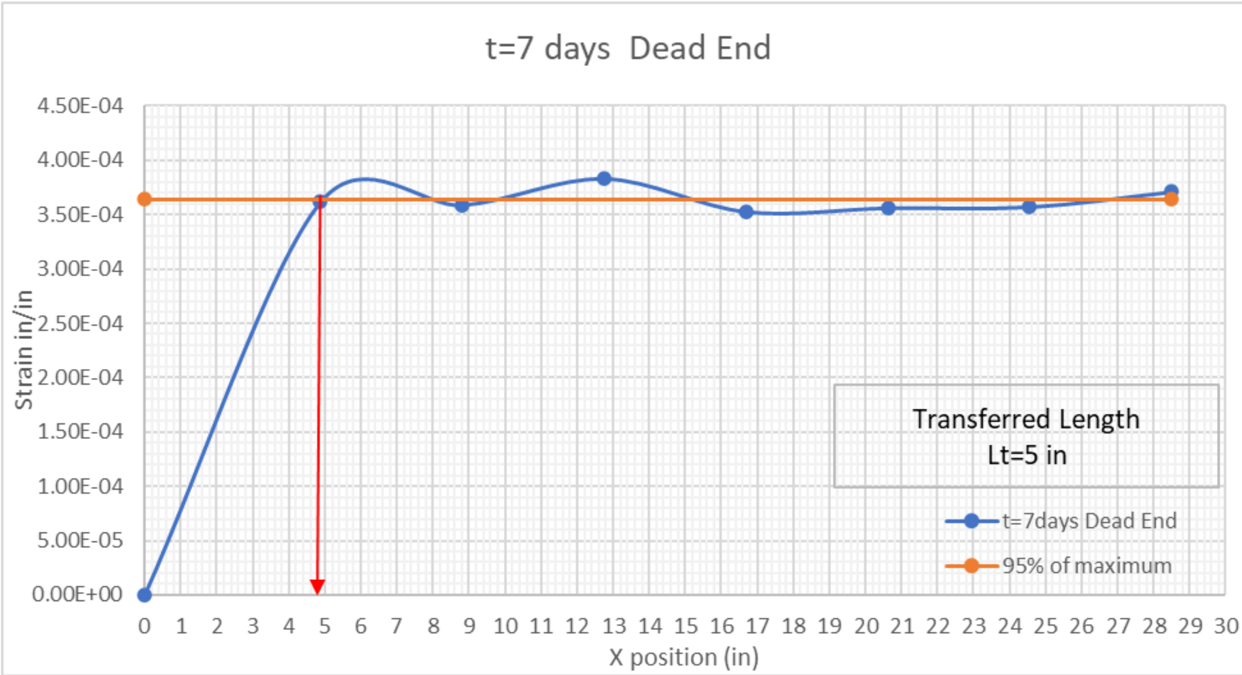

Figure H32: Evaluation of transfer length 7 days after prestress release (Dead End)

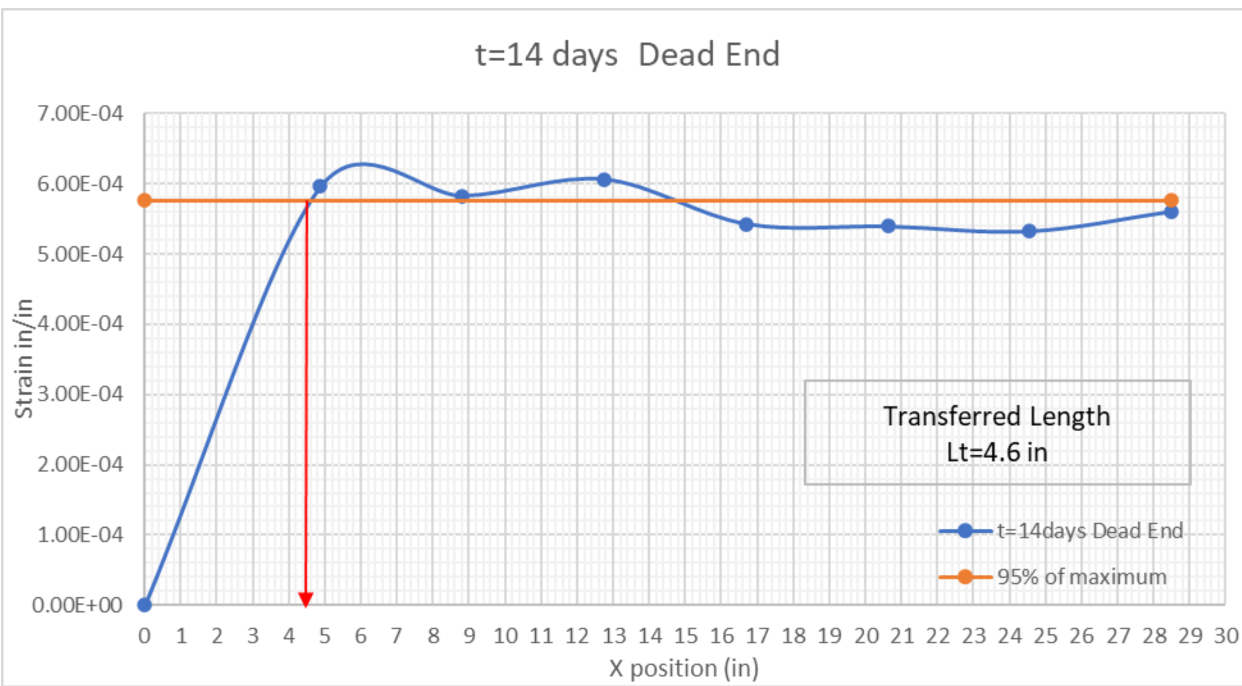

Figure H33: Evaluation of transfer length 14 days after prestress release (Dead End)

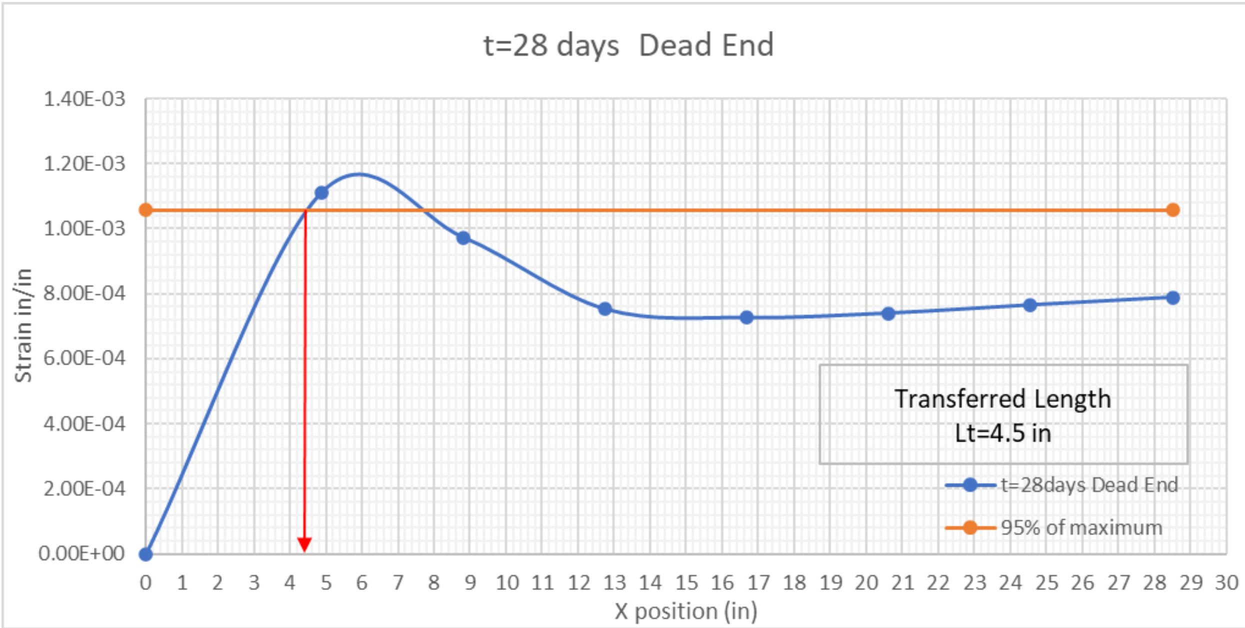

Figure H34: Evaluation of transfer length 28 days after prestress release (Dead End)

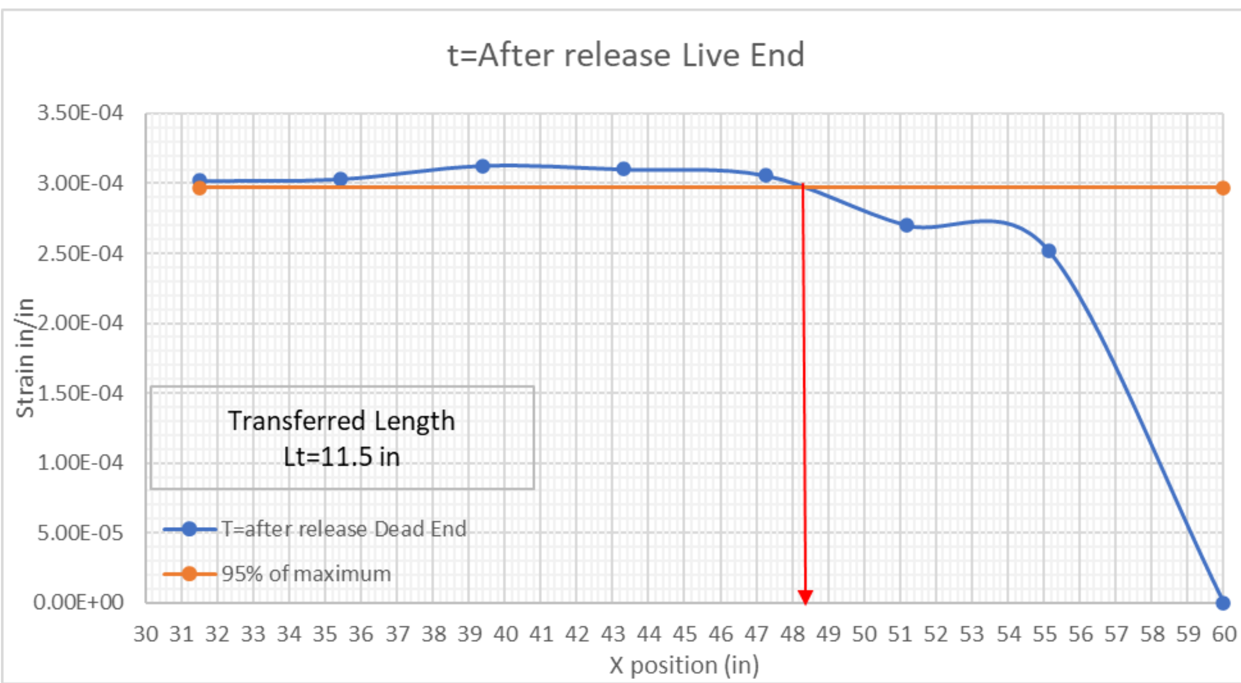

Figure H35: Evaluation of transfer length at the time of prestress release (Live End)

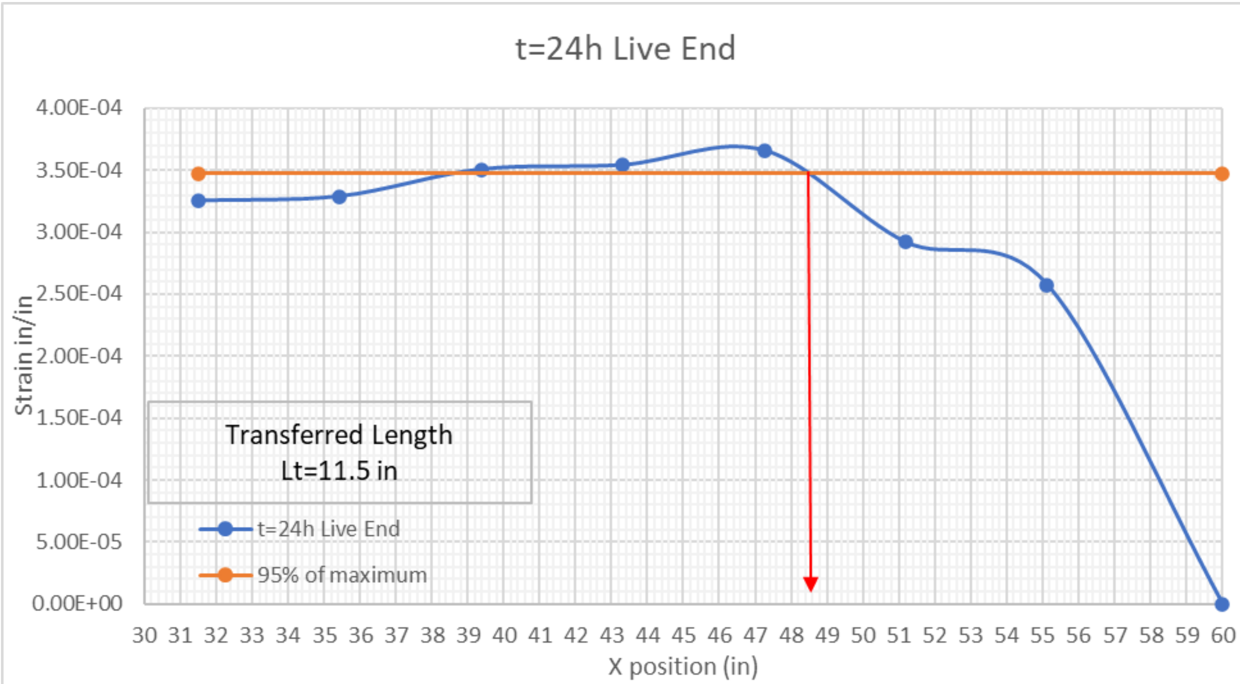

Figure H36: Evaluation of transfer length 24 hours after prestress release (Live End)

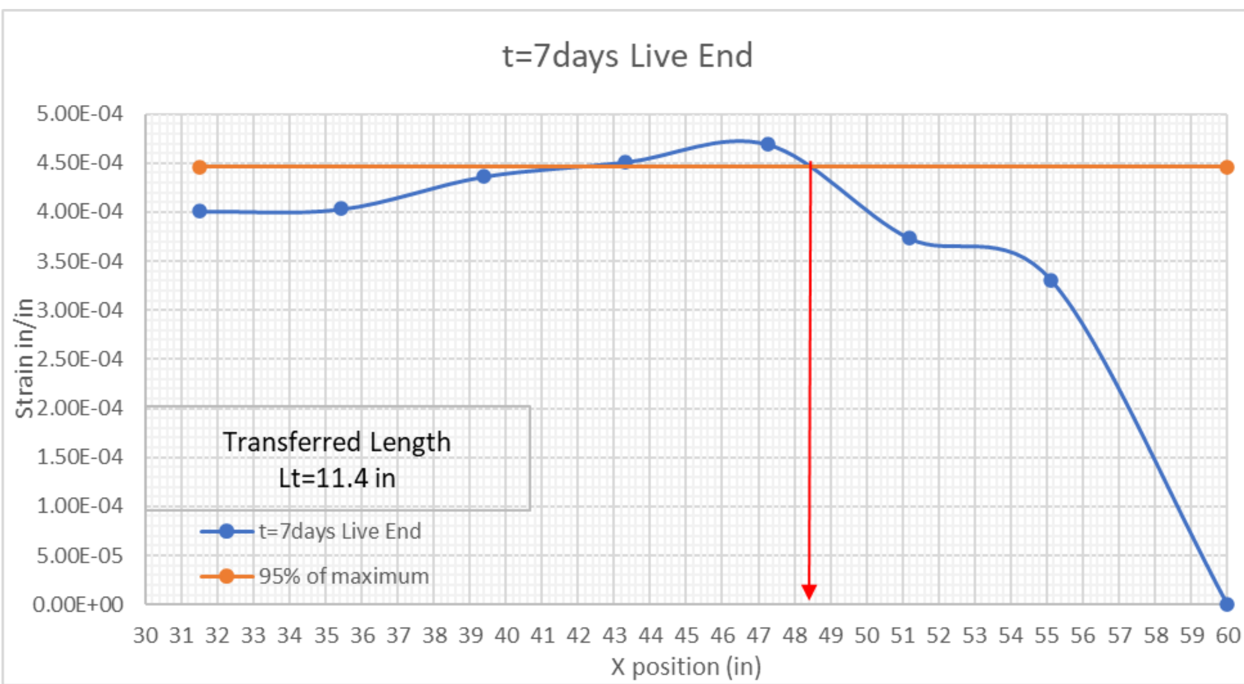

Figure H37: Evaluation of transfer length 7 days after prestress release (Live End)

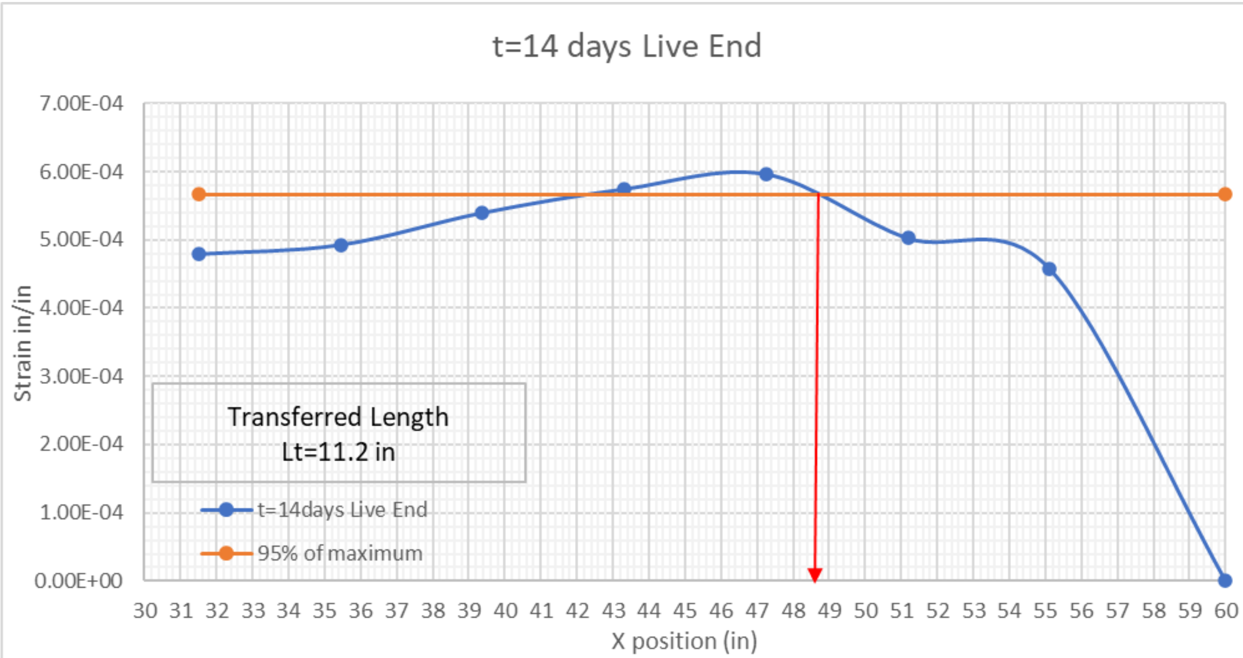

Figure H38: Evaluation of transfer length 14 days after prestress release (Live End)

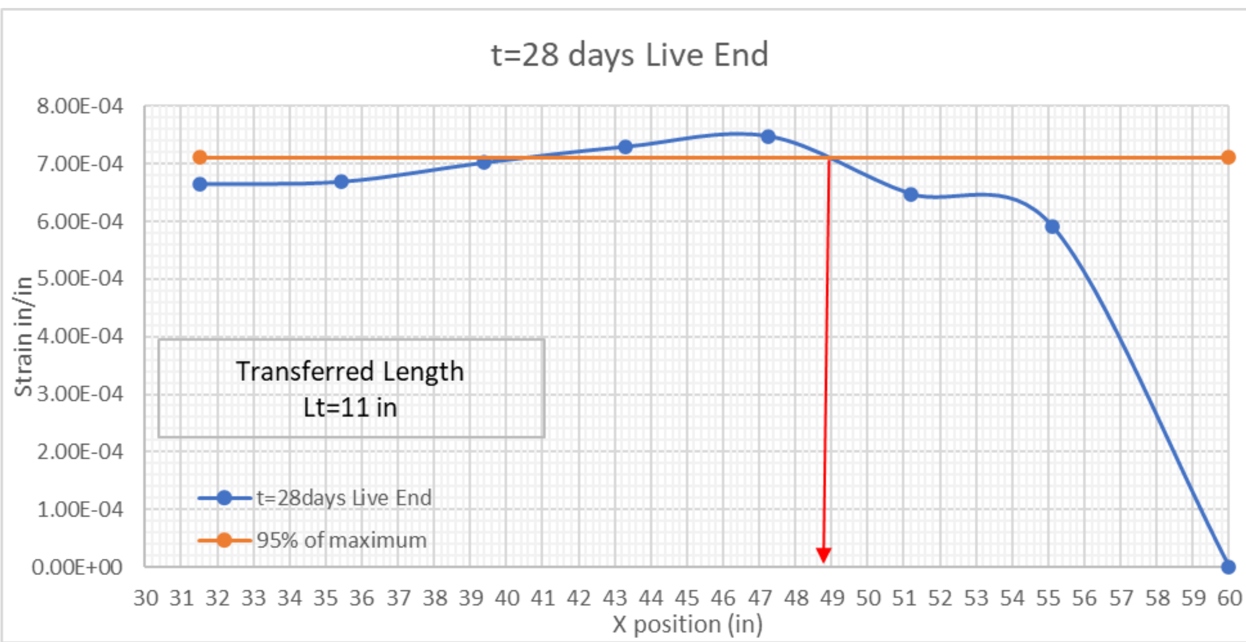

Figure H39: Evaluation of transfer length 28 days after prestress release (Live End)

Appendix I: Calculation of prestress losses

The prestress losses are calculated by following the procedure presented in Appendix B.

Prestressed beam No. 1 (PB1):

Table I1: Calculations of prestress losses for PB1

Properties		
Ac=	24	in2
Aps=	0.223	in2
concrete's weight	150	lb/ft3
Ec=	5525	ksi
Eci=	4371	ksi
Eb=	8702	ksi
I=	72.11137	in4
yb=	2.931878	in
yt=	3.068122	in
ys=	5.69	in
V/S=	1.2	in
w0=	25	lb/ft
e=	1.527	in
LL=	0	lb/ft
f'c=	9396.083	psi
fci'=	5880	psi
fj=	84.30493	ksi
beam span=	4.67	ft

Elastic shortening		
Ppi=	18.8	kips
fcpi=	1.39	ksi
Mo=	0.82	k.in
fg=	0.017	ksi
Kcir=	0.9	SU
fcir=	1.23	ksi
Kes=	1	SU
ES=	2.46	ksi
fbi=	81.85	ksi

Shrinkage		
RH=	65	%
Ksh=	1	SU
SH=	2.32	ksi

Creep		
wsd=	0	lb/ft
Msdl=	0	k-in
fcds=	0	ksi
Kcr=	2	SU
CR=	3.9	ksi

Relaxation		
Kre=	5	ksi
J=	0.04	SU
C=	1	SU
RE=	2.70	ksi

Total losses=	11.36	ksi
f_{be}=	**73**	**ksi**

Prestressed beam No.2 (PB2):

Table I2: Calculations of prestress losses for PB2

Properties		
Ac=	24	in2
Aps=	0.223	in2
concrete's weight	150	lb/ft3
Ec=	6178	ksi
Eci=	4768	ksi
Eb=	8702	ksi
I=	72.06154	in4
yb=	2.949364	in
yt=	3.050636	in
ys=	5.69	in
V/S=	1.2	in
w0=	25	lb/ft
e=	1.544	in
LL=	0	lb/ft
f'c=	11749	psi
fci'=	6996	psi
fj=	86.09865	ksi
beam span=	4.666667	ft

Elastic shortening		
Ppi=	19.2	kips
fcpi=	1.44	ksi
Mo=	0.82	k.in
fg=	0.018	ksi
Kcir=	0.9	SU
fcir=	1.27	ksi
Kes=	1	SU
ES=	2.33	ksi
fbi=	83.77	ksi

Shrinkage		
RH=	65	%
Ksh=	1	SU
SH=	2.32	ksi

Creep		
wsd=	0	lb/ft
Msdl=	0	k-in
fcds=	0	ksi
Kcr=	2	SU
CR=	3.6	ksi

Relaxation		
Kre=	5	ksi
J=	0.04	SU
C=	1	SU
RE=	2.76	ksi

Total losses=	10.99	ksi
f_{be}=	**75.11**	**ksi**

Prestressed beam No.3 (PB3):

Table I3: Calculations of prestress losses for PB3

Properties		
Ac=	24	in2
Ab=	0.223	in2
concrete's weight	150	lb/ft3
Ec=	6101	ksi
Eci=	4578	ksi
Eb=	8702	ksi
I=	72.0662	in4
yb=	2.94748	in
yt=	3.05252	in
ys=	5.69	in
V/S=	1.2	in
w0=	25	lb/ft
e=	1.542	in
LL=	0	lb/ft
f'c=	11456.48	psi
fci'=	6452	psi
fj=	86.08072	ksi
beam span=	4.666667	ft

Elastic shortening		
Ppi=	19.196	kips
fcpi=	1.43	ksi
Mo=	0.82	k.in
fg=	0.017	ksi
Kcir=	0.9	SU
fcir=	1.27	ksi
Kes=	1	SU
ES=	2.42	ksi
fbi=	83.66	ksi

Shrinkage		
RH=	65	%
Ksh=	1	SU
SH=	2.32	ksi

Creep		
wsd=	0	lb/ft
Msdl=	0	k-in
fcds=	0	ksi
Kcr=	2	SU
CR=	3.6	ksi

Relaxation		
Kre=	5	ksi
J=	0.04	SU
C=	1	SU
RE=	2.75	ksi

Total losses=	11.12	ksi
f_{be}=	**74.96**	**ksi**

Appendix J: Calculations of moment capacity

All notations are described in Appendix A and B.

Nonprestressed BFRP concrete beam No.1 (NPB1):

Table J1: Calculations of moment capacity for NPB1

Sections properties		
b=	4	in
h=	6	in
d=	4.595	in
L=	56	in
f'c=	9396	psi
fy=	60	ksi
Ec=	5525.204	ksi
E steel=	29000	ksi
E bfrp=	8702	ksi
n1=	1.57	DN
n2=	5.25	DN
As'=	0.2	in^2
Ab=	0.223	in^2
Ac=	23.58	in^2
A1=	0.351217	in^2
A2=	1.049735	in^2
Ag=	24	in^2
Atr=	24.98	in^2
e=	1.53	in
ygB=	1.405	in
ygS=	4.595	in
ygC=	3	in
ytr=	2.93	in
Ig=	72	in^4
Itr=	72.11137	in^4
cb=	2.93	in
ct=	3.068122	in

Strain compatibility		
i=1		
c=	2	in
β=	0.65	SU
a=	1.3	in
ε,s'=	0.000893	in/in
f's=	25.8825	ksi
C=	46.70719	kips
ε3=	0.003893	in/in
ff=	33.87254	ksi
T=	7.553575	kips
%	518%	
i=2		
c=	0.786	in
β=	0.65	SU
a=	0.5109	in
ε,s'=	0.002363	in/in
f's=	60.000	ksi
C=	28.32156	kips
ε3=	0.014538	in/in
ff=	126.5111	ksi
T=	28.21198	kips
%	0.39%	

Mn=	**108.63**	**kip.in**
Pu=	**7.69**	**kips**

Nonprestressed BFRP concrete beam No.2 (NPB2):

Table J2: Calculations of moment capacity for NPB2

Sections properties		
b=	4	in
h=	6	in
L=	56	in
d=	4.595	in
f'c=	11749	psi
fy=	60	ksi
Ec=	6178.279	ksi
E steel=	29000	ksi
E bfrp=	8702	ksi
n1=	1.41	DN
n2=	4.69	DN
As'=	0.2	in^2
Ab=	0.223	in^2
Ac=	23.58	in^2
A1=	0.314092	in^2
A2=	0.938773	in^2
Ag=	24	in^2
Atr=	24.83	in^2
e=	1.54	in
ygB=	1.405	in
ygS=	4.595	in
ygC=	3	in
ytr=	2.95	in
Ig=	72	in^4
Itr=	72.06154	in^4
cb=	2.95	in
ct=	3.050636	in

Strain compatibility		
i=1		
c=	2	in
β=	0.65	DN
a=	1.3	in
$\varepsilon_{,s}'$=	0.000893	in/in
f'_s=	25.8825	ksi
C=	49.3765	kips
ε_3=	0.003893	in/in
f_f=	33.87254	ksi
T=	7.553575	kips
%	554%	
i=2		
c=	0.73	in
β=	0.65	DN
a=	0.4745	in
$\varepsilon_{,s}'$=	0.002774	in/in
f'_s=	60.000	ksi
C=	30.95398	kips
ε_3=	0.015884	SU
f_f=	138.2188	ksi
T=	30.82278	kips
%	0.43%	

Mn=	**120.30**	**kip.in**
Pu=	**8.53**	**kips**

Nonprestressed BFRP concrete beam No.3 (NPB3):

Table J3: Calculations of moment capacity for NPB3

Sections properties		
b=	4	in
h=	6	in
d=	4.595	in
L=	56	in
f'c=	11456	psi
fy=	60	ksi
Ec=	6101	ksi
Esteel=	29000	ksi
Ebfrp=	8702	ksi
n1=	1.43	DN
n2=	4.75	DN
As'=	0.2	in^2
Ab=	0.223	in^2
Ac=	23.58	in^2
A1=	0.318	in^2
A2=	0.951	in^2
Ag=	24	in^2
Atr=	24.85	in^2
e=	1.54	in
ygB=	1.405	in
ygS=	4.595	in
ygC=	3	in
ytr=	2.95	in
Ig=	72	in^4
Itr=	72.07	in^4
cb=	2.95	in
ct=	3.053	in

Strain compatibility		
i=1		
c=	2	in
β=	0.65	DN
a=	1.3	in
$\varepsilon_{,s}$'=	0.000893	in/in
f'_s=	25.8825	ksi
C=	46.70719	kips
ε_3=	0.003893	in/in
f_f=	33.87	ksi
T=	7.553575	kips
%	518%	
i=2		
c=	0.735	in
β=	0.65	DN
a=	0.47775	in
$\varepsilon_{,s}$'=	0.002735	in/in
f'_s=	60.000	ksi
C=	30.60933	kips
ε_3=	0.015755	in/in
f_f=	137.10	ksi
T=	30.5735	kips
%	0.12%	

Mn=	**119.19**	**kip.in**
Pu=	**8.45**	**kips**

Prestressed BFRP concrete beam No.1 (PB1):

Table J4: Calculations of moment capacity for PB1

Sections properties		
b=	4	in
h=	6	in
L=	56	in
d=	4.595	in
f'c=	9396	psi
fy=	60	ksi
fci'=	5880	psi
Ec=	5525	ksi
E steel=	29000	ksi
E bfrp=	8702	ksi
n1=	1.57	DN
n2=	5.25	DN
As'=	0.2	in^2
Aps=	0.223	in^2
Ac=	23.577	in^2
A1=	0.351	in^2
A2=	1.050	in^2
Ag=	24	in^2
Atr=	24.98	in^2
e=	1.53	in
ygB=	1.405	in
ygS=	4.595	in
ygC=	3	in
ytr=	2.93	in
I=	72	in^4
Itr=	72.11	in^4
cb=	2.93	in
ct=	3.07	in

Strain compatibility		
i=1		
c=	2	in
β=	0.65	DN
a=	1.3	in
ε,s'=	0.000893	in/in
f'c=	25.8825	ksi
C=	46.70719	kips
ε1=	0.008382	DN
Pe=	16.27	kips
e=	1.527	in
ε2=	0.000213	DN
ε3=	0.003893	DN
εpb=	0.012488	DN
fpb=	108.6684	ksi
T=	24.23305	kips
%	93%	
i=2		
c=	1.11	in
β=	0.65	DN
a=	0.7215	in
ε,s'=	0.009419	in/in
f'c=	60	ksi
C=	35.04953	kips
ε1=	0.008382	DN
Pe=	16.26605	kips
e=	1.527	in
ε2=	0.000213	DN
ε3=	0.009419	DN
εpb=	0.018014	DN
fpb=	156.7593	ksi
T=	34.95732	kips
%	0.264%	

Mn=	**135.56**	**kip.in**
Pu=	**9.62**	**kip**

Prestressed BFRP concrete beam No.2 (PB2):

Table J5: Calculations of moment capacity for PB2

Sections properties		
b=	4	in
h=	6	in
L=	56	in
d=	4.595	in
f'c=	11749	psi
fy=	60	ksi
fci'=	6996	psi
Ec=	6178.279	ksi
Esteel=	29000	ksi
Ebfrp=	8702	ksi
n1=	1.408483	DN
n2=	4.693864	DN
As'=	0.2	in^2
Aps=	0.223	in^2
Ac=	23.577	in^2
A1=	0.314092	in^2
A2=	0.938773	in^2
Ag=	24	in^2
Atr=	24.82986	in^2
e=	1.544364	in
ygB=	1.405	in
ygS=	4.595	in
ygC=	3	in
ytr=	2.949364	in
I=	72	in^4
Itr=	72.06	in^4
cb=	2.95	in
ct=	3.05	in

Strain compatibility		
i=1		
c=	2	in
β=	0.65	DN
a=	1.3	in
$\varepsilon_{,s}$'=	0.000893	in/in
f'c=	25.8825	ksi
C=	57.10522	kips
ε_1=	0.008631	DN
Pe=	16.74946	kips
e=	1.544	in
ε_2=	0.000199	DN
ε_3=	0.003893	DN
ε_{pb}=	0.012723	DN
f_{pb}=	110.7132	ksi
T=	24.68904	kips
%	131%	
i=2		
c=	1	in
β=	0.65	DN
a=	0.65	in
$\varepsilon_{,s}$'=	0.010785	in/in
f'c=	60	ksi
C=	37.96436	kips
ε_1=	0.008631	DN
Pe=	16.74946	kips
e=	1.544	in
ε_2=	0.000199	DN
ε_3=	0.010785	DN
ε_{pb}=	0.019615	DN
f_{pb}=	170.6917	ksi
T=	38.06425	kips
%	0.262%	

Mn=	**149.51**	**kip.in**
Pu=	**10.62**	**kips**

Prestressed BFRP concrete beam No.3 (PB3)

Table J6: Calculations of moment capacity for PB3

Sections Properties		
b=	4	in
h=	6	in
L=	56	in
d=	4.595	in
f'c=	11456	psi
fy=	60	ksi
fci'=	6452	psi
Ec=	6101	ksi
E steel=	29000	ksi
E bfrp=	8702	ksi
n1=	1.43	DN
n2=	4.75	DN
As'=	0.2	in^2
Aps=	0.223	in^2
Ac=	23.577	in^2
A1=	0.32	in^2
A2=	0.95	in^2
Ag=	24	in^2
Atr=	24.85	in^2
e=	1.54	in
ygB=	1.405	in
ygS=	4.595	in
ygC=	3	in
ytr=	2.95	in
I=	72	in^4
Itr=	72.07	in^4
cb=	2.95	in
ct=	3.05	in

Strain compatibility		
i=1		
c=	2	in
β=	0.65	DN
a=	1.3	in
$\varepsilon_{,s}$'=	0.000893	in/in
f'c=	25.8825	ksi
C=	55.81413	kips
ε_1=	0.008614	DN
Pe=	16.7158	kips
e=	1.542	in
ε_2=	0.000201	DN
ε_3=	0.003893	DN
ε_{pb}=	0.012707	DN
f_{pb}=	110.578	ksi
T=	24.6589	kips
%	126%	
i=2		
c=	1.02	in
β=	0.65	DN
a=	0.663	in
$\varepsilon_{,s}$'=	0.010515	in/in
f'c=	60	ksi
C=	37.82519	kips
ε_1=	0.008614	DN
Pe=	16.7158	kips
e=	1.542	in
ε_2=	0.000201	DN
ε_3=	0.010515	DN
ε_{pb}=	0.019329	DN
f_{pb}=	168.2045	ksi
T=	37.5096	kips
%	0.841%	

Mn=	**147.26**	**kip.in**
Pu=	**10.46**	**kips**

REFERENCES

- ❖ JiriiMilitky, Vladimir Kovacic, Jitka Rubnerova, 2002, “Influence of thermal treatment on tensile failure of basalt”.

- ❖ Fareed Elgabbas, Patrick Vincent, Ehab A. Ahmed, Brahim Benmokrane, Department of Civil Engineering, University of Sherbrooke, 6 February 2016, “Experimental testing of basalt-fiber-reinforced polymer bars in concrete beams”.

- ❖ A. M. Fairuz, S. M. Sapuan, E. S. Zainudin, and C. N. A. Jaafar, 5 October 2016, “Pultrusion Process of Natural FibreReinforced Polymer Composites”.

- ❖ David Trejo, PhD, page 6,7,8, original submittal: October 2018, “Assessment of GFRP Properties”.

- ❖ M. N. Fardis, H. H. Khalili, A. L. Marshall , December 1982, “Magazine of Concrete Research: FRP-encased concrete as a structural material”

- ❖ S. Paul Bunea, 1991, “Concrete Reinforced With GFRP (glass-Filament-Reinforced-Plastic) in Lieu of Conventional Steel”

- ❖ ACI 440 committee, 2015, “ACI 440.1R-15 Guide for the design and construction of structural concrete reinforced with fiber-reinforced polymer (FRP) bars”.

- ❖ Raghavendra Vasudeva Upadhyaya, December 2018, retrieved from (PDF) Advances in FRP retrofit bonders part-I: State-of-the-art review (researchgate.net).

- ❖ Mohammed Abdulqader Jalil Alsalihi, December 2014 page 6-7, “Mechanical Properties of Glass Fiber Reinforced Polymer Bars After Exposure to Elevated Temperatures”.

- ❖ Ahmed H. Ali, Hamdy M. Mohamed, Brahim Benmokrane, 21 April 2020, “Bar size effect on long-term durability of sand-coated basalt-FRP composite bars”.

- ❖ V-ROD, 2021, Product Data sheet BFRP rods grade 60GPa, https://fiberglassrebar.com/wp-content/uploads/2021/08/V-ROD-BASALT-60-Spec-Sheet-EN.pdf.

- ❖ ACI committee 440, 2015, “ACI 440.1R-15 Guide for the design and construction of structural concrete reinforced with fiber-reinforced polymer (FRP) bars”.

- ❖ Gerhardus H. Koch, Michiel P.H. Brongers, and Neil G. Thompson, Y.Paul Virmani and J.H. Payer, 2002, “Corrosion Costs and Preventive Strategies in the United States”.

- ❖ Ash, 2022 retrieved from Prestressed Concrete - Types of Prestressing in Concrete (civilengineersforum.com).

- ❖ Eythor, THORHALLSSON Bjorgvin Smari JONSSON, January 2012, “TEST OF PRESTRESSED CONCRETE BEAMS WITH BFRP TENDONS”.

- ❖ Ali Alraie, Dipti Ranjan Sahoo and Vasant Matsagar, 2021, “Development of Optimal Anchor for Basalt Fiber–Reinforced Polymer Rods”.

- ❖ ACI Committee 440, 2004, “ACI 440.4R-04 Prestressing Concrete Structures with FRP Tendons”.

- ❖ Thorhallsson, E. and B. S. Jonsson, 2012, “Test of prestressed concrete beams with BFRP tendons.” Workshop Structural Engineering and Composites Laboratory, Reykjavik University.

- ❖ Canadial Standard Association, 2002, "Design and construction of building components with fibre-reinforced polymers.", S806-02, Canadial Standards Association.

- ❖ Alraie, A., D. R. Sahoo and V. Matsagar, 2021, "Development of Optimal Anchor for Basalt Fiber–Reinforced Polymer Rods." Journal of Composites for Construction 25(3): 04021011.

- ❖ ACI Committee 318, 2019, ”Building code requirements for structural concrete (ACI 318-19) : an ACI standard”

- ❖ Zia, P., H. K. Preston, N. L. Scott and E. B. Workman, 1979, "Estimating prestress losses." Concrete International 1(6): 32-38.

- ❖ American Society for Testing and Materials, ASTM C 1611/C1611M, 2014, “Standard Test Method for Slump Flow of Self-Consolidating Concrete”

- ❖ Andrawes, B., M. Shin, and A.M. Pozolo, 2009, “Transfer and development length of prestressing tendons in full-scale AASHTO prestressed concrete girders using self-consolidating concrete", Illinois Center for Transportation (ICT).

- AASHTO 1998, Standard Specifications for Highway Bridges, LRFD. US Customary Units, Second Edition, American Association of State Highway and Transportation Officials, Washington,D.C.
- Zia, P., and Mostafa, T., September-October 1997, "Development Length of Prestressing Strands," PCI JOURNAL, V. 22, No. 5, pp. 54-65
- Cousins, T. E., Johnston, D. W., and Zia, P., July-August 1990, "Transfer and De velopment Length of Epoxy Coated and Uncoated Prestressing Strands," PCI JOURNAL, V. 35, No. 4, , pp. 92-103.
- Shahawy, M. A., Issa, M., and Batchelor, B., , May-June 1992, "Strand Transfer Lengths in Full Scale AASHTO Prestressed Concrete Gird ers," PCI JOURNAL, V. 37, No. 3, pp. 84-96.
- Russell, B. W., and Burns, N. H., September-October 1996, "Measured Transfer Lengths of 0.5 and 0.6 in. Strands in Pretensioned Concrete," PCI JOURNAL, V. 41, No. 5, , pp. 44-65.
- Mitchell, D., Cook, W. D., Khan, A. A., and Tham, T., , May-June 1993 "Influence of High Strength Concrete on Transfer and Development Length of Pretensioning Strand," PCI JOURNAL, V. 38, No. 3, pp. 52-66.
- ACI-ASCE Committee 423, September 2016, "Guide to Estimating Prestress Loss", American Concrete Institute, Section 4.4.4 pp.20